DETERMINATION OF MECHANICAL PROPERTIES OF GEOPOLYMER BASED COMPOSITES SUITABLE FOR 3D ADDITIVE MANUFACTURING

3D BASKI ALINABİLİR JEOPOLİMER BAĞLAYICILI KOMPOZİTLERİN MEKANİK ÖZELLİKLERİNİN BELİRLENMESİ

NAZIM ÇAĞATAY DEMİRAL

PROF. DR. MUSTAFA ŞAHMARAN

Supervisor

Submitted to

Graduate School of Science and Engineering of Hacettepe University

as a Partial Fulfillment to the Requirements

for be Award of the Degree of Master of Science

in Civil Engineering

2022

ABSTRACT

DETERMINATION OF MECHANICAL PROPERTIES OF GEOPOLYMER-BASED COMPOSITES SUITABLE FOR 3D ADDITIVE MANUFACTURING

NAZIM ÇAĞATAY DEMİRAL

Master of Science, Department of Civil Engineering

Supervisor: Prof. Dr. Mustafa ŞAHMARAN

June 2022, 99 pages

The use of traditional concrete for many years until today has brought many problems. The production and use of Portland cement are the most responsible for the problem caused by conventional concrete. It is estimated that the use of concrete will continue to increase as the needs of humanity such as sheltering, and transportation continue. The detrimental influence on the environment of Portland cement so far can be understood by the fact that it accounts for 8-9% of CO2 emissions worldwide. It is obvious that this effect will negatively affect our sustainable future. Therefore, it is necessary to eliminate the production of concrete by offering a new binding material that will meet the needs of humanity with a novel, sustainable and "green" alternative. In addition to the environmental damage caused by concrete produced with Portland cement, the storage and recycling of construction demolition waste in the world are another problem that humanity must deal with. About 1/3 of the total annual waste of the European Union is covered by construction demolition waste. In developed European countries, most of this waste is reused, while in countries that do not have large economies, this rate is quite low. In addition, in European Union countries with large economies, the rate of production of value-added goods by the reuse of construction demolition is very low/limited. These materials are used in transportation projects such as road pavements and filling materials. In addition to materials related issues, traditional production methods used in the construction industry are considered to be very slow, risky and costly in today's

technology. Occupational accident risk is of great importance in-molded construction productions used until today. Mold and labor costs are another issues that needs to be optimized during the production stages. Therefore, researchers carried out studies focusing on innovative and sustainable ways in production methods.

The aim of this thesis is to develop innovative, sustainable and “green” 3 dimensional (3D) printable geopolymer-based composites developed within the scope of the thesis, to minimize the harmful effect of cement production on the environment, to reuse construction demolition waste with added value, and to expand automation by developing 3D production in the construction industry. In this context, the rheological properties of geopolymer binders suitable for 3D printing were determined. After that, the mixtures suitable for printing were produced by 3D additive manufacturing (AM) and their mechanical properties were determined. The anisotropic behavior and interlayer bond strength properties of the produced mixtures were determined as a result of curing at ambient conditions for 7, 28, 56 and 90 days. As a result, it is believed that the produced geopolymer composites suitable for 3D-AM will bring sustainable solutions to many problems encountered in the construction industry, such as global warming, excess cost, occupational accidents and management of construction demolition wastes.

Keywords: 3D-printing, construction and demolition waste, geopolymer, anistropy, alkaline content, bond strength

ÖZET

3D BASKI ALINABİLİR JEOPOLİMER BAĞLAYICILI KOMPOZİTLERİN MEKANİK ÖZELLİKLERİNİN BELİRLENMESİ

NAZIM ÇAĞATAY DEMİRAL

Yüksek Lisans, İnşaat Mühendisliği Bölümü

Tez Danışmanı: Prof. Dr. Mustafa ŞAHMARAN

Haziran 2022, 99 sayfa

Geleneksel betonun günümüze kadar uzun yıllar boyunca kullanılması birçok problemi beraberinde getirmiştir. Geleneksel betonun sebep olduğu problemin en büyük sorumlusu Portland çimentosunun üretimi ve kullanımıdır. İnsanlığın barınma ve ulaşım gibi ihtiyaçları devam ettikçe beton kullanımının artarak devam edeceği tahmin edilmektedir. Şimdiye kadar Portland çimentosunun çevreye zararlı etkisi dünya çapındaki CO_2 emisyonunun %8-9'unu oluşturduğu gerçeğiyle anlaşılabilir. Bu zararlı etkinin sürdürülebilir geleceğimizi kötü yönde etkileyeceği aşikârdır. Bu yüzden insanlığın ihtiyaçlarını karşılayacak beton üretimini, yeni, sürdürülebilir ve "yeşil" alternatif bağlayıcı malzemeler sunarak giderilmesi gerekmektedir. Portland çimentosu ile üretilen betonun çevreye verdiği zararın yanı sıra, dünyada inşaat yıkıntı atıklarının depolanması ve geri dönüştürülmesi de insanlığın başa çıkması gereken bir diğer problemdir. Avrupa birliğinin yıllık toplam atığının yaklaşık 1/3'ünü inşaat yıkıntı atıkları karşılamaktadır. Gelişmiş Avrupa ülkelerinde bu atığın büyük bir kısmı yeniden kullanılırken, büyük ekonomilere sahip olmayan ülkelerde bu oran oldukça düşmektedir. Bunun yanı sıra büyük ekonomiye sahip Avrupa Birliği ülkelerinde inşaat yıkıntı atıklarının yeniden kullanımıyla katma değerli mal üretilme oranı oldukça düşük/kısıtlıdır. Bu malzemeler yol kaplamaları, dolgu malzemesi gibi ulaştırma projelerinde değerlendirilmektedir. İlgili sorunlarla ilişkili malzemelerin yanı sıra, inşaat endüstrisinde kullanılan geleneksel

üretim yöntemleri, günümüz teknolojisinde oldukça yavaş, riskli ve maliyetli olduğu düşünülmektedir. Günümüze kadar kullanılan kalıplı yapı imalatlarında iş kazası riski büyük önem taşımaktadır. Kalıp ve işçi maliyetleri de üretim aşamalarında optimize edilmesi gereken bir diğer konudur. Bu yüzden araştırmacılar üretim yöntemlerinde yenilikçi ve sürdürülebilir yollara odaklanan araştırmalar yapmaktadır.

Bu tezin amacı, tez kapsamında geliştirilen yenilikçi, sürdürülebilir ve "yeşil" 3 boyutlu (3B) baskı alınabilir jeopolimer bağlayıcılı kompozitler geliştirerek çimento üretiminin çevreye zararlı etkisini en aza indirmek, inşaat yıkıntı atıklarının katma değerli olarak yeniden kullanımını sağlamak ve inşaat endüstrisinde 3D üretimi geliştirerek otomasyonu yaygınlaştırmaktır. Bu bağlamda, 3B baskı almaya uygun jeopolimer bağlayıcıların reolojik özellikleri belirlenmiştir. Daha sonra, baskı almaya uygun olan karışımlar 3B eklemeli imalat (AM) ile üretilerek mekanik özellikleri belirlenmiştir. Üretilen karışımların anizotropik davranışı ve katmanlar arası bağ dayanımı özellikleri 7, 28, 56 ve 90 günlük oda koşullarında kür işlemi sonucunda belirlenmiştir. Sonuç olarak, üretilen 3D eklemeli imalata uygun jeopolimer kompozitlerin inşaat endüstrisinde karşılaşılan küresel ısınma, maliyet fazlalığı, iş kazaları ve inşaat yıkıntı atıklarının yönetimi gibi birçok probleme sürdürülebilir çözümler getireceğine inanılmaktadır.

ACKNOWLEDGEMENT

First of all, I would like to express my sincere deep gratitude to my supervisor Prof. Dr. Mustafa ŞAHMARAN for his support and motivation with great patience, for guidance and knowledge throughout my thesis. In addition to his support for my thesis during my time working with him, he has always been more of a father to me than a mentor.

Also, I have to extend my thanks to Prof. Dr. İsmail Özgür YAMAN, Assoc. Prof. Dr. Cenk KARAKURT, Assoc. Prof. Dr. Mustafa Kerem KOÇKAR, Assoc. Prof. Dr. Gürkan YILDIRIM for giving me the opportunity to defend my master thesis.

I would like to thank all my friends whom I worked with at Hacettepe University Advanced Concrete Research Laboratory. Especially, I would like to express my deep gratitude to Mehmet Özkan EKİNCİ, Oğuzhan ŞAHİN, Hüseyin İLCAN, Anıl KUL, Emircan ÖZÇELİKCİ, Atakan OSKAY and Utku BELENDİR for their support.

The author gratefully acknowledges the financial assistance of the Scientific and Technical Research Council (TUBITAK) of Turkey provided under Project: 119N030.

Finally, I have to express my deep gratitude to my parents and siblings for their endless support and encouragement, both throughout the writing process of this thesis and throughout my life. I would especially like to thank my father, Doğan DEMİRAL, for guiding me throughout my education life.

NAZIM ÇAĞATAY DEMİRAL

June 2022, Ankara

TABLE OF CONTENTS

LIST OF TABLES

LIST OF FIGURES

1. INTRODUCTION

1.1 General

Structuring is inevitable for humanity due to shelter requirements throughout the human history. Traditional cement-based concrete, which is mostly used to meet the need for shelter, is the main part of the building materials. Concrete provides numerous advantages in the construction industry, including high strength, fire resistance, and durability [1]. However, this widely usage of concrete causes global warming and environmental pollution since CO_2 emissions due to the production of cement fabrication. Therefore, cement decarbonation is defined as one of the most difficult emission types [2]. Concrete production accounts for 7.8% of anthropogenic nitrogen emissions, 5.2 percent of anthropogenic sulfur emissions, and 6.4 percent of particles smaller than 2.5 microns [3]. At the same time, while global cement production was 0.94 billion tons in 1970, this value increased to 4.1 billion tons in 2018 [4]. Moreover, it is thought that 45% more of the cement produced today would have been produced by 2050 if alternative binders are not provided [5]. On the other hand, natural resources including water, limestone, and clay are running out during the manufacturing of cement. Humanity must find alternative materials to eliminate the negative impacts of Portland cement and get better the world. Minimizing the use of cement and replacing it with different nature-friendly alternatives will both reduce CO_2 emissions and decrease natural resource consumption. Due to the many detrimental effects of cement, it is inevitable that alternative binders that are less aggressive to the environment should replace cement. However, for the design and production of alternative binding materials to cement, the reasons why cement has been the most widely used binding material for years should be considered.

One of the side effects of concrete manufacturing is the formation of large amounts of construction and demolition waste (CDW), which have an extreme influence on the environment due to improper final disposal [6]. CDW makes for over 35% of total waste output in the European Union, or over 700 million tons per year [7], with the United States producing roughly 143 million tons [8]. Although Germany, Denmark, and the Netherlands reutilize 80 percent of CDW material, the rates in the remaining countries average less than 30 percent [6, 9]. However, the majority of CDW materials reutilized in those countries are not used as value-added. These materials are reused in road

pavement or as footpaths. [10-12] By using CDW-based geopolymer, a product having market value can be produced in the construction industry. CDW-based geopolymers produced by three-dimensional additive manufacturing (3D-AM) can be shown as an alternative concrete type that can solve all these environmental problems by reducing the use of cement production and increasing the added value production of waste materials.

A geopolymer is an innovative concrete type that can alleviate all these environmental issues while also reducing cement production. Alkaline-activated or geopolymer binders are among the alternative binders that have gained attention in both research and practice, despite their lack of widespread commercialization. Several industrial by-products and wastes, as well as alumina-silicate raw materials, have been used to design and produce alkali activated materials or geopolymer binders. However, there have been few investigations on using CDW as an alternative ingredient for alkaline activation or geopolymer binders' development.

Recently, the geopolymerization technology used successfully with various industrial wastes, has motivated the search for other alternatives such as CDW in geopolymerization process. Based on this logic, performing geopolymerization by CDW, which will provide a great benefit in terms of nature protection and sustainability, has been one of the subjects studied comprehensively in late years. However, the geopolymerization of CDW is still a difficult mission.

Apart from the requirement of solutions to waste material problems, operation-based innovations are needed for the sustainability of the construction industry. Therefore, enabling CDWs to be used with autonomous systems in the construction sector is important to the sustainable construction industry. Automation in the construction sector has a number of benefits, including cost savings, increased efficiency, and improved quality [13]. In addition, robotization in the construction industry also reduces accidents and injuries considerably [14]. Although robotic systems have been applied in the building industry since 1960, it has not progressed as fast as in fields such as the automotive industry [15]. 3D applications could be given as an instance among the areas where robots are used in construction in the world. 3D-AM is one of these autonomous revolutions in the building industry. This revolution makes it inevitable to apply AM in other words 3D printing production technology in structuring. Construction companies

are seeking new ways to improve productivity and cut expenditures [16]. 3D printing can provide many economic and environmental benefits compared to traditional methods in the construction field. Furthermore, this method can reduce manufacturing errors, time, safety risk of labor, and cost [17]. Therefore, 3D-AM can play a significant role in construction in a changing world [18]. Compared to traditional methods, 3D-AM also provides significant advantages in terms of formwork costs. As known, the cost of formwork is a large part of the construction industry. By using this novel technology, which does not need formwork, savings between 35% and 60% can be achieved in total construction expenses [19, 20]. Additionally, reducing environmental impacts in the 3D-AM method will create a much more sustainable construction process. The amount of post-manufacturing waste is expected to decrease, thanks to a production process in which construction waste is managed correctly and optimized material consumption [21, 22].

1.2 Research Objectives and Scope

The major goal of this thesis is to reduce the negative influence of CDWs on the environment and to improve their use in autonomous construction applications. Thanks to the study, CDWs emerged due to ongoing structuring are utilized. Produced "green mortars" are combined with 3D-AM technology and provide cost-effective solutions that prevent work accidents by contributing to automation in the construction field. In this regard, extrudability and mechanical properties of CDW-based geopolymer mortar produced by 3D-AM technology were determined. Utilizing more concrete waste (CW) by producing geopolymer mortars from 100% recycled concrete aggregate (RCA) is another goal of the current study. On the other hand, by producing geopolymers from 100% CDW, the current study provides the reuse of materials including, roof tile (RT), hollow brick (HB), red clay brick (RCB), CW and glass waste (GW). Innovative, applicable, and measurable objectives designed to achieve the main objectives of the study are listed below.

- Developing an environmentally friendly alternative geopolymer binder to cement, which accounts for most of the world's CO_2 emissions.

- Producing viable, economical, and environmentally friendly building materials that minimize the damage of CDWs such as RT, RCB, HB, CW, GW to the environment by utilizing in the production of geopolymer.

- Using 3D-AM technology to develop novel and sustainable manufacturing methods using the geopolymer mortars produced with 3D-AM technology.

- Determining the anisotropic behavior of 3D printed specimens by performed various mechanical properties tests.

Within the scope of the thesis the fresh state properties of geopolymer mortars were investigated to determine the printability properties of 3D printable green products produced entirely from waste materials. Then, mixtures suitable for 3D printing were selected. Eventually, anisotropic and bond strength properties of 100% CDW-based mixtures were investigated. The methodology of all processes in the study is detailed below.

In the first stage of the study, alumina silicate source precursors (RCB, HB, RT, CW, GW) originated from CDW were obtained. These materials were grouped and reduced to the required dimensions for the geopolymerization process by crusher and ball mill. In addition, after the crushing process was applied to the CW, the material that was sieved from the 2mm sieve was used as RCA.

In the second step of the study, the quantities of the powder components, RCA, and alkaline activators were determined, and the fresh state characteristic of the mixtures were tested. The workability and 3D printability qualities of geopolymer mortars composed entirely of CDW were investigated using flow table and ram extruder tests performed in open-time on the mixtures.

In the final stage of the study, mold-casted and printed samples were produced by selecting mixtures suitable for 3D-AM. The anisotropic characteristic of the manufactured 3D-printed samples was evaluated using compressive strength tests in three different loading axes and three-point bending tests in two different loading directions. The influence of 3D-AM on mechanical properties was evaluated by comparing

compressive and bending performances of 3D printed samples to mold-casted samples. The interlayer bond strength of 3D printed samples was also determined using direct tensile and splitting tensile tests. Furthermore, at the end of the study, the effect of activators on mechanical properties was determined.

1.3 Thesis Outline

The details of this thesis consisting of 5 stages are mentioned below.

In the first part titled “Introduction”, general information, main problems and solutions are mentioned within the scope of the study. The study’s goal is specified in detail.

In the second part titled “Literature Review”, the studies conducted in the past years on the development of geopolymer binders are detailed. In addition, automation in the construction industry, 3D technologies and studies on geopolymer in 3D-AM technology are mentioned.

In the third part titled “Materials and Methodology”, detailed information is given about precursor materials, alkaline activators and RCA. Besides, detailed information about mixing ratios, preparation of the mixture and test samples, curing conditions and applied tests are presented.

The fourth stage, “Results and Discussion,” included extensive information on the rheological characteristics, compressive, flexural, and interlayer bond strength test results of mixtures manufactured solely of CDW materials. The impact of activators on the workability and extrudability properties of open-time flow table and ram extruder tests are discussed, as well as potential reasons. In addition, open-time rheological performances of the mixtures were evaluated. The results of mechanical characteristics testing on 3D printed samples were compared to samples produced with standard manufacturing methods. The anisotropic behavior of 3D-printed samples was investigated, as well as the potential causes of these results. Mechanical parameters (compressive, flexural, and interlayer bond strength) were investigated to alkaline activator proportions.

In the last stage, titled “Conclusions”, the tests performed within the study, the results and possible causes are summarized.

2. LITERATURE RESEARCH

PC is one of the most often utilized building materials, and it is the primary source of greenhouse gas emissions and unmanageable CDW issues. According to reports, cement, the second most commonly used material by humankind after water, is responsible for 8-9 percent of worldwide CO2 emissions [23]. In addition, the effect of PC on CO_2 emission is related not only to the CO_2 released by the produced concrete, but also the CO_2 released in the production process. The greenhouse gas formed as a result of PC production, prevents the reflection of the sun rays coming into the world and returning to space, causing the air temperature to be 15-18 degrees on average every season [24]. Along with the CO_2 emission, natural resources required in the manufacturing of cement-based concrete, which includes limestone, sand, and gravel are also at risk. The continuous use of these materials makes it impossible to create a sustainable future for the environment. Therefore, it has become inevitable to develop alternative materials to the PC. Researchers have conducted many scientific studies to enhance environmentally friendly and sustainable alternative materials. The development of a material called alkali-activated geopolymer has also been one of the focal points in the literature to develop alternative binder materials.

The aim of the development of innovative and sustainable geopolymer binders is to reduce the emission of CO_2 as an alternative candidate to PC. In this study, geopolymer binder material was used as an alternative to PC. Joseph Davidovits was the first to use the term geopolymer in the literature. [25]. Author defined geopolymer as an alkali alumina silicate material obtained whereby combining alumina silicates with alkali activators. Depending on the type of material to be selected in production, geopolymers can have low thermal conductivity, high strength, fire resistance, long or short setting time, acid resistant building material properties. The fact that geopolymers can be produced with different types of industrial and construction wastes also provides cost-effective binder material production.

The alkali activation of alumina-silicates is the geopolymerization process. The process of amorphous precursor materials converting to a compact structure in a highly alkaline medium is known as alkali activation. The resulting compact structure is an amorphous

gel that gains binding property. At the end of the geopolymerization process, amorphous alumina silicate gel is formed [26].

The geopolymerization mechanism is described in three steps by Glukhovsky [27], (i) dissolution of in an alkaline precursors such as silicon and aluminum (ii) agglomeration of dissolved components (iii) polycondensation of the dissolved components. On the other hand, Davidovits [28] described geopolymerization as the result of a polycondensation reaction and reported that such reactions form three-dimensional tecto-alumina silicates. The following formula represents these reaction products:

$$M_n[-(SiO_2)_z - AlO_2]_n . wH_2O$$

Where M stands for alkalis such as sodium, potassium, and calcium, while n stands for the degree of polycondensation. All oxygen atoms are shared in the formation of SiO4 and AlO4. Si-O-Al bridges are made up of chains and rings.

When the alkali activator solution and the precursor materials combine, in the first step of the reaction, the Si-O-Si bonds in the precursor material are broken by the OH- ions in the alkali activator solution. Broken Si elements form silanol (Si-OH) and sialate (Si-O) bonds. Poly silicon-oxo-aluminate (polysialate) is defined by Davidovits [28] as semi-crystalline and amorphous polymers in which silicon and aluminum are bonded by oxygen bonds. This structure can be seen in Figure 2.1.

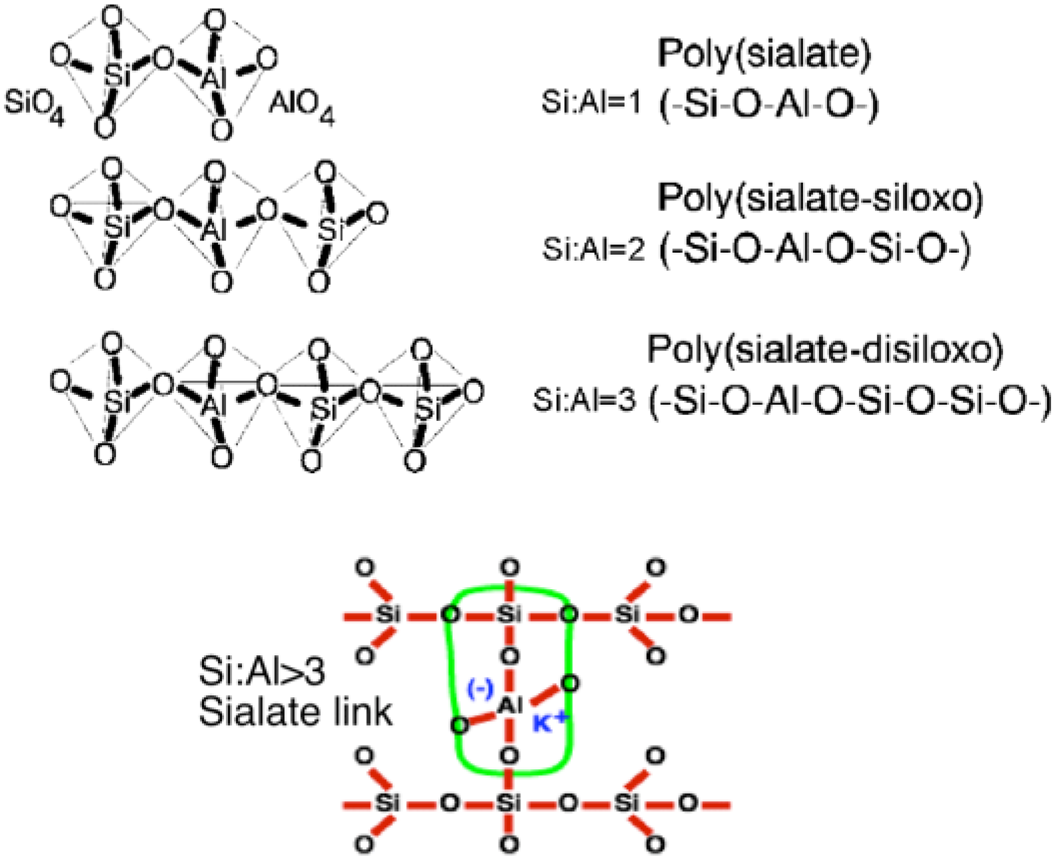

Figure 2.1 Structure of geopolymer [28]

At the end of the chemical process of geopolymerization, these 3D sialate chains are formed. In another study Chanh et al. [29] the geopolymerization reaction stages were schematized in two steps. The chemical reaction steps and the geopolymer formation mechanism shown in Figure 2.2 and Figure 2.3.

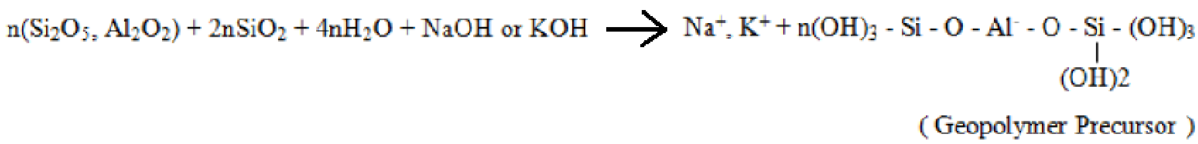

Figure 2.2 Schematic of geopolymer monomers formation [29]

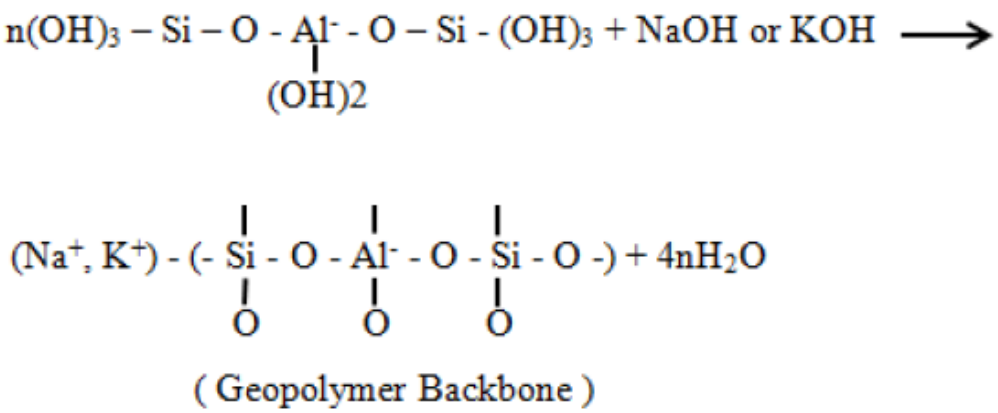

Figure 2.3 Schematic of polymerization of geopolymer monomers into polymeric structure [29]

According to Duxson et al. [30], the geopolymer mechanism takes place in 5 steps, as seen in Figure 2.4. The five reaction steps identified in the study are described below:

- In the first stage of the reaction, alumina-silicates dissolve in a highly alkaline medium to form aluminates and silicates. Aluminate and silicates, which dissolve rapidly in a high pH environment, provide the formation of a highly saturated alumina silicate solution.

- Second, the dissolved aluminates and silicates speciate and maintain ion balance. This process is called speciation equilibria [31].

- Third, an infinite number of monomers formed in the medium form a connection by condensation and the solution takes the gel structure. This gelation process release water consumed at formation of aluminates and silicates. The water that provides the dissolution during the reaction then exist in the gel structure. Duxson said that such gel structures are often called biphasic. The structure is made up of two phases: alumina silicate binder and water.

- In the fourth step of the reaction, the gels continue to link and result in three-dimensional alumina silicate gels. These gels are called geopolymers.

- Finally, the gels formed and reorganized during the reaction, harden and form the geopolymer structure.

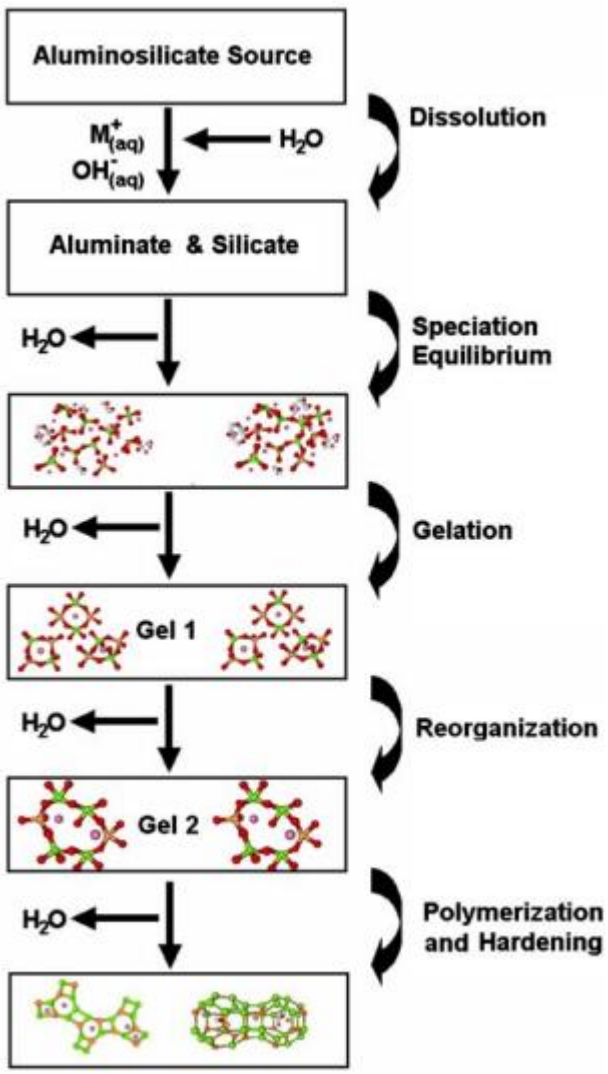

Figure 2.4 Geopolymerization process model [30]

In a recent study of Provis and Bernal [32], a new model was designed for the geopolymerization process of precursors with high calcium content. The diagram schematizing the geopolymerization steps reported in the study Is shown in Figure 2.5.

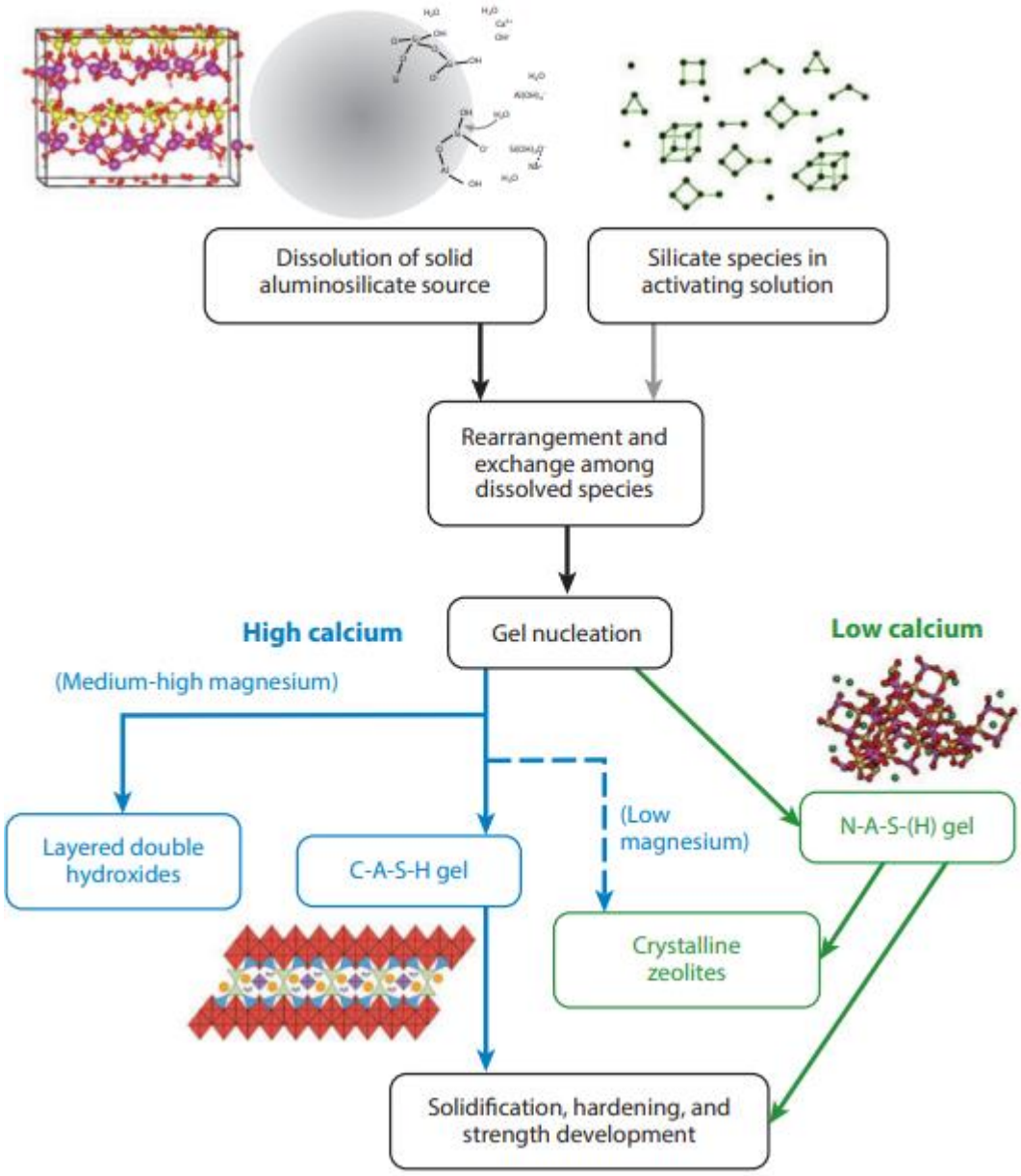

Figure 2.5 Geopolymerization process model of precursors with high calcium content

2.1 Utilization of CDW in Production of Geopolymer

Among the alumina-silicates required for geopolymerization, the most widely used ones are metakaolin (MK), granulated blast furnace slag (GBFS) and fly ash (FA) [33-35]. Nevertheless, FA is not sustainable due to the harmful effects of thermal power plants on the environment. Likewise, GBFS will lose its usability in the coming years. In addition, the precursors are mineral admixtures very suitable to produce conventional PC-based concrete. These materials, which will be less accessible today and soon, have reached higher costs than PC due to high demand. The transportation of these precursor materials

is also one of the factors that increase the cost. It is critical to find alternative precursor materials in the production area to minimize transportation costs.

CDWs are becoming an increasing problem in the world due to the constant increase of materials, limited storage area and reutilization. In addition, with the growth of cities, the completion of the life of the buildings and urban transformation the waste rate increases. Natural disasters can also be considered as another factor that causes CDW generation. Many of the existing structures in the world, which are located in the earthquake zone, are not resistant to earthquakes. Considering the damage caused by earthquakes to structures, it has become obligatory to demolish the structures that do not meet the minimum criteria against earthquakes in developing countries and to construct new, safe structures that meet the requirements of the day, and the governments to take regulatory measures. It is stated in the constant statements of the public authority on this subject that over 6.5 million buildings will be affected by urban transformation [36]. Considering that Turkey's total building stock is around 19-20 million, the demolition wastes that will emerge even with a simple proportional calculation have reached quite high amounts even in the current situation, and this has become a very serious problem. In recent years, in terms of both economic sustainability and efficient use of natural resources, CDW has become increasingly popular in building construction, particularly in industrialized countries. Today, the recycling issue has become very common, with demolition companies realizing that metal waste has a material value. However, apart from metal wastes, the CDWs that have emerged so far are mostly stored in landfills without recycling. The main reason for this situation is that it is a simple, easy, and economical method. Undoubtedly, the fact that there is a limited advanced attempt in the evaluation of waste, especially in developing and economically struggling countries is also effective in threatening our world by CDW. Therefore, the rapid consumption of available resources in the world, the decrease in waste disposal areas and the emergence of increasingly larger problems for local governments make recycling these wastes mandatory. All these reasons show the fact that the demolition activities encountered today and the storage of demolition wastes in landfills cannot always be done with traditional methods. Considering the current developments in demolition wastes in the world, the studies carried out under the name of selective demolition ensure that the wastes have high economic value. In the context of all these handicaps, more effective waste management and reuse can be achieved by using CDW materials (e.g., concrete,

tiles, ceramics, bricks, glass) as an alumina-silicate source in geopolymer production. Studies of CDW-based geopolymers, which are less than mainstream alumina silicates (e.g., FA, GBFS, MK), are available in the literature.

The following is a comprehensive review of the literature on CDW-based geopolymer development:

In a study by Allahverdi and Najafi [37], setting time, compressive strength tests and Fourier transform infrared spectroscopy (FTIR), scanning electron microscopy (SEM) analyzes geopolymer concrete produced with CW, brick waste (BW) and different combination of sodium hydroxide (NaOH), sodium silicate (Na_2SiO_3) were investigated. In the study, 100% brick waste samples with 8% Na_2O obtained 40 MPa strength at the end of 28 days.

Sun et al. [38] studied the high-temperature behavior of waste ceramic-based geopolymers. The samples produced by combining NaOH, Na_2SiO_3 and potassium hydroxide (KOH) in different combinations were cured at 100% relative humidity and 60 °C temperature. X-ray diffraction (XRD), TGA, FTIR and SEM/EDX analyzes were performed for mechanical and microstructural analysis. In addition, to determine the high-temperature behavior, the samples were exposed to a temperature of 100, 200, 400, 600, 800 and 1000 °C for 2 hours and compressive strength tests were performed. The compressive strengths of the samples were ranging from 26 to 71 MPa, in accordance with the research. The compressive strength of the mixtures is increased as the temperature is raised to 1000 °C.

Sata et al. [39] analyzed the properties of permeable concretes obtained with a high calcium FA-based geopolymer and two types of recycled aggregates (crushed structural concrete element and crushed clay brick). The results of splitting tensile strength, compressive strength, total void ratio and water permeability coefficient of permeable geopolymer concrete showed that both types of recycled aggregates could be utilized in permeable concrete.

Pathak et al. [40] worked on the geopolymer produced by using two precursor materials such as CW and BW, which are CDW-based materials activated with NaOH and Na_2SiO_3, at different usage rates. After the samples were kept at 60 °C for 24 hours, they were

stored at 30-35 ℃ temperature until the end of curing. The samples were tested for compressive strength and XRD, FTIR and SEM-EDX analyzes were performed to determine the structural differences between the mixtures. The maximum compressive strength of the mixture produced from BW at the end of the 28-day was reported as 11.43 MPa.

Komnitsas et al. [41] examined manufacturing geopolymers manufacturing with concrete, brick, and tile waste materials as raw materials. Researchers used Na_2SiO_3 and NaOH as alkali activators. They conducted research by changing the molarity of Na_2SiO_3, curing at 60°C and 90°C for 7 days, and performing tests at different high temperatures for one hour. As a result, they reported that the geopolymer reached a compressive strength of 49.5 MPa produced with brick and 57.8 MPa produced with tile. The researcher also stated that brick-based geopolymers can be used as insulation and coating materials with their behavior in their resistance to heat.

Torres-Carrasco & Puertas [42] investigated the use of GW in an alkali activator solution to activate FA-based geopolymer. They prepared a variety of alkali activators by dissolving various quantities of GW in various molarities of NaOH+Na_2SiO_3 solution. The geopolymer samples prepared with the addition of glass powder waste were cured at 20 ± 2 ℃ for 1, 2, 7 and 28 days. Sample behaviors were compared with geopolymers prepared with NaOH alkaline activators. Based on the mechanical, mineralogical (XRD, FTIR) and microstructure (porosimeter, Nuclear magnetic resonance spectroscopy and SEM/EDX) analysis of the samples, researchers have confirmed that the GW is dissolved in pH = 13.6 in the NaOH solution. In the study, it was reported that 10M+15% Na_2SiO_3 and 10M+15 grams GW alkaline activators had a significant effect on geopolymerization.

Robayo-Salazar et al. [43] produced geopolymer by substituting ordinary Portland cement (OPC) up to 30% for RCB, CW and GW-based mixtures. The mixtures were activated with NaOH and Na_2SiO_3 and heat cured at 25 and 70 ℃ for 24 hours. The study reported that the geopolymers produced without using OPC reached adequate strength. The maximum compressive strength of the samples produced at different Na_2O ratios and cured at 25 °C for 28 days was reported as 102, 33 and 57 MPa for RCBW, CW- and GW-based geopolymers, respectively.

Vafaei and Allahverdi [44] conducted a study on GW-based geopolymer mortar with different Na_2O content, activated with NaOH and Na_2SiO_3. In the manufacturing of geopolymer mortar, up to 24 percent by weight of calcium aluminate cement was added to the mixtures. The free alkaline ratio, efflorescence tendency, setting time, workability and compressive strength of the mortar samples were all tested. The morphology and microstructure analyses of the mortars were also determined using FTIR and SEM analyses. The best mixture was found to have a maximum compressive strength of 87 MPa as a result of the research. According to the findings, the calcium alumina cement led to the production of an alumina silicate gel in the matrix, increasing strength.

Shoaei et al. [45] conducted a study focusing the influence of alkali solution to binder (S/B) ratio and curing temperature on waste ceramic powder-based geopolymer mortar. In this context, the geopolymers were exposed to 60, 75, 90 and 105 ℃ temperatures for 24 hours at an S/B ratio between 0.4 and 0.7 with an increase of 0.1 and cured in ambient conditions after 24 hours of heat curing period. Flow table test was performed to fresh specimens, compressive strength and flexural strength tests were performed on the specimens, and cured during 3, 7, 14 and 28 days. In addition, the densities of the samples were also determined. As a result of the study, optimum curing temperature and S/B ratio were reported as 90 ℃ and 0.6, respectively. At the reported optimum conditions, 23.7, 24.3, 24.9, and 27.9 MPa strengths were reached at the end of the 3, 7, 14, and 28 days, respectively.

De Rossi et al. [46] studied the effect of sand substitution by CDW with different particle sizes on fresh and hardened state characteristics of FA and MK-based geopolymer mortars activated with NaOH and Na_2SiO_3. Mixtures using CDW as fine aggregate showed lower flowability than mixtures using standard sand. It has been reported that the mixtures in which CDW is used as aggregate show higher compressive and flexural strength than the standard sandy mixtures. As a result of the study, 8.5 MPa flexural strength and 40.5 MPa compressive strength were reached in mixtures with CDW aggregates.

In a study by Hwang et al. [47], the influence of GBFS addition on mechanical characteristics of waste brick powder-based geopolymers activated by NaOH and Na_2SiO_3 was determined. Mixtures using GBFS in substitutions with 10% increase

between 10% and 50% were cured in ambient conditions. Water absorption, ultrasonic pulse velocity (UPV) tests, porosity, compressive strength were performed to the samples cured for 3,7,28 and 56 days. At the end of the experimental research, it has been reported that the compressive strength of the samples was between 24-93 MPa, and the UPV values were between 2112-4086 m/s.

Mahmoodi et al. [48], produced a RCB-based geopolymer binder activated with alkali activators NaOH and Na_2SiO_3. The mixtures were stored at ambient, 50 °C, 75 °C, and 100 °C temperatures. In the study, the influence of incorporating MK, C and F class FA and GBFS precursors was investigated. At 50 °C, 75 °C and 100 °C temperatures for 24 hours, 15%, 30%, 45% MK, FA and GBFS were incorporated to the mixtures and their influence on mechanical characteristics were investigated. In addition, microstructure analyzes (SEM, FTIR, XRD and energy dispersive X-ray analysis) were performed. In the study conducted with different Na_2O/SiO and SiO_2/Al_2O_3 and ratios, the optimum ratios in terms of geopolymerization degree, density and compaction were determined as 7.1 and 0.24, respectively. More C-A-S-H and N-A-S-H formation were observed at 75 °C. 100 °C temperature caused a decrement in compressive strength. The RCB-based geopolymer cured at 75 °C reached a compressive strength of 53.4 MPa in 7 days and 58.1 MPa in 28 days.

Mahmoodi et al. [49] investigated the utilization of CW in geopolymer. In the study, NaOH and Na_2SiO_3 alkali activators were used to activate the precursors. Different molarity of alkali activators was used to obtain mixtures with different SiO_2/Al_2O_3, Na_2O/SiO_2 ratios. In the study, materials such as FA, GBFS, MK were substituted by 15%, 30%, and 45% instead of CW, and the samples were cured at 50, 75, and 100 °C for 24 hours. In the study, flowability, mechanical properties and setting time tests were carried out. Moreover, FTIR, SEM and XRD and analyzes were performed on samples with different cure and mixing ratios. Authors reported that the increment of Na_2O/SiO_2 and SiO_2/Al_2O_3 ratios increased the flowability. The compressive strength of the mixtures showed optimum behavior determined under ambient conditions increa7sed up to 100 °C temperature cure. In addition, it was determined that GBFS substituted CW-based geopolymers increased their strength. At the end of 7 and 28 days, the maximum compressive strength was reached at 31.9 and 37.1 MPa, respectively, under 100 °C curing.

Ulugöl et al. [50], manufactured a CDW-based (RCB, RT, HB, GW) geopolymer paste. The mechanical properties of pastes with 10%, 12.5% and 15% NaOH concentrations exposed to different temperatures (0, 65, 75, 85, 95, 105, 115, 125 ℃) for different curing times (24, 48, 72 hours) were tested. In addition, XRD, SEM, TG/DTG analyzes were performed for microstructure analysis. According to the results, HB-based mixtures cured at 115 ℃ for 24 hours have a strength of 45 MPa. Among the precursors, HB was reported to be the most effective precursor due to its more compact microstructure. The investigation found that GW had the lowest compressive strength among the precursors, owing to its coarser particle size.

Ilcan et al. [51] investigated the rheological properties of geopolymers for 3D-AM composed entirely of CDW materials. In the study, RCB, HW, RT, CW and GW were used as precursors, and the mixtures were activated by Na_2SiO_3, calcium hydroxide ($Ca(OH)_2$) and NaOH. The rheological characteristics of geopolymer mortars were determined using modified mini slump, vane shear and flow table tests. Furthermore, to evaluate mechanical characteristics of the samples compressive strength tests were performed on 7- and 28-day cured samples. As a result of the research, it was revealed that completely CDW-based geopolymers showed rheological properties suitable for production with 3D-AM without the need for chemical additives. In the study, it was reported that at the end of 28 days, samples produced with a single use of NaOH reached a strength of 11 MPa, samples produced with $Ca(OH)_2$ reached a strength of 17.9 MPa, and samples produced with the addition of Na_2SiO_3 reached a strength of 36 MPa.

Akduman bet al. [52], produced reinforced geopolymer concrete using waste masonry materials (RCB, RT, HB) and glass precursors and RCA (D_{max}=16mm). As a result of the preliminary tests to determine the optimum alkali activator content, 10M NaOH solution and two times NaOH by weight Na_2SiO_3 was the most convenient alkali activator content. A total of 4 different mixtures were prepared as geopolymer and conventional concrete using normal aggregate (NA) and RCA. The samples were cured under ambient conditions. The compressive strengths of cylindrical geopolymer and conventional concrete manufactured with RCA reached 36.6 MPa and 35.2 MPa, respectively, according to the research. In addition, the fracture pattern of the samples produced with NA and RCA during the bending test was examined. At the conclusion of this research,

it was revealed that RCA drastically reduced the capacity of geopolymer samples to disperse energy.

Yıldırım et al. [53], produced geopolymer mortar using CDW-based masonry materials such as RCB, RT, HB. Within the scope of the study, the effect of the NaOH concentration (10,15, 19 M), the curing temperature (95, 105, 115, 125 ℃) and period (1, 2 and 3 days) of the samples were investigated. Microstructure analyzes such as XRD, SEM / EDX were also performed along with compressive strength tests. According to the results of compressive strength tests, HB is the most efficient precursor to compressive strength. The sample cured for 48 hours at 115 °C with 25% RCB activated with 15M NaOH and 75% HB content reaching a maximum compressive strength of 80 MP, according to the researchers. The study found that high-strength building members can be manufactured with CDW-based masonry precursors.

2.2 Automation in Construction Industry/3D-AM

2.2.1 History of AM Technology

Although the idea of AM dates back to past history, it is known that the first emerging system started in 1987 with the commercialization of the plastic processing technique known as Stereolithography. The process is the first commercially produced AM system in the world. The 1990s were a turning point for AM technologies. In the same year, commercialization of Laminated Object Manufacturing (LOM), Solid Ground Curing (SGC) and Fused Deposition Modeling (FDM) occurred [54]. Shortly after these methods, the Selective Laser Sintering (SLS) method was developed. In 1994, the German company EOS introduced the M160 machine based on Direct Metal Laser Sintering (DMLS) technology and produced the M250 machine in 1995 [54, 55]. In the past 20 years, developments in AM technologies have accelerated considerably. As existing technologies continue to evolve, important new technologies such as Direct Metal Laser Melting (DMLM) have been developed and commercialized. In 2002, it started to sell Direct Metal Deposition (DMD) systems. In early 2016, a new technology, a new product, a new material or a new application appeared almost every week. Over time, these systems have become more reliable and more efficient, and the variety of suitable materials has increased significantly [56-58].

The advantages of AM technology are listed below.

- Reduces production processes and costs,
- Accelerates product improvement,
- Special products can be produced,
- Provides fast modeling,
- Very difficult shaped parts can be produced,
- Reduces design times,
- Provides harmony between design and production,
- Allows the product to be functionally optimized,
- Reduces the number of production machines,
- Shorter delivery times allow lower stock requirements,
- Provides freedom of design,
- It does not need any mold,
- Consumes less material, reduces the amount of waste,
- Facilitates logistics

2.2.2 Additive Manufacturing in Construction Technology

According to ASTM F2792-10 [59], AM is defined as the layer adding on the layer. In recent years, AM is widely used in commercial aviation, medical applications, and other technological areas. In recent years, the fabrication of concrete structures AM technology has been one of the ways that may be solutions to the issues of the existing concrete industry. The use of AM technology in concrete production reduces the material's environmental effect, improves product quality, and allows for the rapid building of the completed project [60, 61]. In the construction industry, when the production methods developed in recent years have been considered, it is proved that the use of AM as a large-scale production method could be available [62, 63]. 3D-AM is also defined as a layer-based manufacturing method without the use of the formwork [62, 64]. In comparison to traditional methods, 3D-AM also provides significant advantages on formwork costs. As is known, the formwork cost has a large share in the construction industry. Using 3D-AM technology without formwork, total construction expenditures can be saved from 35% to 60% [19, 20]. In addition, compared to formwork workmanship, using the 3D-AM

method with the support of technological equipment will significantly reduce the need for labor apart from the formwork cost. In this way, significantly reductions will be observed in both accidents and labor costs [21]. In traditional concrete production, designer is designed in certain limits, and in production with 3D-AM this obstacle in the production of the designer is eliminated and designer could design in line with their thoughts free. Today, aesthetic, functional, and optimized designs come to the fore. In addition, the reduction of environmental impacts in the 3D-AM method will result in a much more sustainable construction process. Thanks to a production process and optimized material consumption of construction waste correctly, it is expected to decrease the amount of waste after manufacturing [21, 65]. Furthermore, because the 3D-AM technology is widely used in the buildings, significant reductions in post-production CO_2 emissions are expected due to reasons such as low waste material (around 30%), lower energy use, on-site manufacturing, less resource requirement, and wide design freedom [17, 66, 67]. As summarized above; in comparison to traditional concrete manufacturing processes, 3D-AM building of structures is a cheaper, faster, more affordable, and more sustainable method that allows for far more design freedom.

One of the benefits of using 3D-AM technology in the construction business is to ensure that production is completed at a stable speed and shorter time. Buswell et al. [62] has compared completion time of wall produced with 3D-AM and traditional methods (Figure 2.6). The 3D printed wall is seen to be manufactured at constant speed and in a shorter time, it is observed that the wall of the wall produced by traditional methods should be expected without production for curing.

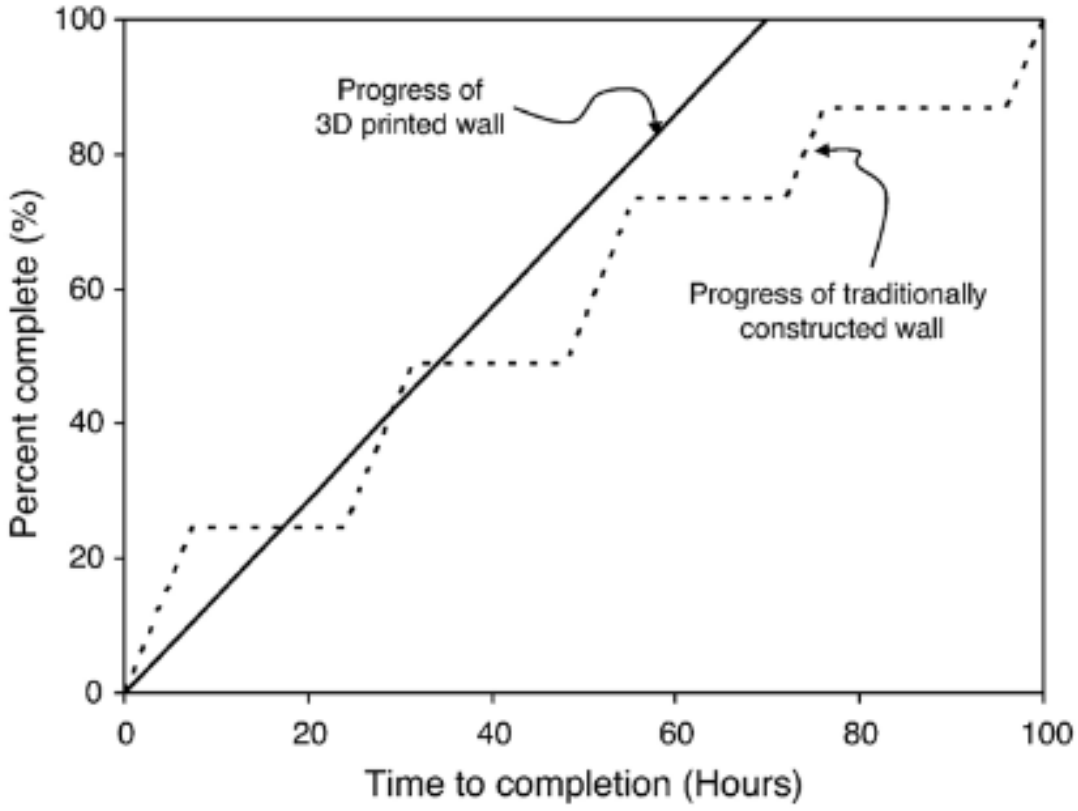

Figure 2.6 Time comparison between production of wall produced with 3D-AM and traditional method [62]

Developments in technology have brought new expectations regarding the potentials of design tools and possibilities. The problems in today's mobile lifestyles with their rapid changes require specific solutions which follow digital technologies. 3D printing, with its digital fabrication, raises as a methodology for addressing these challenges. 3D printing provides the manufacturing of complex shapes and structures due to integrating digital models through 3D modeling. It has usually been achieved by converting a digital model into an assembly of parallel horizontal slices. There are many advantages of 3D printing, such as faster construction, low cost, safe working conditions [63, 68]. Although there are some challenges of 3D printing, it provides customizable, flexible, and modular housing possibilities [69]. Furthermore, employing traditional manual construction methods, this technology allows architects to produce structures with useful and uncommon and difficult-to-achieve geometry, giving for increased design flexibility (Figure 2.7). Laboratory-scale preliminary studies are needed to design these viable, sustainable building materials and elements. Therefore, experimental studies are carried

out with laboratory-scale 3D printer systems. Laboratory scale 3D printer systems consist of many elements. In a study by Hojati et al. [70], the schematic of the system was presented.

Figure 2.7 Bloom; an experimental pavilion that produced with 3D printed Portland cement [71]

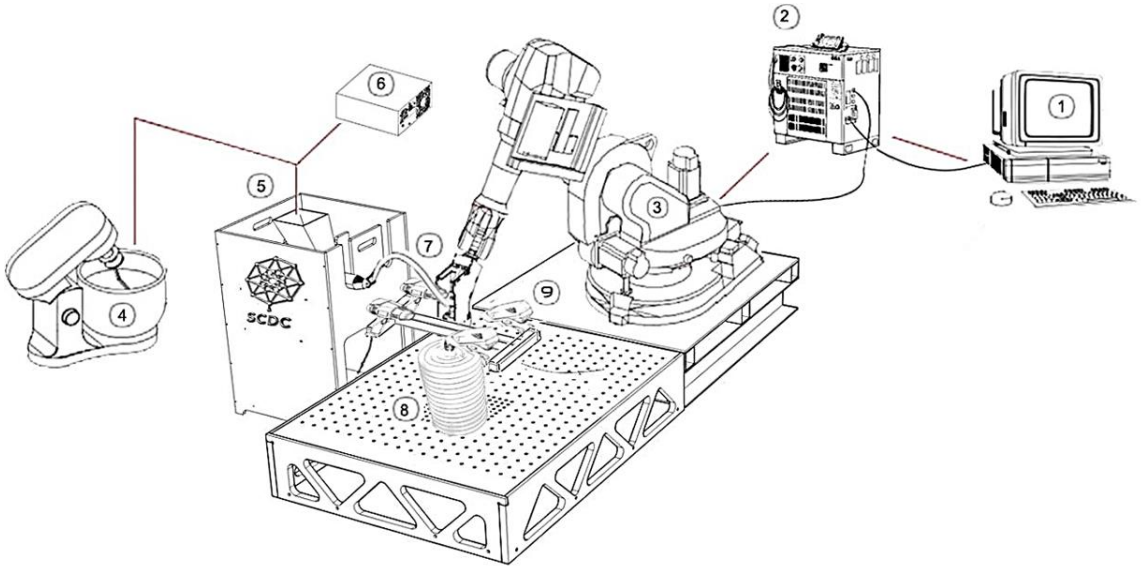

Figure 2.8 Diagram of the 3D-printing concrete system: (1) Computer for designing the toolpath and generating the G-code; (2) Robot controller for reading the generated code and controlling the robot, (3) Robot for moving the extruder

nozzle along the generated toolpath; (4) Mixer for material preparation; (5) Developed pump; (6) Pump controller for running the code and controlling the pump speed; (7) Extruder; (8) Printed specimen; (9) Heat guns for heating the material during printing [70]

2.3 Utilization of Geopolymer in 3D-AM Technology

Only a few research have been conducted in recent years to adapt geopolymer, an ecologically friendly construction material, to 3D-AM technology in order to turn the material and production technique into a more environmentally friendly structure. Studies on geopolymers produced with 3D-AM technology are detailed below.

Panda et. Al. [72] were emphasized that FA-based geopolymers produced with 3D-AM technology showed different mechanical performance depending on different loading direction. Researcher carried out a study focusing the effect of employing different diameters of glass fibers (3-6-8 mm) and different substitutes (0.25-1%) on mechanical properties was investigated. GBFS, SF, sand, potassium silicate (K_2O_3Si), hydroxypropyl methylcellulose and tap water were used in the manufacturing of FA-based geopolymer mortar. In study, geopolymer mortar samples were stored at ambient condition for 28 days and flexural and compression tests were performed. It has been reported that geopolymer mortars increased mechanical properties up to 1% fiber addition. As a result of the 3 different loading compression tests, the maximum difference between the parallel to the printing direction and lateral loading was reported as 23%.

Panda et al. [73] conducted a study focusing the mechanical properties and anisotropic behavior of FA-based 3D printed geopolymers. KOH and K_2O_3Si solution was used as alkali activators in the mixture prepared by adding FA-based geopolymer GBFS, SF, and river sand. Rheology tests were carried out to determine the fresh properties. XRD and SEM analyzes were performed on the waste materials. The mechanical properties were also determined using compressive, flexural, and bond strength tests. In the study, compressive strength tests in 3 different axes and flexural strength tests in 2 different axes were performed to the 3D-printed samples, and the results were compared with the mold-casted samples. Compared to mold-casted samples, printed samples showed 5% less compressive strength under perpendicular and parallel loading and 2% higher under

lateral loading. The findings demonstrated that depending on the loading directions, the 3D printed geopolymer showed anisotropic behavior. Furthermore, the maximum bond strength was stated to be 1.4 MPa.

Quatifi et al. [74], synthesized a study investigating the printability and hardened properties of FA-based, 3D-printed geopolymers. The geopolymer was produced with 0-3 mm sand that activated with NaOH and Na_2SiO_3. The ratio of NaOH/Na_2SiO_3 by weight was chosen as 1. To evaluate the effect of PP fibers and steel on geopolymer mixes, three mixtures were prepared: without fiber, with 1% steel fiber by weight, and with 0.5% PP fiber. The samples were printed in three layers of geopolymer mortars and stored at room temperature for 48 hours. After that, it was exposed to a 2-hour heat cure at 70°C, then held at ambient temperature for 10 days while mechanical properties testing was performed. Moreover, the effect of time intervals (5-10-15 minutes) between the printing of the layers on the mechanical characteristics of the mixtures were also investigated. The flexural strength dropped as the time interval between the layers increased, according to the research. The buildability performance improved when the time interval was increased, as the layers' capacity to bear their own weight increased. The use of steel fibers in AM technology is not suggested, according to the study's conclusion, due to the possibility of developing a roughness between the two layers.

Panda et al. [75] studied the fresh and hardened characteristics of geopolymer synthesized from FA, GBFS, and SF in a study. They produced FA-based geopolymer substituting different combination of GBFS and SF up to %10 by weight. Precursors were activated by NaOH and Na_2SiO_3 solutions with $SiO_2/N_{a2}O$ ratio of 1.8. To determine rheological behavior of geopolymer mortars, yield stress and thixotropy value of mixtures evaluated. The mechanical characteristics of the mortars were determined by the compressive strength test performed on the 3D printed and casted samples. In accordance with the compressive strength tests performed only in the perpendicular direction to examine the compressive strengths of 3D printed and mold-casted geopolymers, the influence of the production technique on the compressive strength is negligible. The printed sample and mold-casted specimens cured at ambient temperature for 7 days had compressive strengths of 18.4 MPa and 16.2 MPa, respectively, according to the study.

Panda and Tan [76], carried on a study examining the printability properties such as extrudability, shape retention, buildability, and thixotropic open-time of geopolymer mortars suitable for 3D printing produced by activating silica fume (SF), GBFS and FA precursors with K_2O_3Si solution. In order to determine the most printable mixture, tests were carried out on 5 different mixture designs within the scope of the study. All mixtures were designed to reach a compressive strength of 25 MPa at the end of 28 days. According to the research, increasing the sand proportion in the mixture decreased extrudability via increasing particle friction. According to the study, increasing yield stress increases the ability of the 3D printed multilayer sample to carry its own weight, which improves shape retention qualities. According to the thixotropic open-time test results, the increase in GBFS content caused a decrease in the setting time. In the study, it was reported that the clay added to a mixture did not cause any discontinuity in the sample, although it exceeded the maximum limit of 1.0 KPa for extrusion.

The influence of polypropylene (PP) fibers on the fresh and hardened characteristics of 3D printed FA-based geopolymer mortars was examined by Nematollahi et al. [77]. Compressive strengths in three loading directions and flexural strengths in two loading directions were studied in addition to the workability and extrudability of the mortars. Only samples tested under perpendicular (perpendicular to the printing path) loading directions revealed that fiber reinforcing had a beneficial influence on compressive strength. According to the compressive strength test results depending on the loading directions, the maximum difference between perpendicular loading and lateral loading was reported as 20.8 MPa (154% of the result in the lateral loading direction).

Nematollahi et al. [78] performed compressive strength test in 3 different axes, flexural test in 2 different axes and time-dependent (2 and 15 minutes delay after the first layer when printing two layers) interlayer bond strength test to the 3D printed geopolymers produced by using FA and GBFS. As a result of the compression tests, the specimens under loading parallel to the printing direction were 72% higher than the samples under lateral loading. On the other hand, in flexural strength, 65% of the lateral loading was obtained in perpendicular loading. Maximum 1.3 MPa strength result has been reported in time-dependent interlayer bond strength.

Nametollahi et al. [79] examined the influence of fiber types on the bond and flexural strengths of 3D printed geopolymers. In this study, the effect of three different fibers called polyphenylene benzobisoxazole (PBO), PP and polyvinyl alcohol (PVA) in FA-based geopolymer mixtures was investigated. The mixtures activated by Na_2SiO_3 and NaOH. The Na_2SiO_3/NaOH ratio of the mixtures was chosen as 2.5. Flexural strength and interlayer bond strength tests were performed on the samples. The test results revealed that the samples with PBO, PVA and PP added showed 34%, 23% and 17% more flexural strength than the samples without fiber addition, respectively. This was attributed to the increase in flexural strength through the bridging of cracks by randomly dispersed short fibers. The PBO added samples reached the maximum flexural strength of 10.3 MPa between samples. According to the interlayer bond strength test results, in contrast to the flexural strength, the interlayer bond strength results were lower in fiber added samples. It has been reported that the samples produced with PBO, PVA and PP fibers show 23%, 15% and 20% less interlayer bond strength, respectively, than the samples without fiber. This is explained by the fact that the mixture using fiber are stiffer than the no fiber added mixture, and the bond area prevents the formation of a sufficiently continuous bond during printing.

Kashani and Ngo [80] produced 3D printed geopolymer mortar using SF, FA and GBFS as precursor. Geopolymer mortar activated by sodium meta-silicate powder. Within the scope of the study, a total of 6 mixtures with 0.31, 0.33 and 0.35 ratios and 8% and 10% alkali activator contents were prepared. In the study, the open-time rheology, and compressive strength properties of the geopolymer were investigated. In addition, 3D printing parameters, extrusion pressure and printhead speed, were also investigated. To determine the rheological properties, yield stress was measured with a rheometer. To determine the time-dependent variation of the yield stress, measurements were made with 15-minute intervals until the 45^{th} minute. In the study, it has been reported that the rise of water/binder ratio reduces the yield strength due to the fact that excess water in the environment covers the particles and facilitates the separation of the particles from each other. In addition, it was determined that increasing the water/binder ratio prolongs the setting time. The maximum compressive strength was reported to be at 50 MPa after 21-day compressive strength tests. A mixture with alkali activator content of 8% and water/binder ratio of 0.33 and was identified as the showed the best rheological and mechanical characteristics.

Chougan et al. [81] conducted a study focusing the 3D printability properties of geopolymer binders produced by FA, GBFS, SF and activating NaOH and sodium silicate (Na_2SiO_3). The 3D printed mixtures' rheology, buildability, and mechanical properties were examined. The effects of nano-graphite platelets were also studied in the research. The results showed that 3D printed mixtures with 1% nano graphite platelet had 90 percent better flexural and 30% better compressive strengths than 3D printed samples without any nano graphite platelet. In addition, the highest compressive and flexural strengths obtained were 50.9 MPa and 15.3 MPa, respectively.

Li et al. [82] conducted a study on improving the mechanical characteristic of geopolymer mortars manufactured with FA and GBFS by adding continuous micro cable steel. To make the thixotropic and microstructural features of the mixtures suitable for 3D printing, silica fume was added to the mixtures. Penta sodium metasilicate was included to dry mixtures in solid form as alkali activator. In order to understand the composite behavior, 3D printed geopolymers were subjected to compression, tensile and shear loading. As a result of the study, the maximum 28-day compressive, tensile and bond strengths were reported as 41.5 MPa, 4.69 MPa and 4.79 MPa, respectively.

Panda et al. [83] carried out a study investigating the rheological behavior (yield stress, viscosity, and thixotropy) of nano clay addition to geopolymers (GBFS+FA+ river sand with the maximum diameter of 2 mm) suitable for 3D printing. The precursors were activated with KOH and K_2O_3Si in different MRs. In the study, rheometer tests in different conditions and Vicat-set time test were performed to assess the buildability and extrudability characteristic of the mixtures. As a result of the study, it was reported that the mixtures with an activator to binder ratio of 0.35, a water to solid ratio of 0.30 with the addition of 0.5% clay of the solid material showed the most convenient rheological behavior.

Şahin et al. [84] carried out a study focusing the rheological properties of entirely CDW-based geopolymers convenient for 3D printing. HB, RCB, RT, G and C as precursors in geopolymer production; $Ca(OH)_2$, NaOH and Na_2SiO_3 were utilized as activators. The vane-shear test, flow table, and modified mini-slump test were performed to evaluate the rheological parameters. Additionally, compressive strength tests on casted specimens

were carried out to evaluate mechanical characteristic of geopolymer samples. The extrudability characteristic of the optimum mixtures determined by the rheological and mechanical properties testing was determined by the ram extruder test. The mixture with 6.25 M NaOH and 10% $Ca(OH)_2$ content was found to have the most convenient mechanical and rheological properties. The maximum compressive strength of 28-day cured sample was reported as 16.8 MPa.

Nematollahi et al. [85] performed compression tests in 3 different axes and flexural test in 2 different axes to class F FA-based geopolymer samples and determined the interlayer bond strength. They used 8M NaOH solution and Na2SiO3 alkali activators with a Na_2SiO_3/NaOH ratio of 2.5. In addition, 6 mm lengths of PVA, PP and PBO fibers were added to the geopolymer mortars produced singly in mixtures. The samples were subjected to a 24-hour thermal cure at 60 °C before being removed from the oven and maintained at ambient condition until the test day. The compressive strength of the sample under parallel loading was 50% higher than that under lateral loading, according to the compressive strength data. In flexural strengths, it was reported that the sample under lateral loading showed 6.5% higher strength than the sample under perpendicular loading. The study reported that Interlayer bond strength results were between 2.33 and 3.03 MPa.

Muthukrishnan et al. [86] performed compressive and flexural tests in 3 directions to geopolymer concrete (GBFS + FA + fine and coarse aggregate + Na_2SiO_3 + magnesium alumina silicate + tap water). In addition, within the scope of the study, the effect of alkaline reactions on rheological properties for 3D printable geopolymer concrete formulation was investigated. The researchers examined the effect of design features including activator content, retarder (sucrose) and thixotropic additive (Magnesium Alumina silicate) dose on the rheological characteristics of concrete. The rheological properties were determined using a device called Viskomat XL (Schleibinger, Germany). During the experiment, the mixer with 6 blades was kept fixed and a shear force was applied to the material by rotating the outer cylinder. The time-dependent variation of the applied torque during the process was recorded. The rheological properties such as viscosity, shear rate and shear stress were determined by using the Reiner-Riwlin equation, which is extended to the torque and minute revolutions (rpm) acquired, was used to determine rheological parameters such as shear stress, shear rate, and viscosity.

In order to determine the mechanical properties, 3D-printed geopolymer samples were stored in a water bath until the test day. According to the test results of 28 days, the compressive and flexural samples loaded in the parallel direction showed 28% and 56% more strength than the specimen loaded in the perpendicular direction respectively.

Guo et al. [87] examined the effect of GBFS and SF on the rheological properties of an FA-based geopolymer manufactured with 3D-AM. By weight, 10-30% of GBFS and SF were substituted by FA in the preparation of the mixtures. The alkali activator was Na_2SiO_3, and the rheological additive was ATTAGEL-50 thixotropic thickener. The rheological parameters of 3D printable FA-based geopolymer were determined using an RVDV-2 type rotational viscometer. The plastic viscosity and yield stress values were calculated using the Bingham Flow Model and the Herschel-Bulkley Model, which were applied to the shear stress data obtained with experimental devices. The mixture ratio with the highest viscosity was reported as a 10 percent GBFS mixture. Furthermore, it has been noted that adding GBFS to the mixtures reduces the time setting time. With the addition of GBFS, the rheological characteristics of FA-based geopolymers were enhanced at first, then reduced. The mixture containing 10% GBFS had the highest rheological properties (plastic viscosity, thixotropic properties apparent viscosity and yield stress), and the best ratio for SF substitution was 10%.

Bong et al. [88] investigated the printability (buildability and open-time extrudability) and mechanical characteristics (compressive strength) of geopolymers that could be used in 3D concrete applications. Two grades of Na_2SiO_3 and sodium metasilicate were utilized to activate FA and GBFS mixtures. The effect of alkali activators used in various proportions on 3D printed geopolymers was researched in order to establish the optimum ratios. Dynamic yield stress, static yield stress, open-time extrudability, plastic viscosity, thixotropy and buildability (shape retention ability) properties of geopolymers were all examined as part of the research. In addition, the samples were subjected to compressive and flexural testing in various loading directions. The SiO_2/Na_2O ratio of sodium silicate and sodium metasilicate activators in the best mixture in terms of setting time, workability, and strength was found to be 2.0 and 0.9, respectively, as a result of the research. Additionally, the ideal mixture's workability (145 mm flow table), initial and final setting times (291 and 475 minutes), and compressive strength (52.6 MPa heat cured casted sample) are all reported. The printed samples had a 10 to 27 percent lower

compressive strength as a consequence of the direction-dependent mechanical characteristics tests. The flexural strength of the printed samples achieved a range of 3.5-8.4 MPa after 28 days as a consequence of the study.

Mechtcherine et al. [89] who performed compression and flexural tests in 2 different loading directions on 3D printable mortars containing CEM I type cement, FA and micro silica, reported that the compressive strengths of the casted samples and the 3D printed samples tested under loading parallel to the printing direction were nearly the same. On the contrary, the printed samples under loading perpendicular to the printing direction exhibited 20% less compressive strength. In flexural strengths, the casted samples showed 18% more strength than the printed samples when loaded in the perpendicular loading direction.

Ma et al. [90] produced the mortars produced with Portland cement, FA and in multi-layered form by 3D printing. The compressive and bending characteristics of the samples extracted into the cube and prismatic shape under loading in 3 directions were examined and the strength results were compared with the casted specimens. In addition, splitting tensile tests were also performed. It was reported that the samples under the compression showed a decrease of 7% and 24.6%, respectively, in the samples under perpendicular and lateral loading to the printing path, compared to the casted samples, while the results were similar in the loading condition parallel to the printing direction. In flexural strengths, compared to the casted samples, the samples perpendicular and parallel to the printing direction showed 56.1% and 20.6% higher strength, respectively, while the samples under side loading showed 24.8% less strength.

In study by Ding et al. [91], the bending behavior of 3D printable Portland cement mortars produced by adding polyethylene fiber in certain proportions was investigated. The 3D printed, multilayered and extracted specimens were subjected to bending tests in all three loading directions and the results were compared with samples manufactured with mold casted. At the end of the research, the maximum flexural strength variation in different directions was reported as 50.7%.

In the existing studies related to 3D-AM, the different mechanical performances obtained in different loading directions are generally explained by the anisotropic property caused

by the weak bond region between the layers depending on the nature of the 3D printing process. However, there is no clear consensus on how the anisotropic effect varies in different loading directions (perpendicular, lateral or parallel direction). In addition, there is no research in the literature investigating the anisotropy performance of 3D printable geopolymers consisting of 100% CDW.

Xia et al. [92] conducted a study focusing printability characteristics and mechanical ofgeopolymers produced with different combinations of GBFS and FA, activated with different ratios of potassium metasilicate (unhydrous), Na_2SiO_3 and NaOH. In the study, printability was determined by linear dimensional accuracy analysis. The analysis is essentially based on the comparing of the error difference between the 3D-printed construction element and the digital model. As a result of the dimensional error values measured in 3 different axes, it was reported that the samples showed anisotropic behavior in dimensional accuracy. In order to determine the mechanical properties, compression tests were carried out in parallel and perpendicular to the nozzle movement direction. In accordance with compressive tests, the maximum compressive strength for 7 days was reported as 29.6 MPa. In addition, among the 3D-printed sample showing the maximum strength, the compressive strength in the parallel to printing path direction was 11.7% greater than the compressive strength in the perpendicular to nozzle movement direction.

Panda et al. [93] produced ”one-part geopolymer” using FA and GBFS as precursor materials. They used solid alkali activators with combinations of K_2O_3Si powder and KOH. Tap water and river sand with grain sizes smaller than 2 mm were used in the production of geopolymer. 3D printed samples were prepared with 3 mixtures in which the alkaline activator content was kept constant and the GBFS amount varied between 15% and 40%, and the GBFS and FA content were kept constant, 2 mixtures in which 10% and 20% activator content, with a total of 5 mixtures. In the study, the water to solid (FA, GBFS and alkali activator) ratio was determined as 0.35. The tests evaluated the flow properties, thixotropic properties, compressive strength, and buildability properties of the samples. Furthermore, XRD analyses were performed to evaluate the microstructural characteristics of the raw materials, and FESEM analyses were carried out to determine the microstructural properties of the samples that had been cured for 28 days. The use of 40% GBFS in the study enhanced the buildability properties Similarly, rising the amount of GBFS showed to enhance mechanical characteristics of geopolymer

samples. It has been revealed that increasing the alkaline content from 10% to 20% improved compressive strength. Furthermore, the compressive strengths of curing period of 28 days were determined under various loading directions. As a result of the study, the sample under loading parallel to the nozzle movement direction was reported as 28.3 MPa, and the sample under loading in the lateral direction was reported as 24.3 MPa.

Ma et al. [94] performed mechanical tests to geopolymer containing SF, FA, GBFS, sodium metasilicate, silica sand and tap water. In addition, the mixture compositions have been added PP fiber and Hydroxyethyl Cellulose to prevent shrinkage and loss of water. The compressive strength and tensile strength of the casted sample of the geopolymer is stated as 40.5 MPa and 2.84 MPa respectively. In the study, it has been reported that the printed micro-cable addition mixtures meet the printing properties. At the end of the study, the 3D printed micro-cable was added to the geopolymer has reached high flexural strength.

The bond strength of construction member produced by the 3D-AM technique has a critical significance in determining the mechanical characteristics of the material. There are limited studies in the literature investigating the bond strength of materials produced with 3D-AM.

Panda et al. [95] synthesized a study focusing the bond strength of 3D printed FA and GBFS-based geopolymer samples and added with micro silica, activated with NaOH and Na_2SiO_3. As a result of the bond strength tests performed at different molar ratios (MR), researcher reported that as the MR decreased, the bond strength decreased because of the decrement of the setting time. The highest bond strength between the mixtures with varying MR was found to be 0.734 MPa at the end of the research.

In the study by Tay et al. [96], the primary objective was to use rheological and visual inspection to explore the time-gap effect on the printed layers for better discussing the material behavior of the additive manufactured layers while they were still fresh. On the 2^{8t}h day following printing, the tensile bond strength between the two layers of manufactured by 3D printing specimens was determined. The interlayer bond strength values of the 3D-printed samples manufactured at 1-minute intervals were between 0.8 and 1 MPa.

Panda, Ting, et al. [97] synthesized a study comparing the flowability and mechanical characteristics of 3D-printed systems with 2 different binders. In the study, cement-based containing OPC and recycled glass aggregate and FA-based geopolymer were produced. Viscosity recovery test, slump test and visual inspection were performed to determine the rheological characteristics. Furthermore, in order to determine the mechanical behavior, both binder systems were produced as casted cubes and 3D printed, and compressive strength test was performed to the samples at the end of 7 days. As a result of the study, it was reported that OPC-based mixtures showed more suitable thixotropic properties. In addition, OPC-based mixtures have shown higher compressive strength in both cast and 3D-printed samples. According to findings, 3D printed OPC samples have reached a maximum of 23.1 MPa at the end of 7 days.

Panda et al. [98], carried out a research examining the the tensile bond strength of a novel FA-based 3D-printed geopolymer mortar about the time interval between production of layers, nozzle distance to printing table or surface of underlayer, nozzle speed. For the interlayer bond strength test, 50 mm long samples were extracted from the 350 mm 3D-printed geopolymer filaments in the hardened state on the test day. In order to investigate the effect of time gap between the printing of layers on bond strength, the samples were printed in two different groups. In the first group, the time interval was prepared to be 5 minutes, up to 20 minutes. In this group, the second layer was prepared from the same mixture batch. In the second group, the interval was determined as 35 minutes–- 3 hours–- 6 hours. Due to the setting of the mixture at the end of the time interval, unlike the first group, the second layer, which was printed on the old first layer, was reprapared and pumped at fresh state. The researchers stated that the time interval for the first group of samples decreased the interlayer bond strength. This was attributed to the decrement in interlocking between the old and subsequent layer due to the setting of the bond region as the time interval increased. According to the bond strength test results of the second group samples, the difference in strength between 35 minutes and 1 hour is greater than between 1 hour and 3 hours. The reason for this was attributed to the freshness of the bonding region in the 35-minute time interval samples. It was determined that the strength difference was lower as the time interval increased. At the end of the study, the tensile strength of the FA-based geopolymer mortar was found to be 1.63 MPa according to the test results.

Marchment et al. [99] conducted research that examined the effect of time gap on bond strength between layers during 3D printing of two layers. Furthermore, other mechanical properties (compressive strength and bending characteristics) of OPC-based mortars were investigated. The interlayer bond strength of 3D-printed concrete is tested at a rate of 1 mm/min. In the study, the layers were printed with a time gap of 3 and 15 minutes. While the samples were being printed, cementitious paste was applied between the layers with a brush, and its effect on the bond strength was also investigated. In addition, two layers were produced in different colors and bond regions were scanned after the interlayer bond strength test. The effective bond area was calculated by determining the color pixels on the scanned images. With an average bond strength of 0.44 MPa, the samples with no interlayer paste formed the weakest bonds. The bond strength of the OPC paste samples was 0.72 MPa, but the bond strength of the pastes with admixtures was 1.26 MPa, and the bond strengths of two additional mixtures with admixtures were 0.98 and 1.00 MPa, respectively.

3. MATERIALS AND METHODOLOGY

3.1 Materials

3.1.1 Precursor Materials

In this section, the characteristics of the precursor materials (CDW) used in the manufacturing of geopolymer, as well as the activators used for geopolymerization and RCA, are discussed.

3.1.1.1 CDW Materials

CDW-based materials including RCB, RT, HB, GW and CW, collected from variety of selective demolition activities performed in Turkey, were used as precursors in the production of geopolymers. RCB, RT and HB were collected from collapsed masonry structures and wall elements for use as precursors. GW, a CDW-based material that usually comes out of the windows of the buildings, was also extracted to be used as an alumina-silicate source. The final CDW-based material, CW, was also used, separating materials from masonry structures, wall elements and demolition wastes of reinforced concrete structures. All these waste materials were first crushed individually with a jaw crusher (Figure 3.1) to reduce in size and then milled for 60 minutes in a ball mill (Figure 3.2) to obtain powder form. Same procedures were followed for each type of waste. The same process was applied in material CW without separating the aggregates. The details of the crushed and milled materials are shown in Figure 3.3-3.4-3.5-3.6-3.7. Milled material was sieved to separate the CW material from the hydrated material and the aggregate that did not decrease in sufficient size. To dehydrate the wastes obtained from the external environment, the CDW-based precursors employed in the study were subjected to a temperature of 105 °C for 24 hours in powder form.

Figure 3.1 Representative image of jaw crusher

Figure 3.2 Representative images of different types of ball mills used in study

Figure 3.3 Crushing and grinding process of HB. a) Raw form, b) Crushed form, c) Ground form

Figure 3.4 Crushing and grinding process of RCB. a) Raw form, b) Crushed form, c) Ground form

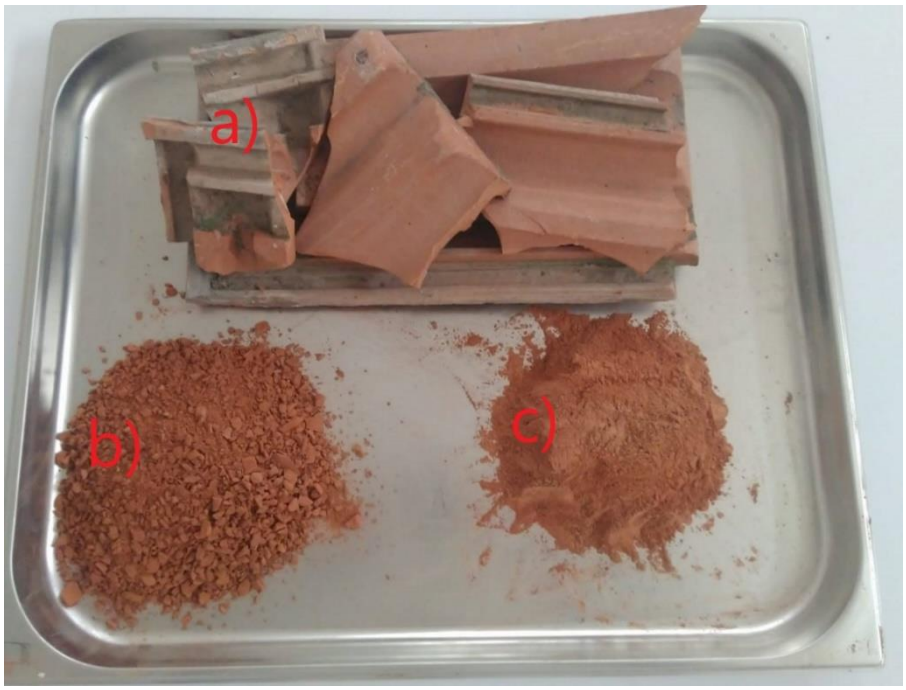

Figure 3.5 Crushing and grinding process of RT. a) Raw form, b) Crushed form, c) Ground form

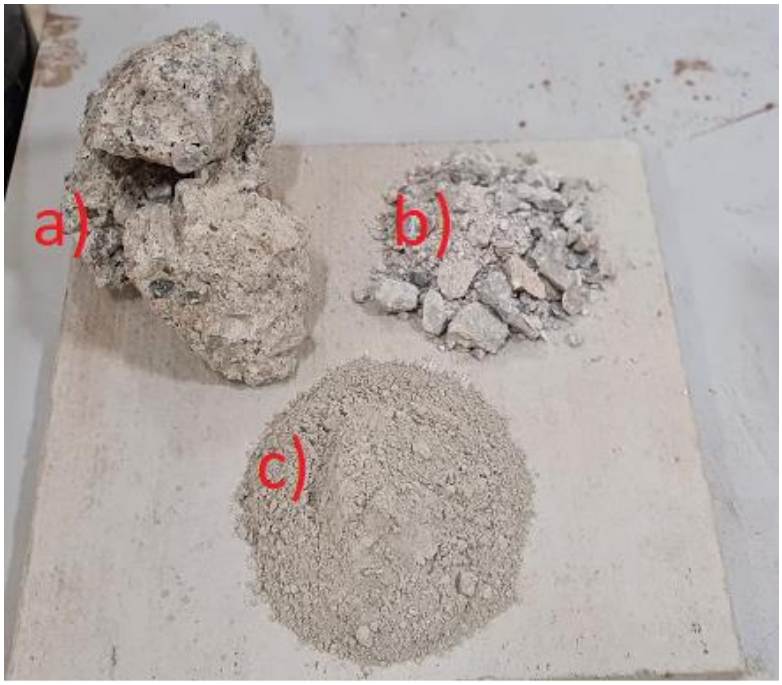

Figure 3.6 Crushing and grinding process of CW. a) Raw form, b) Crushed form, c) Ground form

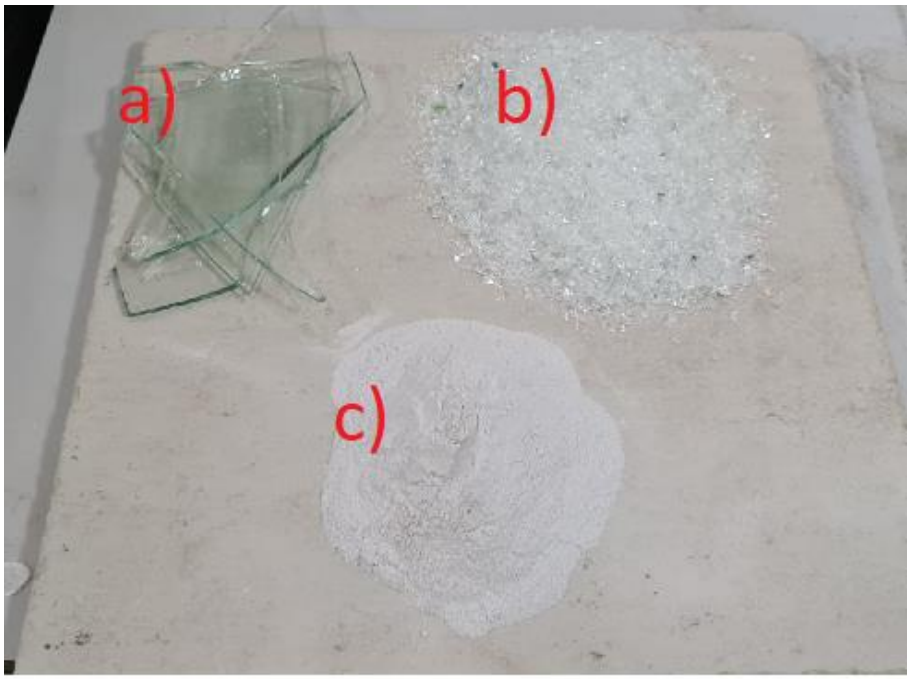

Figure 3.7 Crushing and grinding process of GW. a) raw form, b) crushed form, c) ground form

Following the milling process, the oxide compositions (Table 3.1) and particle size distributions (Figure 3.8) of the precursors were determined using X-ray fluorescence (XRF) analysis (with a wavelength of 0.1-50) and laser diffraction technique (with a size range sensitivity of 0.02–2000 m) on oven-dried powder batch fractions. The specific gravity values of powder materials are also presented in Table 3.1. As seen, SiO_2, Al_2O_3 and Fe_2O_3 oxides, which are substantially required during geopolymerization process [100], were found in high quantity in the content of the clay-based materials (HB, RCB and RT) analyzed. While CDW-based precursors of clay origin show similar oxide composition, CW and GW, which are also CDW-based, contain different amounts of SiO_2, Na_2O and CaO. The SiO_2 value is expected to be high, since the GW, obtained from the glass of the demolished buildings, is a soda-lime-based waste material. In addition, it is seen in Table 3.1 that the CDW-based precursor with the lowest specific gravity is also GW.

Table 3.1 Results of XRF analysis

Oxides %	HB	RCB	RT	GW	CW
SiO2	39.7	41.7	42.6	66.5	31.6
Al2O3	13.8	17.3	15.0	0.9	4.8
Fe2O3	11.8	11.3	11.6	0.3	3.5
CaO	11.6	7.7	10.7	10.0	31.3
Na2O	1.5	1.2	1.6	13.6	0.45
MgO	6.5	6.5	6.3	3.9	5.1
SO3	3.4	1.4	0.7	0.2	0.9
K2O	1.6	2.7	1.6	0.2	0.7
TiO2	1.7	1.6	1.8	0.1	0.2
P2O5	0.3	0.3	0.3	0.0	0.1
Cr2O3	0.1	0.1	0.1	0.0	0.1
Mn2O3	0.2	0.2	0.2	0.0	0.1
Loss on ignition	7.8	8.0	7.5	4.3	21.1
Specific gravity	2.89	2.81	2.88	2.51	2.68

As seen in the Figure 3.8, at the end of 1 hour of identical crushing and milling procedures, obtained powdery form of precursors had different particle size distribution. According to the results, RT, HB, and RCB have almost identical particle sizes, however, CW and GW have coarser particle size. Approximately 90-95% of HB, RCB and RT were finer than 40 μm and the amount of CW finer than 40 μm was ~80%. Among the precursors, GW appears to be the powder material with the coarsest grain size; only 60% of GW remained below 40 μm. Differences in the particle size distributions of the powdery form of different types of precursors after same milling process was most probably related to the variety in grindability index, hardness, density and pore structure of materials.

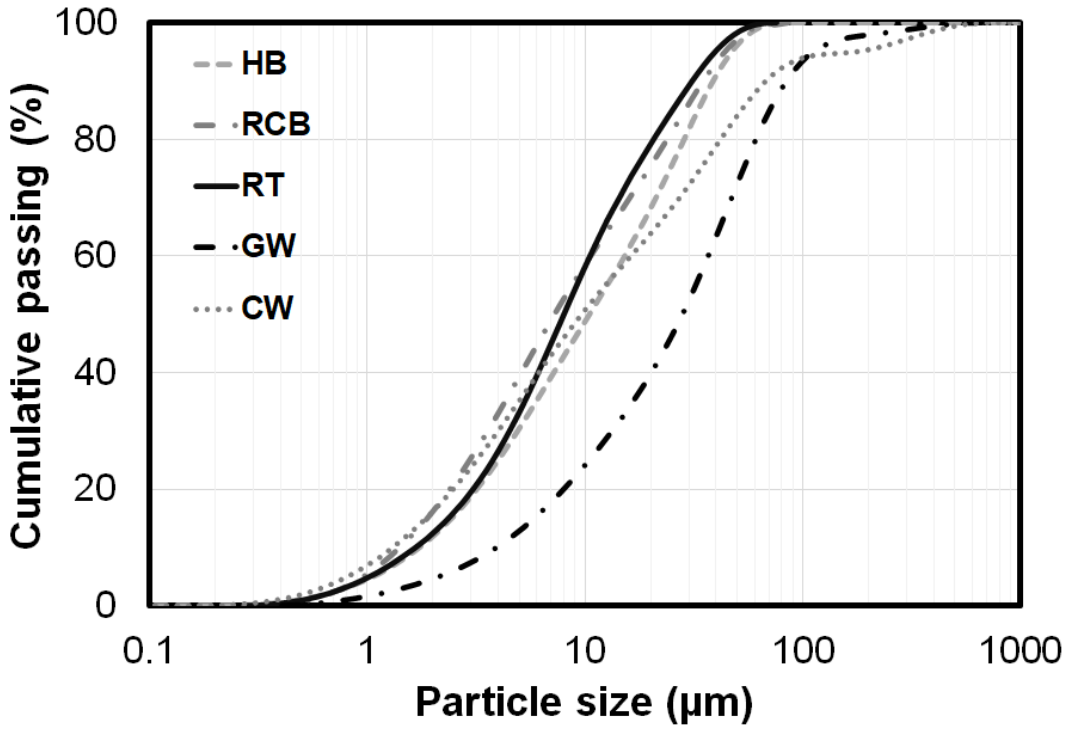

Figure 3.8 Particle size distribution of precursors

Instead of natural aggregate, fine recycled concrete aggregate (RCA) obtained from concrete rubble has been used during synthesis of geopolymer mortar mixture. Considering the printing application procedures, maximum aggregate size was limited as 2 mm for each mixture. At first, a jaw crusher with a 2 mm open side setting was used to reduce the size of the concrete rubble. Then, crushed RCA were sieved via 2-mm sieve. The RCA obtained from the concrete rubble was utilized directly in geopolymer mixtures without being treated in any way to improve the durability and mechanical characteristics of the recycled aggregates. No further application has been made on particle sizes and other properties of RCA and other CDW-based precursors. In accordance with the purpose of the thesis study, the most energy-effective and applicable precursor material was selected. Additional applications, such as the precursors having the same particle size, prevent the study from being cost-effective. The results of SEM analysis made under 30 kV vacuum from 10 mm are shown in Figure 3.9. After the crushing and grinding processes, it is seen that all CDW-based precursor materials were in angular shape.

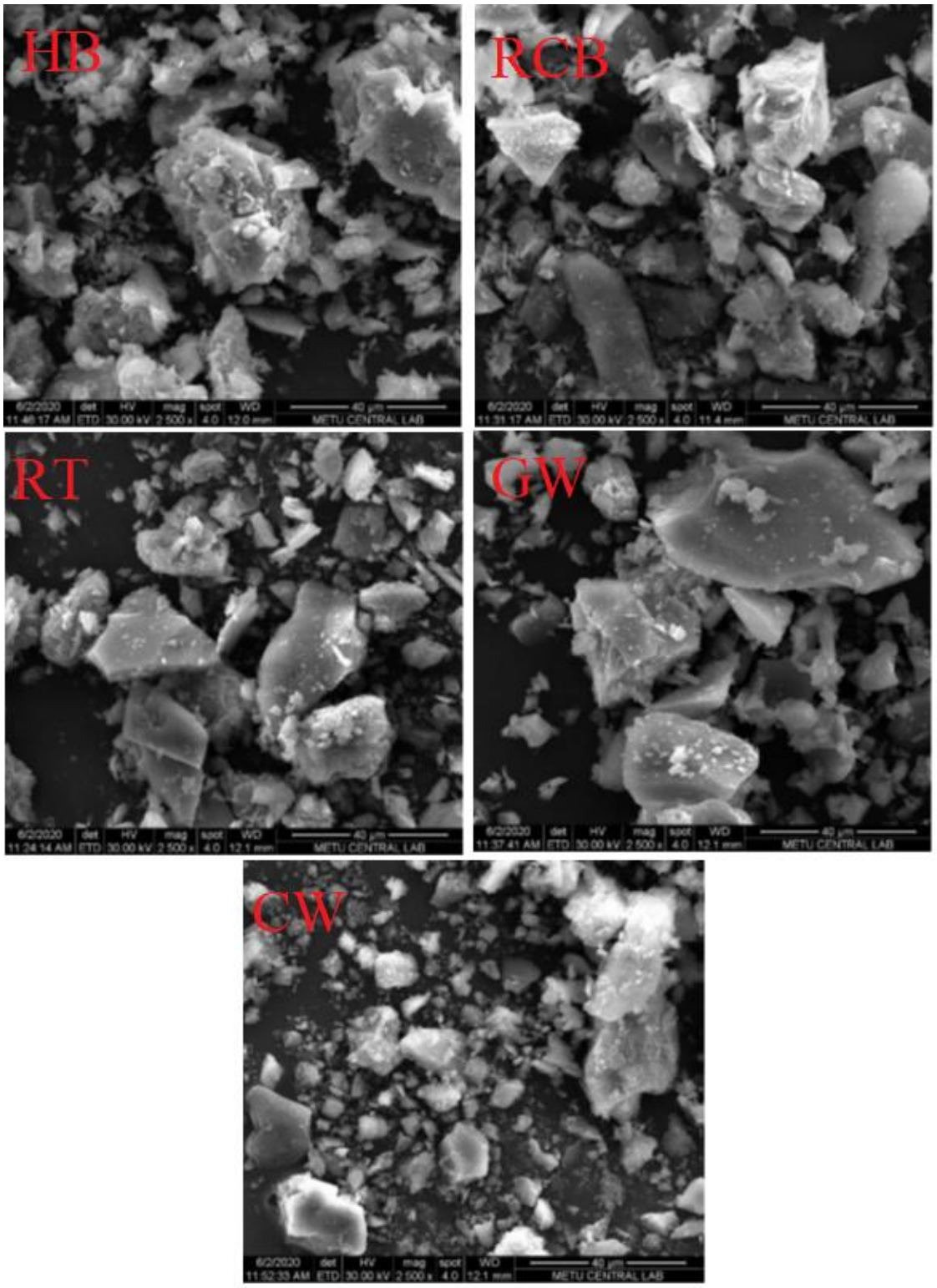

Figure 3.9 SEM micrographs of CDW-based precursors.

As shown in Figure 3.10, the crystalline phases of CDW-based precursors were investigated using the XRD method, which was performed on an Olympus BTX Benchtop XRD Analyzer (with a scan range of 5-55o with a 0.02° increment). The XRD patterns of

the HB, RCB and RT revealed amorphous to semi-crystalline phases and were comparable, with a large hump centered mostly at 2 of 27–29° and varying crystalline peaks of various strengths. Quartz was the most prominent crystalline peak, as expected, with the highest intensities for HB, RT and RCB. All clay-derived precursors have a diopside peak as well. The shape of GW was amorphous, with a broad peak centered on 2 of 28°. Quartz, Diopside, and Calcite were the main peaks scanned for CW, while Muscovite and Foshagite were minor peaks. The powder diffraction file (PDF) and chemical formulas obtained from XRD analysis of CDW-based precursors are shown in Table 3.2.

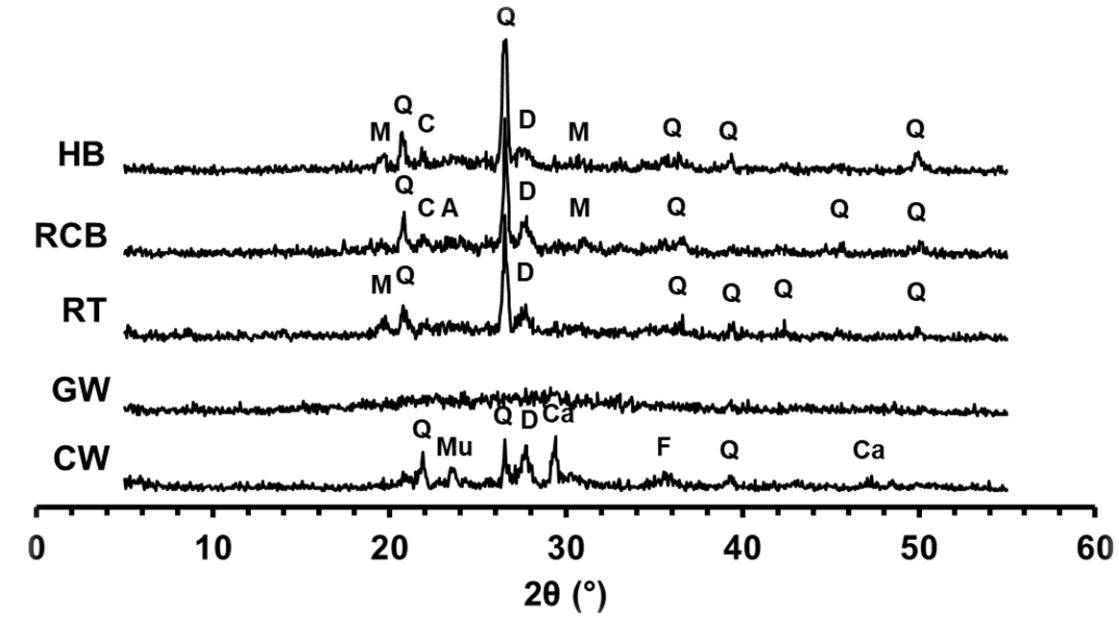

Figure 3.10 XRD graphs of CDW-based precursors.

Table 3.2 PDF numbers and chemical formulations of crystalline phases accordingly XRD analysis

Crystalline Phase	Symbol	PDF Number	Chemical Formula
Quartz	Q	96-101-1160	SiO_2
Crystobalite	Cr	96-900-8230	SiO_2
Diopside	D	96-900-5280	$Al_{0.6}CaMg_{0.7}O_6Si_{1.7}$
Mullite	M	96-900-5502	Al_2O_5Si
Akermanite	A	96-900-6115	$AlCa_2Mg_{0.4}O_7Si_{1.5}$
Calcite	Ca	96-900-9668	$CaCO_3$
Muscovite	Mu	96-101-1050	$Al_3H_2KO_{12}Si_3$
Foshagite	F	96-901-1044	$Ca_4H_2O_{11}Si_3$

3.1.2 Alkaline Activators

In this thesis study, to activate CDW-based precursors, NaOH and $Ca(OH)_2$ were used as alkaline activators, in a different usage rates and combinations which will be discussed in following section.

3.1.2.1 Sodium Hydroxide (NaOH)

NaOH is a widely used basic ingredient in the chemical industry. Caustic soda is another term for NaOH. It has a moisture-absorbing function and is white in color. It is easily dissolved in water. Its structure is smooth, slick, and soap-like. It comes in both liquid and solid form. The electrolysis of a sodium chloride (NaCl) solution produces NaOH, which results in the creation of chlorine gas and the evaporation of the solution's water. It has a fast interaction with water and produces an exothermic reaction. In the geopolymerization stage, this reaction releases Na^+ and $(OH)^-$ ions to the environment. $(OH)^-$ ions decrease the pH of the medium and increase alkalinity. High alkalinity, as previously stated, is critical in the initiation of geopolymerization and the dissolution of aluminosilicate precursors.

In the literature, many factors such as the type of precursor used, the particle size of aggregate and powder materials, etc. have varying effects on the mechanical characteristics of the geopolymer. Therefore, within the scope of the study, the effect of NaOH on geopolymerization and 3D printability was investigated and its effect on mechanical properties was investigated by using NaOH solution at different molars.

NaOH is provided by “Koruma Klor Alkali San. Tic. A.Ş.” and was in white solid flake form, with a minimum of 98% sodium hydroxide, a maximum of 15 ppm iron, 0.1 percent sodium chloride and a maximum of 0.4% sodium carbonate NaOH in flake form used in the study is shown in Figure 3.11.

Figure 3.11 Flaked form of NaOH image

3.1.2.2 $Ca(OH)_2$

Calcination of limestone at temperatures above 900°C produces quicklime, which is subsequently reacted with water to generate $Ca(OH)_2$, also known as hydrated lime. $Ca(OH)_2$ helps to increase the alkalinity of the medium during the geopolymer production. In addition, calcium silica hydrate (CSH) and calcium alumina silica hydrate (CASH) bonds form, allowing the matrix to form a more compact structure. Moreover, with the seeding effect it provides in the system, it enables the geopolymerization material to produce more easily. Much research in the literature have found that the mechanical properties of geopolymer change with the amount of $Ca(OH)_2$, depending on the type of precursors and other alkali activator. As a result, varied ratios of $Ca(OH)_2$ content were employed to examine the mechanical characteristic of the 3D printed and casted specimens. The $Ca(OH)_2$ was provided by “Tekkim Kimya San. ve Tic. Ltd. Şti” and was in powder form (in solid phase with the molecular weight of 74.09 g/mol), with a purity level of 87%. The illustration of $Ca(OH)_2$ is shown in Figure 3.12.

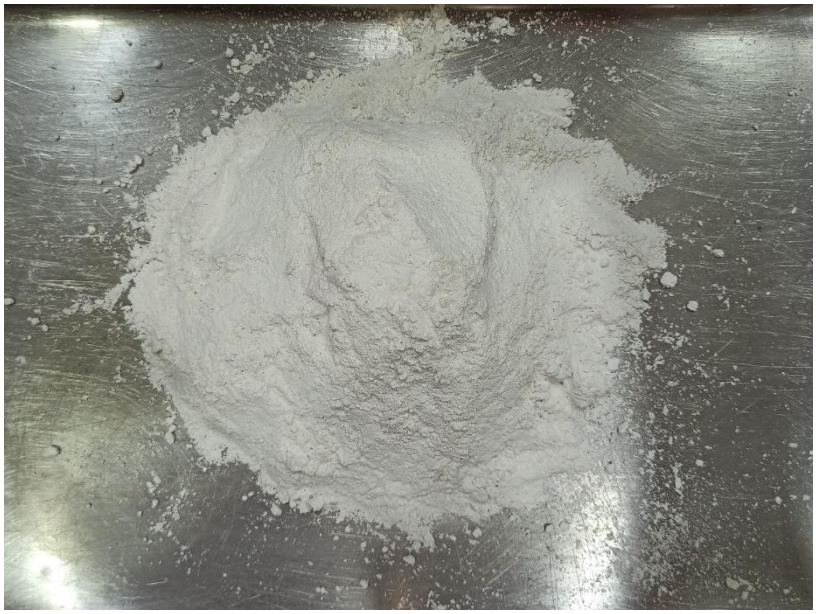

Figure 3.12 Representative image of $Ca(OH)_2$

3.1.3 Recycled Concrete Aggregate (RCA)

It is desired that all binder and aggregate materials used within the scope of the general purpose of the thesis were produced from waste materials. In addition, CW constitutes the largest portion of CDW-based materials that come out today. Therefore, the use of CW as a precursor in the 3D printable geopolymer manufactured within the scope of the thesis, as well as its use as RCA, is of great importance for the reutilization of CDWs. In this context, CDW-based CW materials provided for the use of precursors within the scope of the study were used as RCA. Waste concrete collected from demolition areas in Turkey was first crushed with the help of a jaw crusher without separating it as aggregate or concrete. Then, it was sieved, and RCA of desired dimensions was obtained. The detailed view of the RCA production stages is shown in Figure 3.13. The maximum aggregate size was determined as 2 mm within the scope of the study in order not to cause any blockage in any production pipe and nozzle during pumping and extruding of the geopolymer.

Figure 3.13 Detailed images of RCA a) raw form, b) crushed form, c) sieved form

3.2 Methodology

Experimental studies such as preparation of mixtures, mixing, preparation of samples, curing conditions and testing are detailed below.

3.2.1 Mixture Proportions

Geopolymer mixture proportions have been determined by considering the 3D printable mixtures with optimum rheological properties. In this regard, a dry base mixture was designed to have 80% brick-based materials (RCB, RT and HB), 10% GW and 10% CW. Since the physical and chemical characteristics of HB, RT and RCB were similar, the brick-based material content was chosen to have equal percentages in the mixture (26.67% for each). The usage rate of GW and CW was limited to 10% because of the formation of weaker gel structures and differentiation of the formed gel structures in case the Si/Al balance cannot be maintained in geopolymer systems. Although fine aggregate is used in the mixtures within the scope of the thesis, it is necessary to choose a lower aggregate/binder ratio compared to conventional mortars in order to ensure extrudability property and to prevent a problem in the pumping process during printing. In addition, at the beginning of the geopolymerization, water creates an environment for the dissolution

of alumina-silicates and provides the transport of $(OH)^-$ ions [101-103]. However, it does not participate in the geopolymerization process as a chemical compound. Therefore, the water/binder ratio should be kept at a level where sufficient workability and the necessary liquid medium for the dissolution of Al-Si are formed. In the mixtures prepared for study, aggregate to binder ratio of 0.35 and water to binder ratio (W/B) of 0.33 (by weight) were chosen for each mixture.

To investigate the effect of activators on time-dependent-flowability, time-dependent-extrudability, 10M, 12.5M and 15M NaOH and 0-4-8-12% (by weight) $Ca(OH)_2$ was decided to use in solely and binary combination. Mixtures containing 15M NaOH irrespective of Ca(OH)2 usage and mixtures produced with 12% Ca(OH)2 irrespective of NaOH usage showed unsuitable rheological properties for 3D printing (detailed information is explained later). Therefore, these mixtures were not produced for mechanical property tests. Mixtures comprising solely and binary combination of 0-4-8% $Ca(OH)_2$ and 10M and 12.5M NaOH were prepared for 3D printing to determine bond strength and anisotropic behavior of developed geopolymer and to determine the optimum utilization combination and dosage for best performance. As increasing NaOH molarity leads to increment in viscosity, thereby decreasing the printability performance of mixtures, NaOH molarity was limited to 12.5M. Likewise, since increasing usage rates of $Ca(OH)_2$ increase the amount of geopolymerization products and solid content, hence decreasing the flowability, a usage rate of $Ca(OH)_2$ was limited to 8% by weight of binder. The geopolymer mortar mixtures determined within the scope of the thesis, showed proper the shape retention and extrudability properties required for the 3D-AM process without the need for additional chemical additives. Details of designed mixtures were represented in the Table 3.2.

Table 3.3 Proportions of geopolymer mortar mixtures.

Alkali activators				CDW-based precursors (g) (1000 g)					RCA (g)	W/B Ratio
NaOH		$Ca(OH)_2$								
Molarity (M)	Amount (g)	Rate (%)	Amount (g)	HB	RCB	RT	CW	GW		
10	132	0	0	266.7	266.7	266.7	100	100	350	0.33
		4	40							
		8	80							
		12	120							
12.5	165	0	0							
		4	40							
		8	80							
		12	120							
15	198	0	0							
		4	40							
		8	80							
		12	120							

3.3 Mixture Preparation

The mixture preparation phase was started with the preparing NaOH solutions to be used as alkaline activator. To obtain NaOH solutions of different molar concentrations, white flake-form solid NaOH in required amounts for desired molar concentration was dissolved in the tap water. Then, in order for avoiding the effects related to the heat of solution arising from the exothermic reaction between the NaOH and water, the prepared solutions were kept in the laboratory until they reached the room temperature. On contrary to the NaOH, powdery $Ca(OH)_2$ were directly included into the dry mixtures. Within the scope of the thesis, all of the mixtures were mixed with the pan type mixer shown in Figure 3.14. To achieve homogeneity in the dry mixture, the mixing procedure was begun by mixing all powder materials [CDW-based precursors, RCA, and $Ca(OH)_2$ (if available for a specific mixture) for 2 minutes in a pan type mixer after preparing the NaOH solution. The cooled NaOH solution was then carefully poured into the mixer and mixed for 5 mins to ensure that the solution was equally distributed throughout the dry mixture.

Figure 3.14 Pan type mixer to be used in the study

3.4 Specimen Preparation and Curing

Both 3D-printed and casted geopolymer specimens were produced to examine the influence of manufacturing method on the mechanical characteristics of geopolymer mixtures. After the completion of mixing, for each mixture, prismatic shaped samples with dimensions of 40×40×160 mm were prepared by pouring mixture into the pre-oiled molds in two stages. Pre-oiled mold and poured 40×40×160 mm samples are shown in Figure 3.15. Molds were vibrated by a vibratory table in both stages of pouring in order to prevent air voids in the casted specimens. The casted geopolymer mortar mixtures were stored in the laboratory for 24 hours, then removed from the molds and cured until the testing ages.

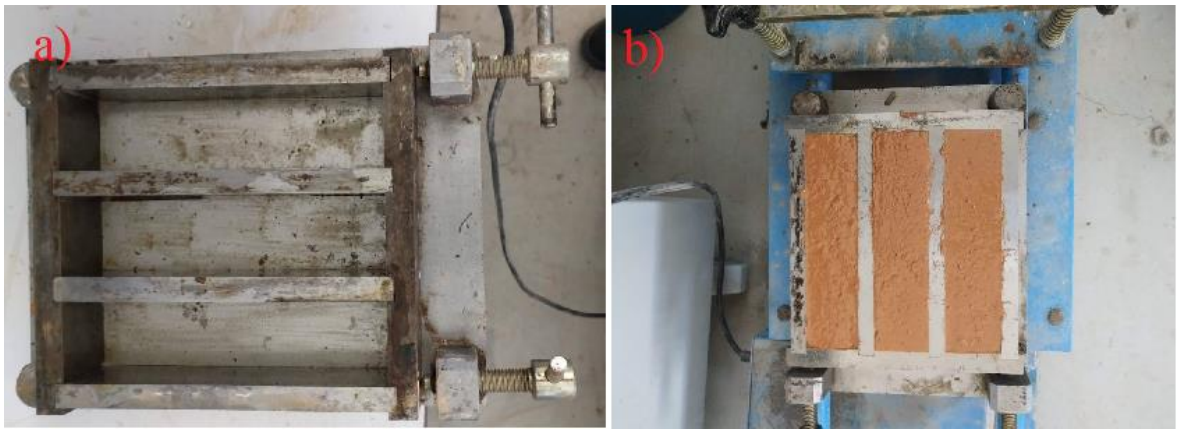

Figure 3.15 Representative images of a) pre-oiled mold, b) fresh poured specimens

A lab-scale gantry system 3D-printer was employed for 3D-printing applications. Details of this 3D-printer can be found in Figure 3.16. Simultaneously with the casting process, prepared geopolymer mortar mixture was loaded to the pump container of the 3D-printer and printing process was performed by using a rectangular nozzle and G-Code-based 3D-printing path design. The nozzle speed was set at 60 mm/s. The print process was carried out by starting the G-code entered in the CNC router control panel and pumping the material loaded into the mortar pump from the transport pipe to the nozzle and printing on the print platform.

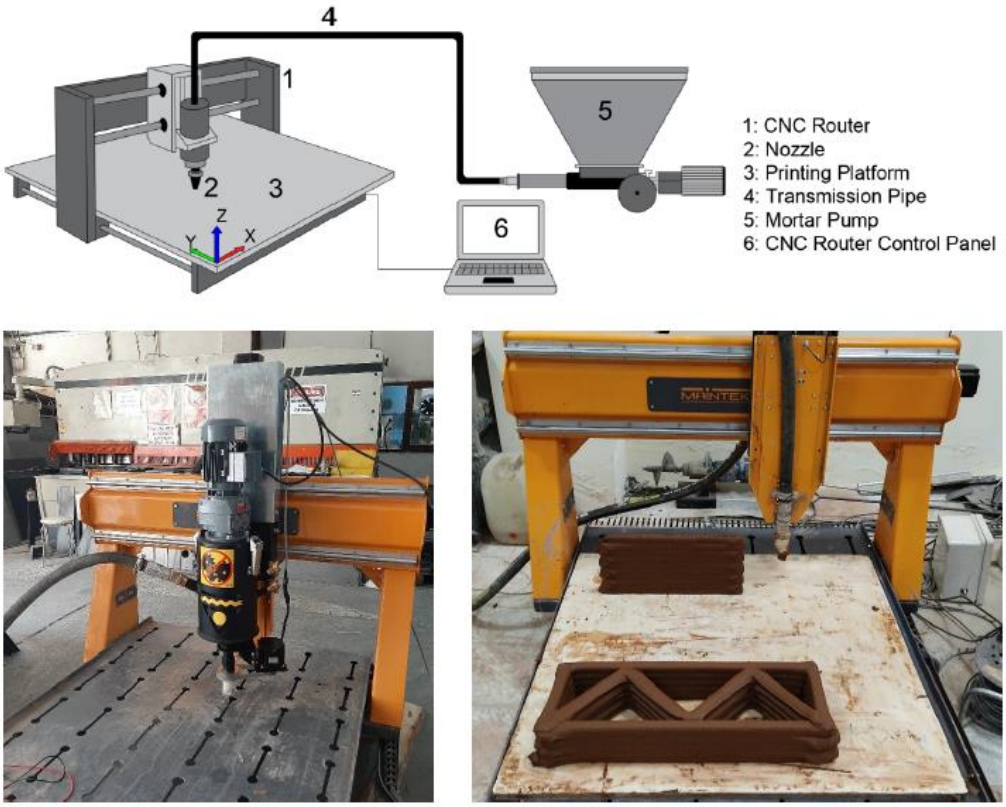

Figure 3.16 Schematic and image of laboratory scale 3D printer

Two-layered filaments with a length of 80 cm and 40x40 mm cross-section were printed uniformly side by side and, immediately after printing process, 40×40×40 mm cubic and 40x40x160 mm prismatic specimens were marked in determined cube and beam dimensions and carefully extracted from these fresh longitudinal two-ply filaments by cutting them with spatula. Prismatic samples were prepared for bending tests in different axes, and cube samples were prepared for bond strength and direction-dependent compression tests. Cubic and prismatic specimens were surface covered for 24 hours on the printing table before being moved to the curing environment to cure. Figures 3.17a and 3.17b show prepared casted prismatic, 3D-printed prismatic, and cube specimens.

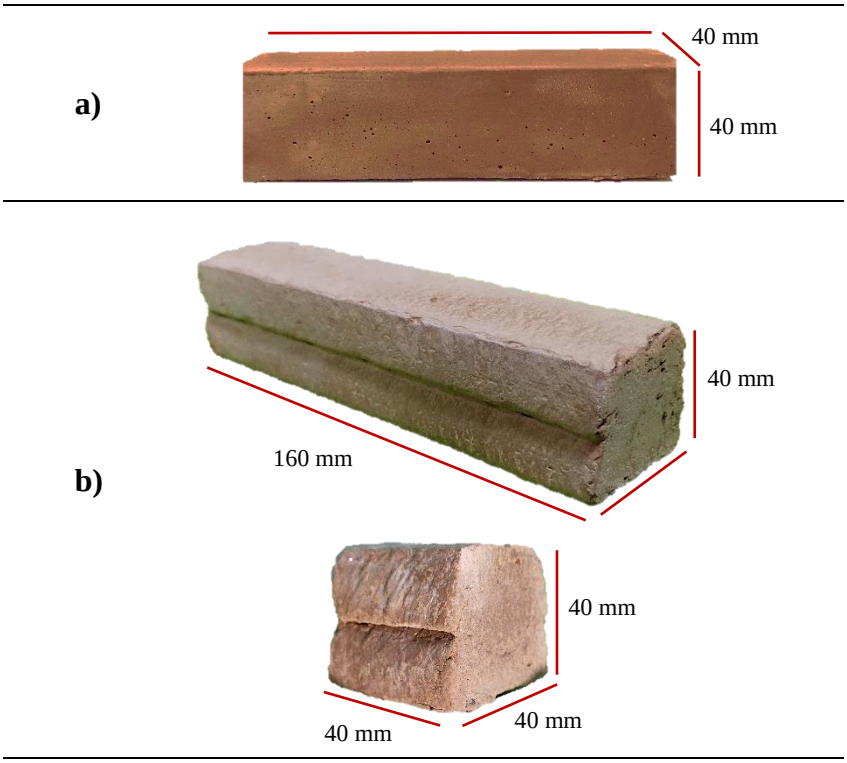

Figure 3.17 Representative images showing details of test specimens: a) Prismatic casted specimen with dimensions of 40x40x160 mm, b) prismatic and cubic 3D-printed specimens

To accurately imitate the field application conditions of the 3D-printing method, the curing procedure was carried out in ambient conditions (Figure 3.18). In this context, both casted and printed specimens were cured under laboratory conditions (23±2 °C) for testing ages of 7, 28 and 90 days.

Figure 3.18 Representative images of 3D printed cubic and prismatic specimens curing at ambient conditions

3.5 Testing

3D printable mixtures must have suitable rheological and mechanical properties. In this context, the flow table and ram extruder tests were performed as a part of this thesis to determine the time-dependent change of rheological properties of the developed mixtures. In addition to the rheological properties suitable for 3D printing, examining the anisotropic behavior and mechanical properties of the products is also an important parameter. In order to examine the mechanical properties, compressive strength tests in 3 different axes and flexural strength tests in 2 different axes were performed. 3D printed samples of 40x40 mm in size for compressive strength, 40x40x160 mm in size for bending strength, and casted samples in 40x40x160 mm dimensions. In order to examine the bond strength between layers, printed samples produced in 40x40 mm dimensions were extracted.

3.5.1 Flow Table Test

Flow table method was conducted to test the flowability properties of the manufactured mixtures as a time - dependent. The ASTM C1437-15 [104] standard was used to conduct the test. The lower diameter of the flow mold in Figure 3.19 is 100 mm, the upper diameter is 70 mm, the height is 60 mm, and the minimum wall thickness is 2 mm. A flow table with a diameter of 300 mm, a straightedge for measuring spreading diameter, a trowel, and a tamper is all included in the system. The mold was positioned in the center of the flow table, and the geopolymer mortar was poured in two stages, with compaction by tamping 20 times with the tamper. The remaining mortar on the mold was removed with the help of a trowel. Mortar on the table and edge of mold was wiped. Afterwards, the mold was lifted, and the flow table was dropped 25 times in 15 seconds and the spread diameter of mortar was measured with the help of a straightedge in two different axes. According to Kazemian et al. [105], there is a correlation between spread diameter and yield stress. As a result, using the spread diameters acquired in the experiments, the "flowability index (τ)" value was derived using the following equation:

$$\tau = \frac{d_1 d_2 - d_0^2}{d_0^2}$$

where, d_0 is the inner diameter of the mold (100 mm), d_1 is the maximum spreading diameter and d_2 is the spreading diameter perpendicular to d_1. The test setup was

represented in Figure 3.19. The test was performed at 0., 30., 60. and 120. min from preparation of the mixture.

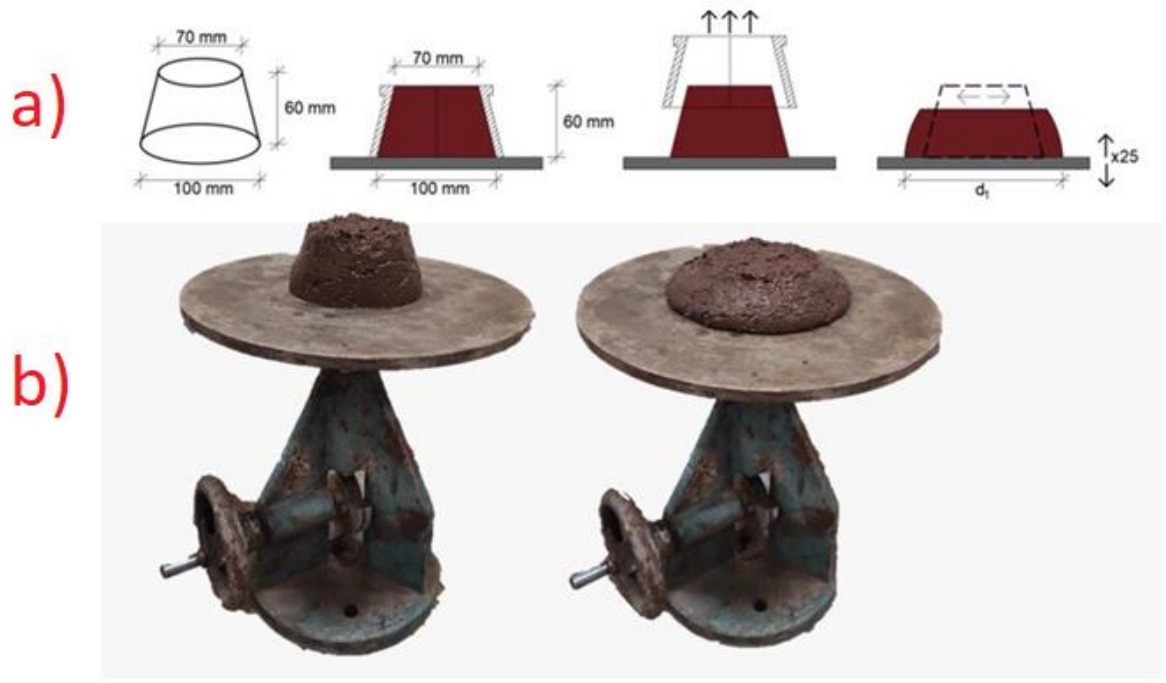

Figure 3.19 a) General schematic view of flow table test, b) illustration of flow table test

3.5.2 Ram Extruder Test

Extrusion capacity of the produced mixture is one of the most essential aspects required within the scope of 3D-AM. The potential of AM is eliminated from the first step if this capacity is not realized. Extrusion capability can be defined as the ability of the mixture to be transmitted easily and reliably from the transmission system and pumped from the nozzle (extrusion tip) with the lowest energy consumption. Figueiredo et al. [106] conducted the ram extruder test and determined the rheological properties of the mixtures using the Benbow-Bridgewater [107] model. Basterfield [108] enhanced this model and a new ram extruder, defined a rigid-viscoplastic material and reported that the extrusion stress value obtained from the test can be converted to shear yield stress. As a result, the shear yield stress value when the material begins to flow could be calculated using the following equation, and the influence of alkali activator types/rates on rheological parameters may be understood:

$$\tau_0 = \frac{\sigma_0}{\sqrt{3}}$$

Where; τ_0 represents shear yield stress and σ_0 represents the extrusion pressure. The extrusion pressure can be calculated as following equation:

$$\sigma_0 = \frac{4F}{\pi} * {D_0}^2$$

Where; σ_0 is the extrusion pressure, F is the average extrusion force measured to obtain the preset piston speed and D_0 is the inner diameter of the chamber, which is equal to 4 cm.

One of the parameters that are thought to have undeniable influences on the rheological characteristics of mortar mixtures with geopolymer binders and therefore important to analyze is the effect of time factor on the fresh characteristics of the mixtures. For this reason, ram extruder test to determine open-time extrudability performances with the ram extruder (0., 30., 60. and 120. minutes from the preparation of the mixture) has been conducted. The ram extruder test used in the current thesis shown in Figure 3.20 was constituted as similar to different studies [109-111] in the literature. In the experiment, 2.25 mm/s piston speed was used to simulate the pump speed during the 3D printing recruitment, and this speed has provided 16 mm/s flow rate. The piston passes through a chamber with a diameter of 4 cm, but the nozzle has a diameter of 1.5 cm, therefore there is a difference in piston speed and flow rate. Furthermore, the distance between the nozzle and the print plate was reduced to avoid any discontinuity or cracking caused by tension.

Figure 3.20 a) General view of ram extruder test setup, b) view of nozzle, c) view of extrusion process

3.5.3 Flexural Strength Test

It is an important parameter to evaluate the anisotropic flexural strengths of the 3D printed samples and the strength differences of these strengths compared to the samples produced by conventional methods. Three-point flexural test was carried out on the prismatic casted and 3D-printed samples (in two different directions such as lateral to and perpendicular to the printing path as shown in Figure 3.21 by using a universal test machine at a crosshead speed of 0.005 mm/sec to evaluate the anisotropic behavior of 3D-printed specimens and manufacturing method-related flexural performance differences. Using the equation below, the flexural strength of geopolymer mortar samples was calculated.

$$\sigma_f = \frac{3F_{max}L}{2bh^2}$$

where F_{max} is maximum load applied; L is span length, b is thickness of the specimen; h is height of the specimen. A minimum of three replicates were used for each case (e.g., testing age, mixture content, loading direction etc.) and averages were calculated.

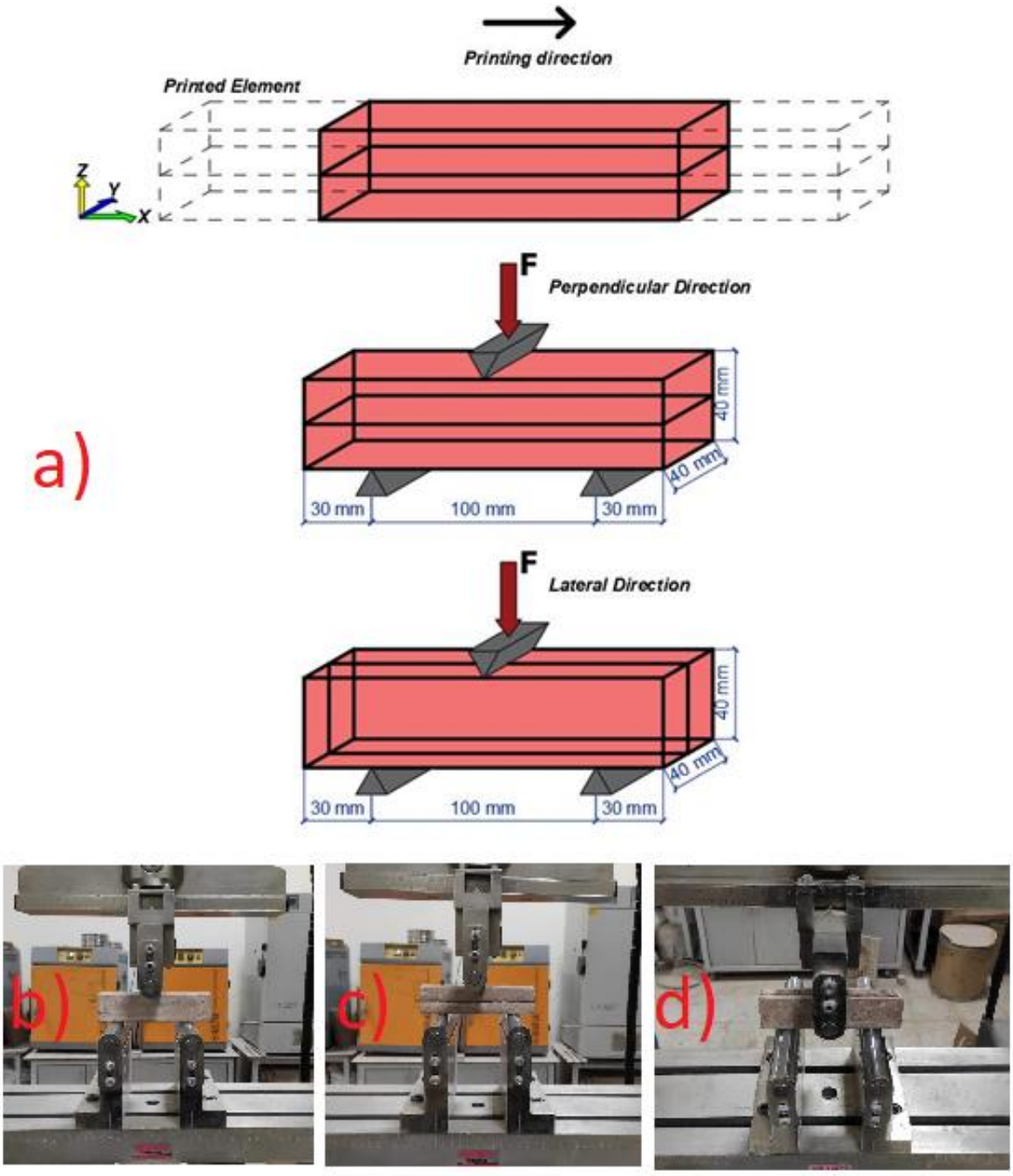

Figure 3.21 Representative images of prismatic specimens for different loading conditions: a) general schematic view, b) mold-casted specimen, c) 3D-printed specimen under perpendicular loading, d) 3D-printed sample under lateral loading.

3.5.4 Compressive Strength Test

Compressive strength tests were carried out on the casted and 3D-printed specimens using a hydraulic testing equipment with a capacity of 150 tons and a loading rate of 0.9 kN/s. In order to examine the direction dependency of 3D-printed samples' mechanical characteristics, the tests were carried out on 3 different directions as perpendicular, lateral and parallel to nozzle movement directions. For the compressive strength test of casted specimens, the broken pieces of the prismatic casted specimens from flexural strength test were used. In order to keep the compression area equal for each specimen, 30x30 mm steel plates were set on the compression areas of the specimens. At least three replicates of each specimen were tested for each case (e.g., loading direction, testing age, mixture content etc.) and strength results were averaged.

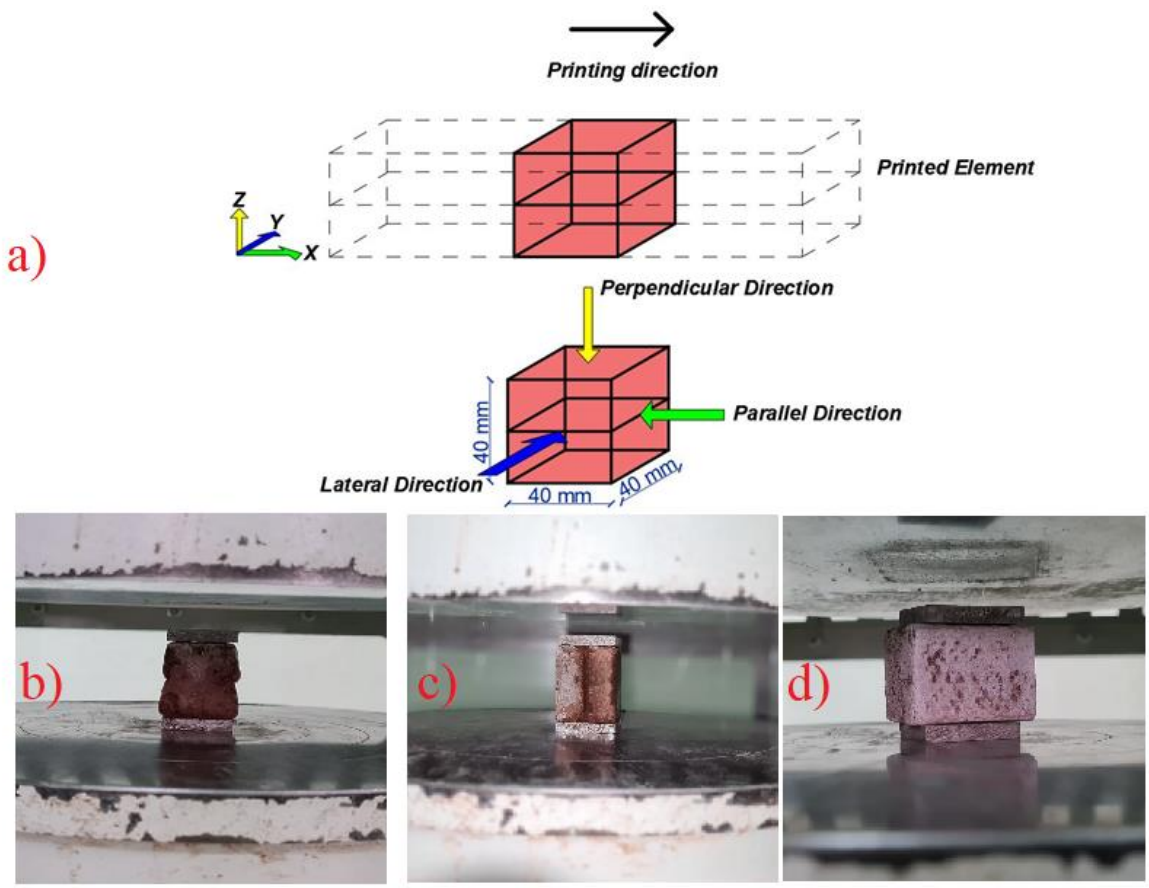

Figure 3.22 Illustration of 3D-printed cubic specimens for 3 types of loading conditions: a) general schematic view, b) perpendicular direction, b) parallel direction, c) lateral direction.

3.5.5 Interlayer Bond Strength

The bond strength between consecutive layers of structures produced with 3D-AM technology is an important parameter in extending the service life of the structure. Due to the nature of 3D-AM, the interlayer bond region can be considered as a relatively weak region. The weakness in the bond is a significant factor in the anisotropic behavior of the samples manufactured with 3D printing. To understand the bonding mechanism, direct tensile test and splitting tensile test performed in the current study.

Splitting tensile test recommended by ASTM 496 [112] "Standard Test Method for Splitting Tensile Strength of Cylindrical Concrete Specimens" and direct tensile strength test inspired by Nematollahi et. al. [85] were performed on 40-mm printed cubic specimens to test the interlayer bond strength between two consecutive 3D-printed layers. For the splitting tensile test, specimens were placed between the compression plates and cylindrical metal rods were placed at the joint of two consecutive layers (Figure 3.23). The compression stress was applied on the rods and the maximum force value required for splitting the layers from each other has been determined. Splitting tensile strength values of each specimen tested were calculated according to Timoshenko [113] formula given below.

$$\sigma_{ST} = \frac{2P_c}{\pi b h}$$

where σ_{ST}: Splitting tensile strength, P_c: Magnitude of the splitting load, b: Width of the specimen and h: Height of the specimen.

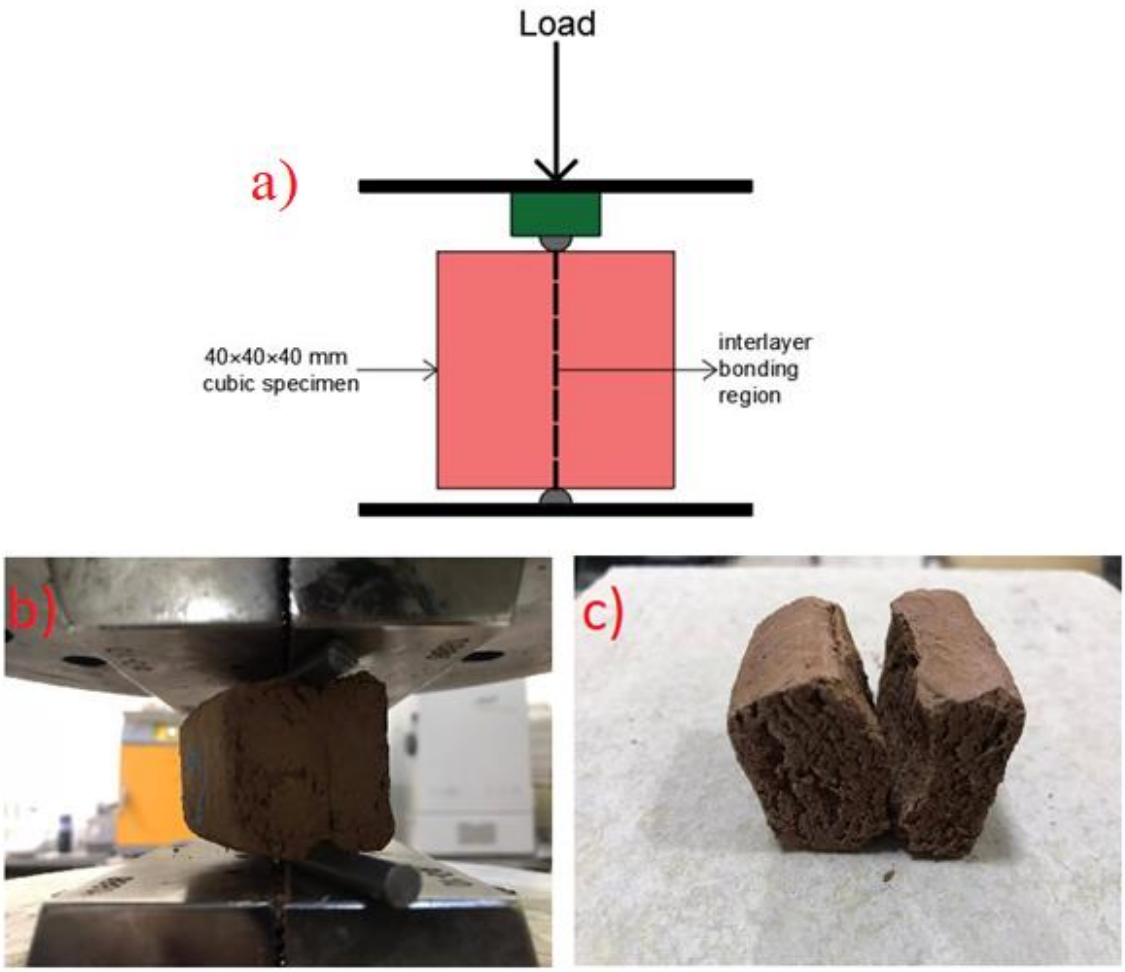

Figure 3.23 Illustration of splitting tensile test: a) general schematic view, b) sample before testing, c) sample after testing

In order to prepare the direct tensile test setup, the web parts of the T-shaped metal plates (Figure 3.24a) and two rectangular plates (Figure 3.24b), which the profile was linked, were drilled on a drill press. For the direct tensile test, the drilled T-shaped steel profiles were glued to the 40-mm printed cubic specimens 4 days before the testing with epoxy-based adhesive. The prepared epoxy was spread to the T-shaped profile and the upper and lower (parallel to bond region) parts of the sample with the help of a toothbrush and glued straightly to avoid any eccentric loading (Figure 3.25). On testing day, T-profiles glued to the specimen were connected to single-hole metal plate carefully with a pintle chain link to avoid any eccentricity during testing. Single-hole metal plates were fixed into the jaws of the tension machine and direct tensile stress was applied on the specimen (Figure 3.26). The direct tensile strength values of the printed specimens were determined by dividing the failure load by the area under tension loading. At least three duplicates of

each sample were evaluated for each curing age in both splitting and direct tensile strength tests, and the results were averaged.

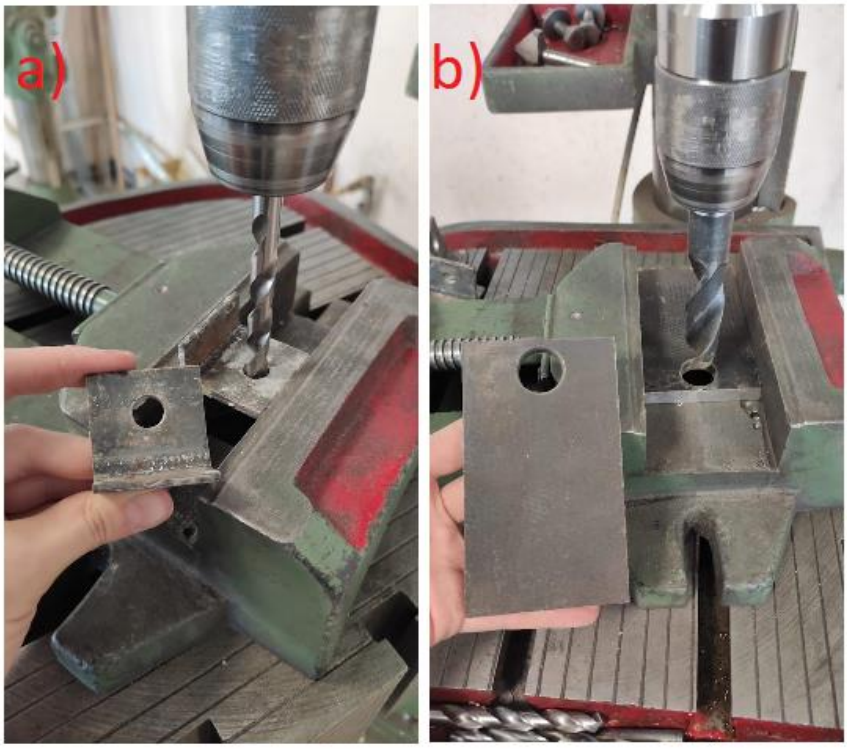

Figure 3.24 Representative images of drilling process: a) T-shaped metal plate, b) rectangular metal plate

Figure 3.25 Representative image showing glued T-shaped plates on sample

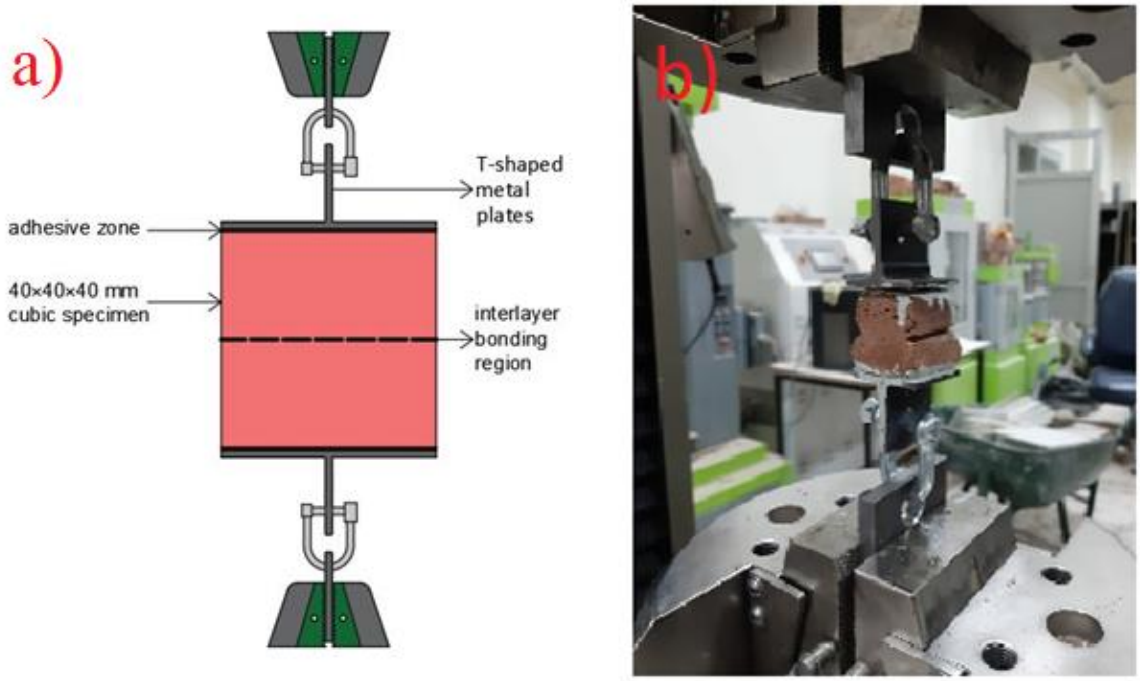

Figure 3.26 Illustration of direct tensile test: a) schematic view, b) test setup

4. RESULTS AND DISCUSSION

4.1 Change of the Open-time Rheological Behavior of Mixtures

Geopolymerization is a complex process including dissolution, gel formation with alkali activation and polycondensation. This process affects the rheology of the mixture depending on the time. The type of alkali activator type and proportion affects the fresh state characteristics of the mixture significantly. Controlling the rheological characteristics of the concrete/mortar used in 3D-AM has critical significance. Because, ensuring that the concrete is pumped uninterruptedly and smoothly from the printer's nozzle during the layering process with the 3D printer, and the production of concrete with a high yield stress in order to ensure shape stability after layer production depends on its rheological properties. For this reason, one of the most important parameters to be considered in order for the concrete to be printable is the rheological property of the concrete. In this part of the thesis, the time-related effect of the alkali activator type and proportion is examined to the flow index and the shear yield stress.

The results of the mixtures are given in Table 4.1, respectively, the results of the time-related flow table test results (flow index values) and ram extruder test results (shear yield stress) respectively. From the Table 4.1, while the shear yield stress results were in an increasing tendency, the flow index results of the mixtures tend to decrease dependent to time. Since the polycondensation reactions and alumina silicate gel precipitation progressed depending on the time, these tendencies are an expected result [114].

Table 4.1 Time-dependent flow table and ram extruder test results

NaOH (M)	$Ca(OH)_2$ (%)	Flow Index (Γ)				Shear Yield Stress (N/mm^2)			
		0.min	30.min	60.min	120.min	0.min	30.min	60.min	120.min
10	0	1,25	1,03	0,96	0,70	0,19	0,26	0,36	0,48
	4	0,77	0,73	0,64	0,44	0,28	0,32	0,43	0,54
	8	0,56	0,54	0,46	0,40	0,39	0,42	0,53	0,67
	12	0,46	0,48	0,44	0,33	0,47	0,53	0,66	0,85
12.5	0	1.02	0,81	0,58	0,44	0,28	0,43	0,51	0,75
	4	0,56	0,55	0,45	0,32	0,43	0,56	0,64	0,81
	8	0,44	0,37	0,25	0,21	0,55	0,65	0,73	1,08
	12	0,35	0,30	0	0	0,66	0,76	0,86	1,23
15	0	0,58	0,43	0,39	0,22	0,48	0,70	0,71	1,06
	4	0,54	0,39	0,42	0,20	0,54	0,74	0,85	1,17
	8	0,36	0,20	0,20	0,17	0,70	0,90	0,98	1,75
	12	0,36	0,23	0,22	0	0,77	0,96	1,15	1,76

4.1.1 Effect of NaOH Proportion on Rheological Properties

When the flow table and ram extruder test results of the mixtures are examined at 0, 30, 60 and 120. minutes, the flow index decreased and shear yield stress increased as the NaOH molarity of the mixtures increased irrespective of the use of $Ca(OH)_2$ for all age conditions. From Table 4.1, when the results of flow table and ram extruder tests performed at various ages (0, 30, 60 and 120 min) starting from the time the mixtures were prepared, irrespective of $Ca(OH)_2$ usage rate for all age, the highest flow index values (lowest shear yield stress) of mixtures were obtained at 10M-NaOH, followed by 12.5M, and 15M NaOH, respectively. Flowability and extrudability decreased when the mixing NaOH molarity increased to 12.5M and 15M. In the process of geopolymerization, Al-Si particles of precursor found in the medium dissolve thanks to OH^- ions from alkaline hydroxides.[115]. Meanwhile, the Na^+ ions that comprise the process of geopolymerization form unbalanced surfaces on the particles, which creates a repulsive force between them, increasing the flowability [116]. The zeta potential formed between the particles depends on the ion concentration and pH value in the medium [116].

However, when the alkalinity of the medium increased, the Na^+ ions formed during the geopolymerization process increased and these ions decreased the repulsive force between the particles. In the mixture containing 10M NaOH, the repulsive force between Na^+ ions, which increases the flowability, decreased when it increased to 12.5M NaOH, because it brought the ion balance on the surface of the particles. Therefore, the flowability decreased above the NaOH concentration value of 10M. The increase in the number of ionic particles with the increment in molarity can be shown as a reason for reducing the flowability and extrudability by restricting the mobility between the ions [117, 118].

4.1.2 Effect of $Ca(OH)_2$ Proportion on Rheological Properties

According to ram extruder test results, increment of $Ca(OH)_2$ usage rate cause increase in shear yield stress value of geopolymer mortar mixtures. In addition, the flow index values of the mixtures reduced irrespective of NaOH molarity for all age states as $Ca(OH)_2$ usage rate increased. The increment in $Ca(OH)_2$ concentration in mixtures with similar NaOH content had a negative effect on workability/fluidity, leading the mixtures to spread less, according to flow table and ram extruder test results. Therefore, as conventional concrete, the water content has an important influence on the workability characteristic of geopolymer mixtures. [119, 120]. Therefore, the increment of $Ca(OH)_2$ which increased the powder content (decreased the water/powder ratio), could be stated as the reason for the decline of workability. Moreover, another cause for this is that more $Ca(OH)_2$ and Ca^{2+} ions accelerated the geopolymerization process by enhancing electrostatic interactions and charge neutralization. [121]. In addition, $(OH)^-$ ions in medium provided from $Ca(OH)_2$, increased dissolution rate of alumina silicate and improved acceleration of geopolymerization. This improvement resulted more rapid constitution of geopolymer matrix and decreased rigidity time of geopolymer [122, 123]. Another possible factor in the decrease of the extrudability and flowability properties with the increment in the amount of $Ca(OH)_2$ in the mixture is that the calcium reacted with the dissolved alumina silicates in the medium to form CSH and CASH products forming a rigid matrix structure [124, 125]. Furthermore, consuming H_2O during the production of CSH and CASH gels enhanced the density of (OH)- ions and alkalinity in the medium. In the high alkali environment, the dissolution rates of alumina silicates increased and geopolymerization accelerated [51, 124-126].

4.1.3 Open-time Rheological Properties

Although it is stated in the literature that the incorporation of $Ca(OH)_2$ with geopolymers prepared with mainstream (commonly used) alumina silicate precursors has an accelerating influence on the setting time of the geopolymers [124, 126, 127], in accordance with the results of flow table and ram extruder, this effect of $Ca(OH)_2$ was not prominent for geopolymer mortar mixtures. The significantly low Si concentration found in CDW-based precursors utilized in this study compared to typical mainstream precursors can be related to the absence of quick curing observed in the presence of Ca(OH)2 (e.g., MK). As it is known, dissolved Ca^{2+} originating from $Ca(OH)_2$ reacts with Si in the medium to create strength-enhancing compounds. In the later stages of the geopolymerization process, the setting time of the mixtures was prolonged due to the insufficiency of Si ions in the system, which reacted with dissolved Ca^{2+} ions and shortened the setting time of the geopolymer.

According to flow table test results mixtures produced with 10M-NaOH were workable after 120 min. from initial mixing and mixture has 12.5M NaOH and %8 $Ca(OH)_2$ was workable after 60 min from initial mixing. As a result of the ram extruder test, all mixtures activated by 10M- and 12.5M NaOH showed workable and printable properties. Mixtures with 10M and 12.5M NaOH contents, which were tested by a ram extruder, retained their extrudability for up to 60 minutes and extruded out of the nozzle continuously, without any clogging and disintegration. (Figure 4.1a). However, the mixtures activated with 15M NaOH lost their extrudability properties 60 minutes after the initial mixing time and extruded discontinuously from the nozzle tip (Figure 4.2b). In addition, incorporation of 12% $Ca(OH)_2$ into all mixtures irrespective of NaOH caused decrement in flow index significantly. The flow was not observed in the flow table test after 60 minutes of mixing in mixtures containing 12.5M NaOH, and after 120 minutes in mixtures containing 15M NaOH. Therefore, within the scope of the thesis, the mechanical properties tests were carried out on 3D printable mixtures activated with the different combinations of 10M, 12.5M NaOH and 0, 4, 8% (by weight of powder content) $Ca(OH)_2$.

Figure 4.1 Representative images of extruded mixtures: a) continuously extruded, b) discontinuously extruded.

4.2 Compressive Strength

Mechanical performances of the 3D-printed specimens including compressive strength can vary with the loading direction since the 3D-printing process is a production method based on adding layer upon layer of material, resulting in interlayer bond (adhesion) zone between successive printed layers. Because the bond interface of layers has weaker mechanical properties than the core region of subsequent layers, a performance dependency, termed as anisotropy, emerges due to the loading and printing direction [128]. Therefore, to evaluate the anisotropic mechanical behavior of the additive manufactured samples and to compare the influences of the manufacturing process on the mechanical performances of the geopolymer mortars produced with entirely CDW, compressive strength tests were performed on both the mold-casted and 3D-printed (for three different loading such as lateral, parallel and perpendicular to printing path) specimens. Figure 4.2 shows the average compressive strength test results of 7-day, 28-day and 90-day-old geopolymer mortar samples manufactured by the single utilize of NaOH and combination of $Ca(OH)_2$-NaOH are presented. Independent of other mixing parameters and loading circumstances, the compressive strength test results of the 7-day, 28-day, and 90-day printed specimens demonstrate that the mechanical performances of the specimens show a trend towards continuous improvement due to the continuation of geopolymerization reactions in the maturing matrix. At the end of 90-day, maximum

compressive strength results recorded for the mold-casted, perpendicular-, parallel-, and lateral-loaded printed specimens were 20.5 MPa [10M NaOH - 8% $Ca(OH)_2$], 21.5 MPa [10M NaOH-4%$Ca(OH)_2$], 19.9 MPa [10M NaOH-4%$Ca(OH)_2$] and, 17.5 MPa [10M NaOH-8%$Ca(OH)_2$], respectively. In general, the findings indicate that printed specimens exhibit comparable compressive strengths to the mold-casted specimens in different loading directions, regardless of the mixture design; however, the loading direction and alkaline activator content cause differences in the mechanical performances. Therefore, a detailed discussion of how the mechanical performances is affected by the production method of the specimens, alkali activator contents, and loading directions is presented in the following sections.

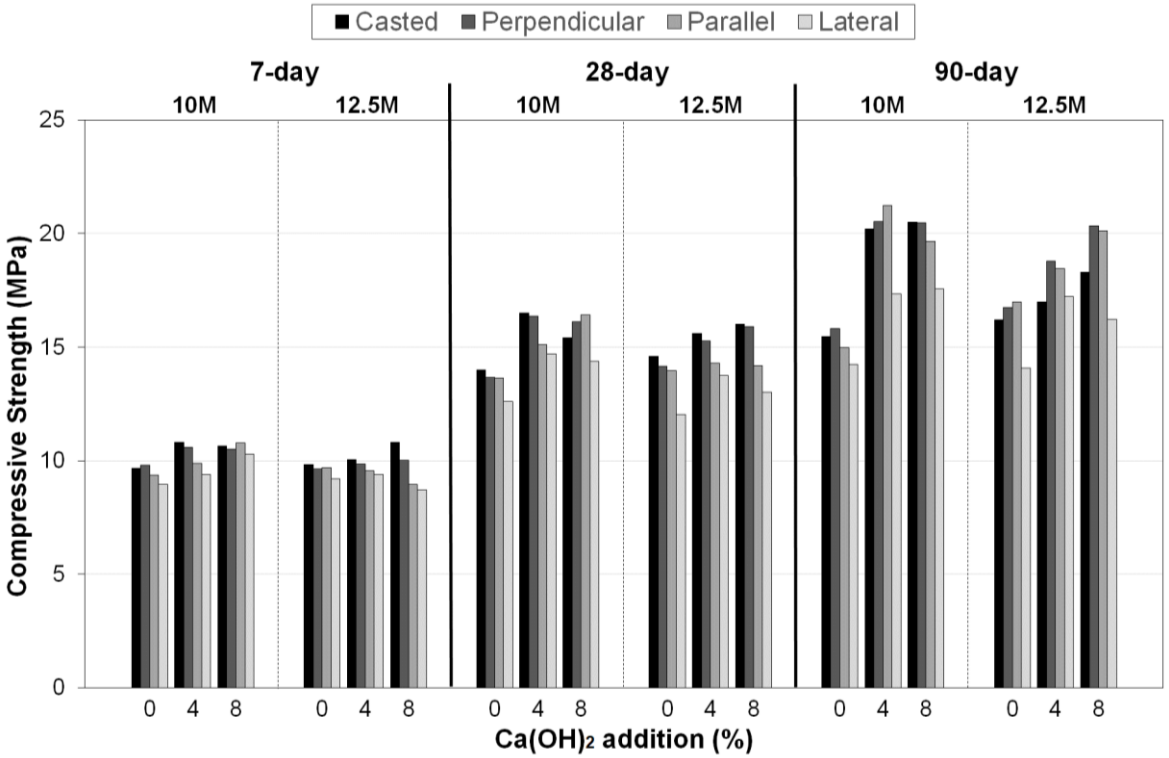

Figure 4.2 Average compressive strength test results of 3D-printed and casted geopolymer specimens

4.2.1 Effect of Alkaline Activators on the Compressive Strength

On the situation that other mixture design parameters were same, although some variations were observable, an increase in the NaOH molarity from 10 to 12.5 resulted in higher compressive strength test results of the mixtures with singly NaOH activation. According to the current literature, when the NaOH molar concentration is increased, an

increment in the strength of the geopolymer mixtures can be expected, but a decrease is also possible. An increase in the NaOH molar concentration increases the alkalinity of the reaction medium and encourages the dissolution of the precursors resulting in increase in dissolved Si and Al ions, which can increase the strength of the geopolymers [129-131]. However, a higher dissolution rate compared to geopolymerization rate results the presence of excess dissolved ions in the reaction medium [117, 132, 133] and this causes (i) due to the obvious repulsive forces between the particles, ion movement is restricted. [117, 118, 134] and (ii) greater Na^+ and $(OH)^-$ ions in the reaction medium cause increased silica coagulation and accelerated hardening. [135]. As a result, the increment in the compressive strength results from the increased NaOH concentration can be linked to higher alkalinity of the geopolymerization medium and thereby higher dissolution of the precursors.

According to the compressive strength test results of both mold-casted and printed specimens given in Figure 4.2, common trends were not noted for the compressive strength test results when the $Ca(OH)_2$ utilization rate of the mixtures were increased from 0 to 8% and other parameters were same. In order to discuss the possible reasons for this, $Ca(OH)_2$-related influencing factors on the compressive strength need to be properly explored and taken into account. Some research in the current literature indicates that the mechanical performance of geopolymer mortars improves as the usage rate of $Ca(OH)_2$ increases, and this has been linked to the (i) enhancement in the dissolution of the alumina silicate precursor with increasing $(OH)^-$ ions in the reaction medium resulting in more active groups available to participate in the geopolymerization reactions [122, 123], (ii) increase in the precipitation of the CSH and CASH gels and nucleation sites for production of geopolymerization products [123-127, 136], (iii) ionic charge balancing and seeding effect [25, 126, 137, 138] and (iv) $CaCO_3$ formation [122, 130]. On the other hand, it was reported that the excessive increase in the utilization rate of $Ca(OH)_2$ decreases the strength of the geopolymer mixtures and the reasons for this were stated as follows: (i) lower ionic mobility because of higher ionic concentration [117], (ii) disruption of the optimal gel binder structure because of excess lime content [126], (iii) presence of unreacted lime in the matrix resulting the creation of the faults in the microstructure [139]. As can be followed from Figure 4.2, the enhancing impact of the $Ca(OH)_2$ on compressive strength results was generally observed for casted and perpendicular-loaded printed specimens. However, as the utilization rate of $Ca(OH)_2$

increased from 4% to 8%, in mixtures activated by 10M-NaOH, decreases in compressive strength were observed. This can be related to the unreacted lime content and observing negative effect of $Ca(OH)_2$ at lower molarities can be attributed to the presence of lower amount of reactive dissolved Si and Al species to be reacted arising from lower dissolution of alumina silicate materials in the reaction medium with lower alkalinity [118, 140]. In addition to the above-mentioned chemical effects, a relationship can be posited between the influence of $Ca(OH)_2$ on the fresh characteristics of mixtures and its effect on the compressive strength and this can be a reason for observed varied behaviors. As known in the literature [51, 84], decrease in the utilization rate of $Ca(OH)_2$ increases the flowability of the geopolymer mortars, and with the increase in flowability it becomes easier to print fresh mixtures more homogeneously and improve the adhesion of two consecutive printed layers. This can influence the compressive strength performance of the mixtures. In this regard, the negative impact of the $Ca(OH)_2$ on compressive strength generally observed for lateral- and parallel-loaded printed specimens (especially for mixtures including 12.5M-NaOH alkaline activator in case of the increment in the usage rate of $Ca(OH)_2$ from 4% to 8%) can be associated with the influence of the $Ca(OH)_2$ on the fresh characteristics.

4.2.2 Anisotropic Behavior and Effect of Loading Direction

When the compressive strength performance of the mixtures is compared, the compressive strength characteristic of the mold-casted specimens was lower than specimens loaded perpendicular to printing directions, irrespective of curing age. Many previous studies that compared compressive strength characteristic of 3D-printed and mold-casted samples have also reported that 3D-printed samples could exhibit greater compressive strength than mold-casted specimens [73, 141]. This can be explained by the formation of a relatively denser matrix due to the pump pressure during printing. When evaluating loading direction dependence of the compressive strength data of the mixtures, it can be concluded that 3D-printed samples loaded in perpendicular to nozzle movement direction generally had better strength results, which is consistent with the studies of [72, 86], although some natural variations were observed. Higher strength results of the perpendicular loaded specimens can be attributed to the fact that the loading direction is perpendicular to the bond region. When compressed under perpendicular direction loading, the bond zone between the successive printed layers is forced to come together

[73]. In this regard, the load is transmitted directly through the printed specimen without any negative effect of the bond zone, that can be possible reason for the higher performance of the printed specimens under perpendicular loading [142]. This can be also evidenced by the fracture patterns of the different-direction-loaded printed specimens. When a uniform compressive stress is applied to specimens, microcracks start to occur in the matrix at early stage of loading. As the stress is increased, the cracks begin to propagate throughout the matrix (a growth in diagonal directions). When the stress rises above the critical value, it causes a bridge to form between the cracks formed in the matrix and failure occurs. Therefore, the expected failure shape after the compression test is hourglass [143]. When the failure patterns of the specimens are examined from Figure 4.3, it can be concluded that perpendicular loaded printed specimens had hourglass-shaped, which means that the compressive stress is distributed uniformly throughout the perpendicular-loaded specimens, as in the mold-casted specimens. On the other hand, parallel- and lateral-loaded specimens exhibited a different fracture pattern than the generally expected one under compressive stress. For lateral and parallel to printing path loading, after cracks created by compressive loading on the specimens reached the interface bond region, these cracks preferred to propagate along this bonding region resulting separating of the layers from each other (Figure 4.3) [73, 142, 144]. These types of crack propagation caused relatively brittle failure mode and hence lower compressive strength results for parallel- and lateral-loaded printed specimens were obtained compared to perpendicular-loaded ones. Taking all of this into account, it is reasonable to conclude that the microcracks' line of propagation has a considerable influence on the mechanical performance of the printed specimens. In addition to the factors given above, it is possible that efficient compaction of the fresh mixtures in the perpendicular direction due to the own weight of the extruded layers might be another factor contributing to superior compressive strength performances under perpendicular loading. The compressive strength characteristics of parallel-loaded specimens were higher than those of lateral-loaded specimens, which can be attributed to the increased intensity of the fresh mixture in parallel to nozzle movement direction due to the effect of the considerable pumping pressure on the 3D-printed layer over the extrusion process [73, 78, 93, 145, 146].

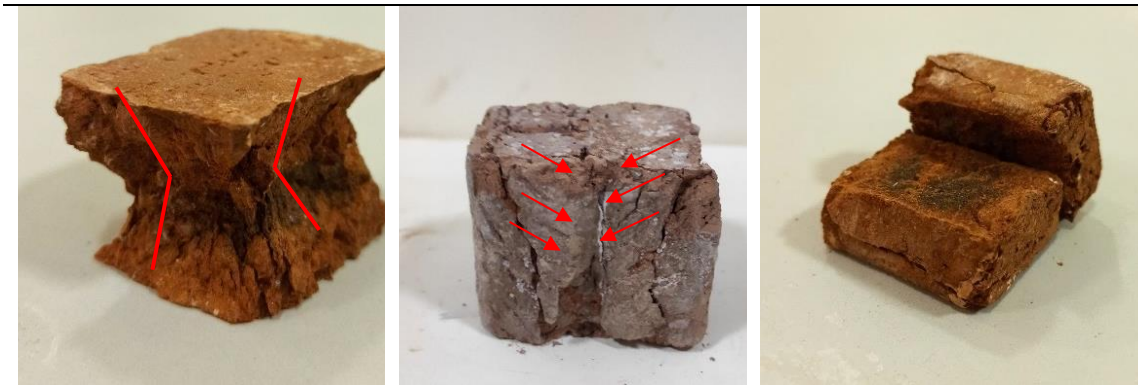

(a) (b) (c)

(d)

Figure 4.3 Representative images showing details of failure mode of compression test specimen in a) perpendicular b) parallel c) lateral direction d) casted specimen

According to TBEC 2018 [147] the mortar compressive strength of masonry walls varies between 1.4 and 14.6 MPa, depending on the mortar class. According to IBC 2015 [148], the compressive strength of the masonry must be 2.07 MPa on average and at least 1.7 MPa. The compressive strengths of masonry structures determined in MSJC and based on the work of Noland and Kingsley [149] should be between 10.34 and 27.58 MPa. According to the compressive strength test results of this study, strength characteristics of the 100% CDW-based geopolymer mortar specimens met the values of all three standards for construction of masonry walls.

4.3 Flexural Strength

Flexural strength of 3D-printed CDW-based geopolymer mortar specimens were tested for the loading in the directions of lateral and perpendicular to the printing path to evaluate performance differences between mold-casted and layered specimens, anisotropic

behaviour of the 3D-printed specimens, and effects of alkaline activator content on the flexural performance of the mixtures. The 7-, 28- and 90-day average flexural strength test results of both mold-casted and 3D-printed specimens cured under ambient conditions are shown in Figure 4.4. The flexural performance of the mixtures improved continuously with prolonged curing ages because of ongoing geopolymerization [150]. Maximum flexural strength results for mold-casted, perpendicular-loaded and lateral-loaded 3D-printed specimens were recorded from the geopolymer mortar mixtures with 10M NaOH and 4% $Ca(OH)_2$ alkaline activator content. The average flexural strength reached the maximum values of 4.9 MPa, 6.6 MPa, and 4.7 MPa for the mold-casted specimens, perpendicular-loaded and lateral-loaded 3D-printed specimens after 90-day ambient curing, respectively. Obtained flexural strength results of perpendicular-loaded and lateral-loaded 3D-printed specimens were compatible with several research results [85, 86, 88, 89, 91, 94, 151, 152]. Results demonstrated that flexural strength of 3D-printed specimens loaded in perpendicular to nozzle movement direction were greater than those of both mold-casted and lateral-loaded 3D-printed specimens. In general, mold-casted and lateral-loaded 3D-printed specimens showed similar performance for early and later age, with slight deviations.

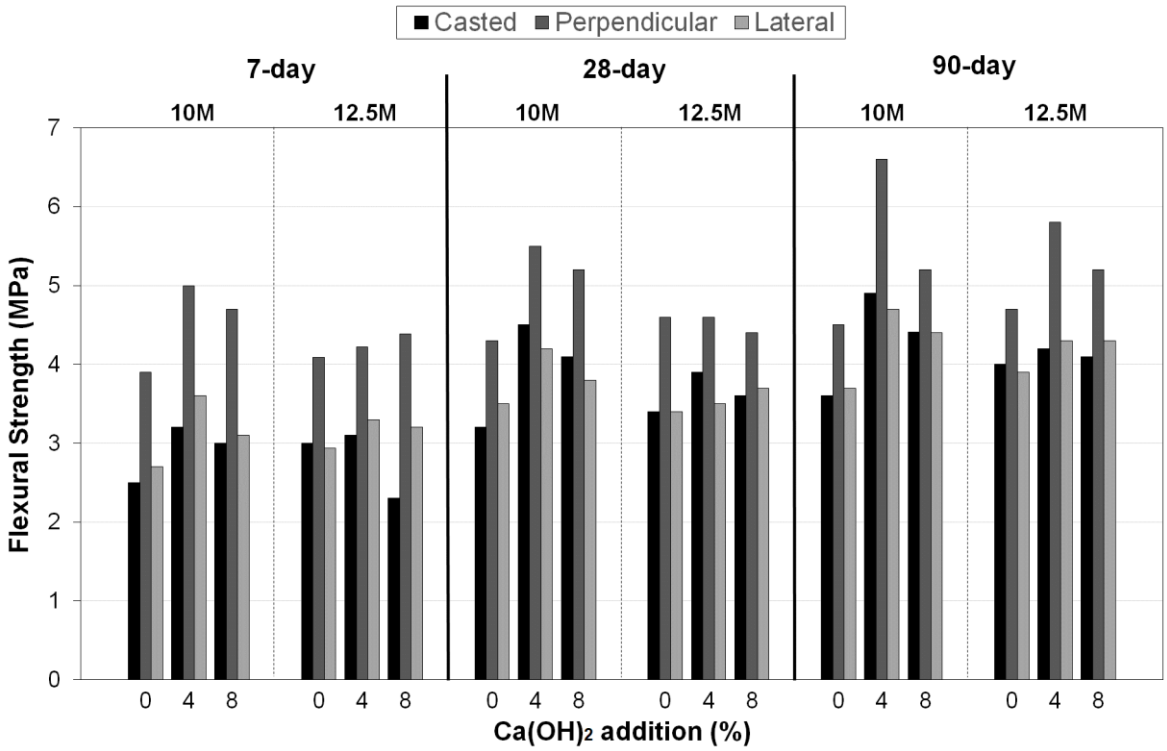

Figure 4.4 Average flexural strength results of mold-casted and 3D-printed geopolymers activated with various combinations of alkaline activators cured at ambient condition.

4.3.1 Effect of Alkali Activators

According to the obtained results, flexural strength result of the mold-casted specimen activated with solely 10M NaOH were lower than those of casted specimen activated with 12.5M NaOH. Similar results were also obtained from the 3D-printed geopolymer mixtures activated with the solely NaOH. Increment of NaOH molarity, therefore, was favorable for the flexural strength characteristic of CDW-based geopolymer mortar mixtures activated with solely NaOH. The possible reasons discussed in compressive strength results for the positive effects of NaOH increment on strength were also valid for flexural strength results.

Inclusion of $Ca(OH)_2$ into solely NaOH activated mixtures yielded increment in flexural strength of both casted and 3D-printed specimens, since increment of "Ca" sources in the medium may lead to the formation of more strength-giving geopolymer products (C(A)SH, NASH, etc.) in the matrix and effective bond area [123-127, 136]. However, addition of 8% $Ca(OH)_2$ either decreased or did not make a positive contribution to the

flexural strength of CDW-based geopolymer mixtures, irrespective of NaOH molarity. The possible effects of 8% $Ca(OH)_2$ addition could be due to lower ionic mobility, disruption of gel structure, presence of unreacted lime [117, 126, 139]. Besides, for the 3D-printed specimen, increment of $Ca(OH)_2$ content in matrix may lead the formation of weakness on effective bond area because of the redundant increment of viscosity.

The trend observed from the compressive strength test results of casted and perpendicular-loaded 3D-printed specimens activated with 12.5M NaOH and 8% $Ca(OH)_2$ did not coincide with flexural strength of same mixtures. The possible reason could be attributed to the variation on the fracture mechanism and load distribution on the specimens and test methods since compression test results of lateral- and parallel-loaded 3D-printed specimens have coincided with flexural strength test results of both mold-casted and 3D-printed specimens. For the flexural strength, applied load was directly delivered to effective bond area that making the bond area more essential than the matrix. Although increment in $Ca(OH)_2$ content may cause more geopolymerization products in matrix, due to more viscous structure, more voids may be formed on the effective bond area which may lead the reduction of flexural strength with increment of $Ca(OH)_2$ from 4% to 8% in the mixtures including 12.5M NaOH [146]. Namely, the effect of the enhancement in the geopolymer matrix in favor of flexural strength could not overcome the negative effect of the high viscosity resulting weakness of the bonding zone.

4.3.2 Direction-dependence of Mechanical Properties

In addition to alkaline activator effects, anisotropic behavior of the mixtures was examined by considering flexural performance of the 3D-printed specimens. In accordance with the obtained test results, flexural strength of the mold-casted specimens was similar or lower than the that of 3D-printed specimens for each testing age. The possible reason for improved performance on flexural strength for 3D-printed specimens (although decrement was expected because of layer by layer production) was due to the better compaction of the mixtures by the high-pressurized pump; by considering the fact that amount of air void in the specimen is significantly effective on the flexural strength [141]. More air void formation was observed in the geopolymer specimens during casting in comparison with the 3D-printed geopolymer specimens, as developed CDW-based geopolymer has sticky nature because of clay origination [51, 84].

During the printing process, because of both the weight of the upper layer and pushing of pressurized consecutive materials by pump, better compaction was achieved on the bottom layer of prismatic specimens. Manufacturing-related factors are significantly effectual on the performance of the mixtures. Moreover, load distribution pattern of 3D-printed specimen was also influential on the performance of CDW-based geopolymer mortar mixtures. In accordance with the obtained results, perpendicular-loaded 3D-printed specimen had higher flexural strength than that of lateral-loaded one for each mixture and testing age. Since, during flexural strength testing in perpendicular direction, first layer, which was more compacted and bonded, was in the tension zone, it yielded better performance. Moreover, 3D-printed specimens loaded in the lateral direction tended to separate from the weak bond area between two consecutive printed layers, causing them to fail quickly in flexural loading. When the fracture behaviors are examined, the fracture behavior presented in Figure 4.5a is close to parallel to the perpendicular reference line. However, when Figure 4.5b is examined, the fracture behavior is parallel to the reference line until it reaches the bond area, then deviated. The weakness in this area may cause deviation in the cracking path and the flexural strength to decrease by up to %29 considering the printing direction.

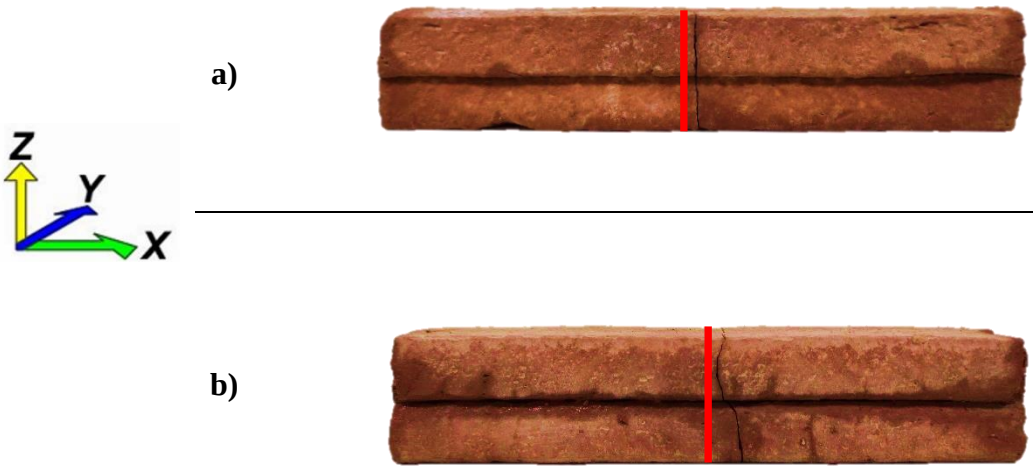

Figure 4.5 Representative images showing details of failure mode of flexural test specimen in a) perpendicular (loaded in z axis) b) lateral direction (loaded in y axis)

4.4 Direct and Splitting Tensile Strength (Bond Strength)

7-, 28- and 90-day direct and splitting tensile test results of the 3D-printed specimens stored at ambient conditions are represented in the Figure 4.6. As followed from the figure, tensile strength results obtained from both splitting and direct test methods were consistent with each other, generally. The bond strength result of the mixtures increased continuously with the prolonged curing ages as a result of ongoing geopolymerization reaction. 10M NaOH and 4% $Ca(OH)_2$ activation provided maximum strength in geopolymer mortars with regards to splitting and direct tensile strength for each curing age. The direct and splitting tensile strength results reached the maximum values of 1.35 and 1.79 MPa after 90-day ambient curing, respectively.

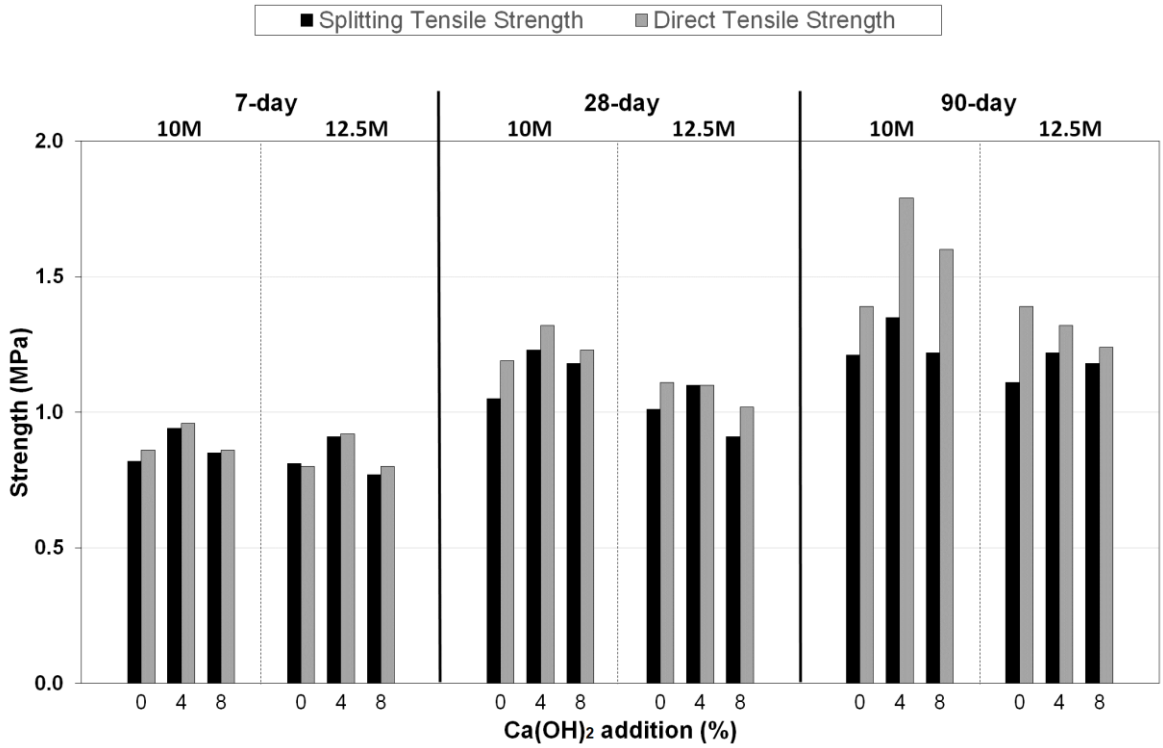

Figure 4.6 Average splitting and direct tensile strength results of 3D-printed CDW-based geopolymer mixtures.

On contrary to the compressive and flexural strength test results, increment in NaOH molarity did not lead to increment in splitting and direct tensile strength test results of the CDW-based geopolymer mortar mixtures. Basically, on one hand, increment in NaOH molarity may increase in the dissolution of precursor materials and, resulting increase in the production of geopolymerization products, on the other hand, the viscosity of the mixtures may increase, leading to the formation of voids in the matrix and weak bonding capacity (weak effective bond area) between consecutive printed layers [51, 84, 146]. According to the obtained results, the bond strength of CDW-based geopolymer mixtures rose with the usage of $Ca(OH)_2$ up to 4%, irrespective of NaOH molarity. Increment in bond strength could be attributed to formation of more geopolymerization products on effective bond area and matrix (Figure 4.7a), and improved interfacial transition zone between geopolymer paste and aggregate due to lower porosity with the existence of high calcium content [153-155]. The relatively low tensile strength results of geopolymer mixtures activated with 10M and 12.5M NaOH containing more than 4% $Ca(OH)_2$ can be explained by the fact that, unreacted excessive alkaline activator content disrupts the

homogeneity of the mixture and, decreased workability with the increased $Ca(OH)_2$ content may lead to having weak bonding between layers as formed voids prevent the synthesis of strength-giving products between layers (Figure 4.7b). The tensile strength results of CDW-based geopolymer mortars in the current research were comparable with those reported by several researchers [95, 96, 98, 152].

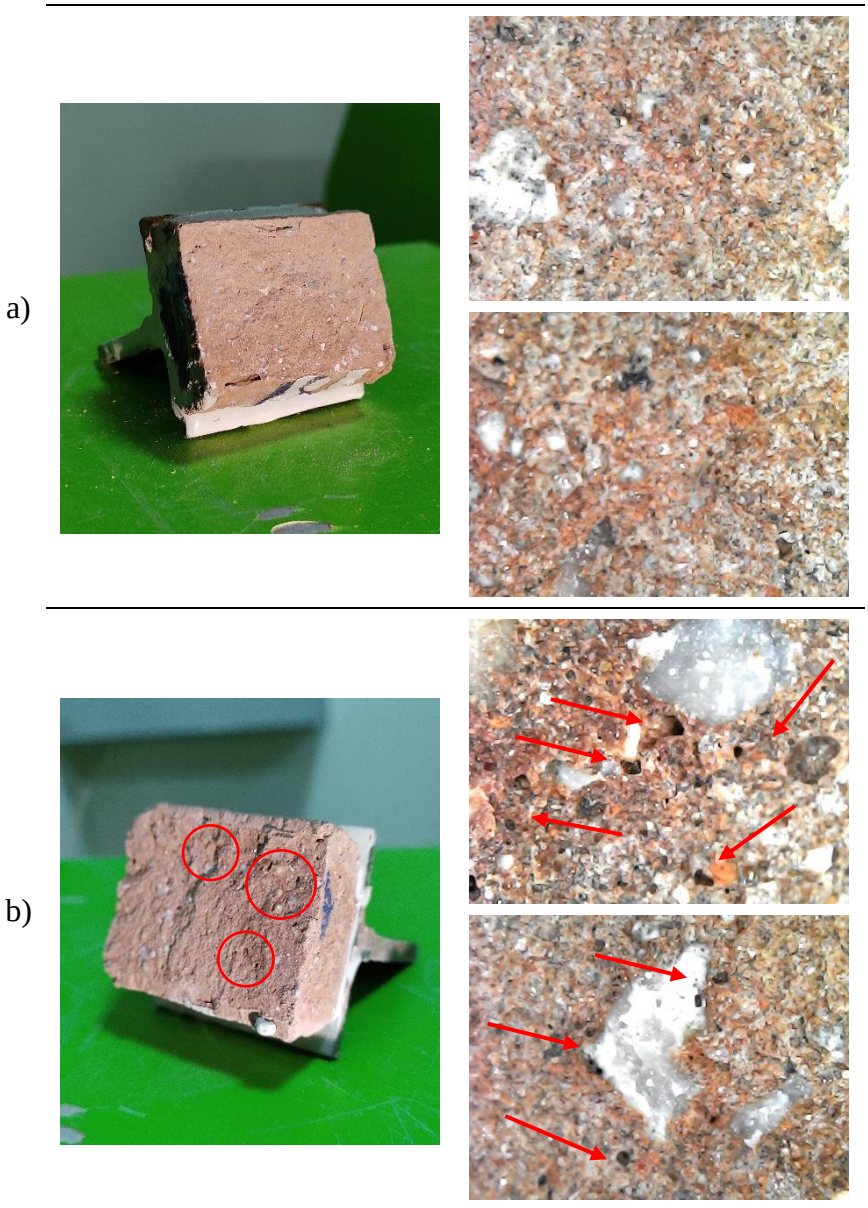

Figure 4.7 Representative general and close-up (area with the size of 3.2 x 2.4 mm) views of a) non-porous and, b) porous bond zone.

Results showed that mechanical properties of 3D-printed 100% CDW-based geopolymer mortars are driven by viscosity of the mixtures and geopolymerization simultaneously. Improvement in the matrix due to alkaline content was more influential for the mechanical performance of mold-casted and also for the perpendicularly-loaded printed specimens due to the formation of less stress on the bond area. However, viscosity properties had more dominant effects on mechanical properties of the parallelly- and laterally-loaded specimens since the applied load concentrated on the bond area, and adhesion between

layers was mainly affected by fresh properties. Findings proved that bond performance between layers is one of the main reasons for the anisotropic behavior of 3D-printed structures. Furthermore, bond strength evaluation showed that although the matrix was enhanced with the alkaline content optimization, due to higher viscosity properties resulting in poor adhesion between layers, lower bond strength performance was recorded from geopolymer mortars. Outcomes of the current study pointed out that to eliminate the anisotropic performance of printed structures, bond adhesion between layers should be taken into account considering viscosity properties in addition to matrix performance while designing mixtures. With the improved bond adhesion, therefore it will be possible to diminish directional performance variations for the 100% CDW-based geopolymer systems.

5. CONCLUSIONS

This thesis study aimed to evaluate rheological and direction-dependent performance of 3D-printed 100% CDW-based geopolymer mortars. In addition to this, the study focused on determining the influence of alkaline activators on the mechanical characteristics of 3D-printed geopolymer mortars including compressive, flexural and bond strength. 3D-printed and mold-casted specimens' performances were also compared with each other to examine manufacturing method-related variations in the mechanical properties of the geopolymer mortars. A combination of RT, HB, RCB, CW and GW were used in mixtures as precursors and solely grinded and sieved CW was used as fine aggregates. The geopolymer mixtures were activated with 7.5M, 10M, 12.5M and 15M NaOH and 0%, 4%, 8% and 12% (by total weight of precursor) $Ca(OH)_2$ in various combinations, and specimens were cured in ambient conditions. To determine open-time rheological behavior of geopolymer mortars, flow table and ram extruder test were carried out. Anisotropic behavior of manufactured samples was determined by mechanical tests including compressive and flexural strength test in different loading directions. Moreover, interlayer bond strength of layer-by-layer manufactured samples was determined by direct tensile and splitting tensile test.

Within the scope of the thesis, the following conclusions of the tests examining the rheological properties of the mixtures and the anisotropic behavior of 3D printed samples were presented:

- Workability properties of geopolymer mixtures showed decreasing trend when NaOH molarity increased. In accordance with the flow table test results, the flow index values revealed a decreasing trend as NaOH increased. Another result showing that NaOH reduced the workability was also seen in the ram extruder test results. A clean increasing trend was observed with the shear yield stress value as the NaOH molarity increased. This trend was attributed to the ion balance of dissolved particles which reduced repulsive force between them.

- Activation of the mixtures with $Ca(OH)_2$ had a negative influence on the workability of the mixtures. Combination of $Ca(OH)_2$ decreased the flow index value and increased the shear yield stress value regardless of NaOH molarity. This is explained by the fact that the utilize of $Ca(OH)_2$ increased the amount of powder in the mixture and accelerated the geopolymerization process.

- Incorporation of 10M, 12.5M NaOH and 0, 4, 8% $Ca(OH)_2$ into mixtures showed 3D printable properties at open-time. However, the workability and extrudability properties of mixtures containing 15M NaOH and all mixtures activated with 12% $Ca(OH)_2$ were found to be incapable for 3D-AM in that the mixtures extruded the nozzle fractured and discontinuously 60 minutes after mixing.

- Increment of the NaOH molarity from 10 to 12.5M enhanced the flexural and compressive strengths of the mold-casted and 3D-printed specimens, regardless of the curing age, for mixes activated by utilizing singly NaOH. However, when the NaOH molarity increased, the 3D-printed samples' splitting and direct tensile strength dropped, most likely owing to an increase in the viscosity of the mixtures, resulting in weaker adhesion at the interface bonding area between the layers.

- The incorporation of $Ca(OH)_2$ at a 4% usage rate enhanced the mechanical characteristics of CDW-based geopolymer mortars. However, beyond a 4% $Ca(OH)_2$ usage rate, no positive influences of $Ca(OH)_2$ utilization on mechanical characteristics (excluding compressive strength) were detected, most likely because large increases in mixture viscosity suppressed the positive influence of $Ca(OH)_2$ in geopolymerization.

- After 90-day ambient curing, the highest compressive strength results recorded for the casted, perpendicular-, parallel-, and lateral-loaded 3D-printed specimens were 20.5, 21.5 MPa, 19.9 MPa and, 17.5 MPa, respectively. These results met the values of relevant standards for construction of masonry walls. Maximum 90-day flexural strength results for the casted, perpendicular- and lateral-loaded 3D-printed specimens were obtained as 4,9 MPa, 6.6 MPa and 4.7 MPa. For the tensile strength, maximum direct and splitting tensile strength results of 1.35 and 1.79 MPa were reached after 90-day ambient curing, respectively.

- In accordance with mechanical properties tests carried out in different directions, the samples produced by 3D-printing showed anisotropic behavior. According to compressive strength test results in three different loading direction such as lateral, perpendicular and parallel to nozzle movement direction, irrespective of the curing age, perpendicular-loaded specimens showed the highest compressive strength among the three different loading direction. In addition to this, mold-casted specimens exhibited lower compressive strength performance compared to

perpendicular-loaded 3D-printed specimens whereas showed higher strength results than parallel- and lateral-loaded 3D-printed specimens.

- As a result of the flexural strength tests carried out in two different directions, the sample under loaded in the perpendicular direction to the nozzle movement showed more flexural strength than the sample loaded in the parallel direction to the nozzle movement. As in the compressive strength tests, perpendicular-loaded specimens exhibited higher flexural strength performance than mold-casted ones. In addition, lateral-loaded and mold-casted specimens showed similar flexural performances.

- It can be concluded that geopolymer specimens showed anisotropic properties in compressive strength and flexural strength tests. In compressive strength results of the 3D-printed specimen loaded in different directions, the maximum direction-dependent variations reached the level of 20%, while this level was 30% for flexural strength. The anisotropic behavior of the 3D-printed geopolymer mortar specimens is thought to be a natural feature of the layer-by-layer printing process.

6. REFERENCES

[1] A.P. Gursel, C. Ostertag, Comparative life-cycle impact assessment of concrete manufacturing in Singapore, The International Journal of Life Cycle Assessment, 22 **(2017)** 237-255.

[2] S.J. Davis, N.S. Lewis, M. Shaner, S. Aggarwal, D. Arent, I.L. Azevedo, S.M. Benson, T. Bradley, J. Brouwer, Y.-M. Chiang, Net-zero emissions energy systems, Science, 360 **(2018)** eaas9793.

[3] S.A. Miller, F.C. Moore, Climate and health damages from global concrete production, Nature Climate Change, 10 **(2020)** 439-443.

[4] U.G. Survey, Mineral commodity summaries, US Geological Survey, 198 **(2019)** 2011.

[5] M. Taylor, C. Tam, D. Gielen, Energy Efficiency and CO2 Emissions from the Global Cement Industry, 50 **(2006)**.

[6] M.M. Sabai, M.G.D.M. Cox, R.R. Mato, E.L.C. Egmond, J.J.N. Lichtenberg, Concrete block production from construction and demolition waste in Tanzania, Resources, Conservation and Recycling, 72 **(2013)** 9-19.

[7] C. European, E. Directorate-General for, Resource efficient use of mixed wastes improving management of construction and demolition waste : final report, Publications Office**2017**.

[8] H. Yuan, A.R. Chini, Y. Lu, L. Shen, A dynamic model for assessing the effects of management strategies on the reduction of construction and demolition waste, Waste management, 32 **(2012)** 521-531.

[9] M. Bravo, J. de Brito, J. Pontes, L. Evangelista, Mechanical performance of concrete made with aggregates from construction and demolition waste recycling plants, Journal of Cleaner Production, 99 **(2015)** 59-74.

[10] A. Arulrajah, M. Ali, M.M. Disfani, J. Piratheepan, M. Bo, Geotechnical performance of recycled glass-waste rock blends in footpath bases, Journal of Materials in Civil Engineering, 25 **(2013)** 653-661.

[11] M. Contreras, S.R. Teixeira, M.C. Lucas, L.C.N. Lima, D.S.L. Cardoso, G.A.C. da Silva, G.C. Gregório, A.E. de Souza, A. dos Santos, Recycling of construction and demolition waste for producing new construction material (Brazil case-study), Construction and Building Materials, 123 **(2016)** 594-600.

[12] A. Arulrajah, M. Ali, M.M. Disfani, S. Horpibulsuk, Recycled-glass blends in pavement base/subbase applications: laboratory and field evaluation, Journal of materials in Civil Engineering, 26 **(2014)** 04014025.

[13] B. García de Soto, I. Agustí-Juan, J. Hunhevicz, S. Joss, K. Graser, G. Habert, B. Adey, Productivity of digital fabrication in construction: Cost and time analysis of a robotically built wall, Automation in Construction, 92 **(2018)**.

[14] D. Castro-Lacouture, Construction automation, Springer handbook of automation, Springer**2009**, pp. 1063-1078.

[15] T. Bock, The future of construction automation: Technological disruption and the upcoming ubiquity of robotics, Automation in Construction, 59 **(2015)**.

[16] R. Maskuriy, A. Selamat, P. Maresova, O. Krejcar, O. David, Industry 4.0 for the Construction Industry: Review of Management Perspective, Economies, 7 **(2019)** 14.

[17] F. Bos, R. Wolfs, Z. Ahmed, T. Salet, Additive manufacturing of concrete in construction: potentials and challenges of 3D concrete printing, Virtual and Physical Prototyping, 11 **(2016)** 209-225.

[18] G. Beersaerts, S.S. Lucas, Y. Pontikes, An Fe-Rich Slag-Based Mortar for 3D Printing, RILEM International Conference on Concrete and Digital Fabrication, Springer, **2020**, pp. 3-12.

[19] E. Lloret, A.R. Shahab, M. Linus, R.J. Flatt, F. Gramazio, M. Kohler, S. Langenberg, Complex concrete structures: Merging existing casting techniques with digital fabrication, Computer-Aided Design, 60 **(2015)** 40-49.

[20] P. Shakor, J. Sanjayan, A. Nazari, S. Nejadi, Modified 3D printed powder to cement-based material and mechanical properties of cement scaffold used in 3D printing, Construction and Building Materials, 138 **(2017)** 398-409.

[21] J. Biernacki, J. Bullard, G. Sant, K. Brown, F. Glasser, S. Jones, M. Ley, R. Livingston, L. Nicoleau, J. Olek, F. Sanchez, R. Shahsavari, P. Stutzman, K. Sobolev, T. Prater, Cements in the 21 st Century: Challenges, Perspectives, and Opportunities, Journal of the American Ceramic Society, 100 **(2017)**.

[22] S. Keating, N.A. Spielberg, J. Klein, N. Oxman, A compound arm approach to digital construction, Robotic Fabrication in architecture, art and design 2014, Springer**2014**, pp. 99-110.

[23] P.J.M. Monteiro, S.A. Miller, A. Horvath, Towards sustainable concrete, Nature Materials, 16 **(2017)** 698-699.

[24] P. Baskar, A. Shalini, J.K. Kumar, Rice husk ash based geopolymer concrete - A Review, Chem Sci Rev Lett, 3 **(2014)** 288-294.

[25] J. Davidovits, Geopolymers: inorganic polymeric new materials, Journal of Thermal Analysis and calorimetry, 37 **(1991)** 1633-1656.

[26] M. Abdullah, L.Y. Ming, H.C. Yong, M. Tahir, Clay-based materials in geopolymer technology, Cement Based Materials, 239 **(2018)**.

[27] V. Glukhovsky, Ancient, modern and future concretes, Proceedings of the First International Conference on Alkaline Cements and Concretes, Kiev, Ukraine, **1994**, pp. 1-9.

[28] J. Davidovits, Geopolymer chemistry and sustainable development, **2005**.

[29] N. Van Chanh, B.D. Trung, D. Van Tuan, Recent research geopolymer concrete, The 3rd ACF International Conference-ACF/VCA, Vietnam, **2008**, pp. 235-241.

[30] P. Duxson, A. Fernández-Jiménez, J.L. Provis, G.C. Lukey, A. Palomo, J.S.J. van Deventer, Geopolymer technology: the current state of the art, Journal of Materials Science, 42 **(2007)** 2917-2933.

[31] T.W. Swaddle, Silicate complexes of aluminum(III) in aqueous systems, Coordination Chemistry Reviews, 219-221 **(2001)** 665-686.

[32] J.L. Provis, S.A. Bernal, Geopolymers and Related Alkali-Activated Materials, Annual Review of Materials Research, 44 **(2014)** 299-327.

[33] A. Mehta, R. Siddique, Sustainable geopolymer concrete using ground granulated blast furnace slag and rice husk ash: Strength and permeability properties, Journal of Cleaner Production, 205 **(2018)** 49-57.

[34] X.Y. Zhuang, L. Chen, S. Komarneni, C.H. Zhou, D.S. Tong, H.M. Yang, W.H. Yu, H. Wang, Fly ash-based geopolymer: clean production, properties and applications, Journal of Cleaner Production, 125 **(2016)** 253-267.

[35] C.B. Cheah, M.H. Samsudin, M. Ramli, W.K. Part, L.E. Tan, The use of high calcium wood ash in the preparation of Ground Granulated Blast Furnace Slag and Pulverized Fly Ash geopolymers: A complete microstructural and mechanical characterization, Journal of Cleaner Production, 156 **(2017)** 114-123.

[36] F.N. Genç, Gecekonduyla mücadeleden kentsel dönüşüme Türkiye'de kentleşme politikaları, Adnan Menderes Üniversitesi Sosyal Bilimler Enstitüsü Dergisi, 1 **(2014)** 15-30.

[37] A. Allahverdi, E. Najafi, Construction Wastes as Raw Materials for Geopolymer Binders, International Journal of Civil Engineering, 7 **(2009)** 154-160.

[38] Z. Sun, H. Cui, H. An, D. Tao, Y. Xu, J. Zhai, Q. Li, Synthesis and thermal behavior of geopolymer-type material from waste ceramic, Construction and Building Materials, 49 **(2013)** 281-287.

[39] V. Sata, A. Wongsa, P. Chindaprasirt, Properties of pervious geopolymer concrete using recycled aggregates, Construction and Building Materials, 42 **(2013)** 33-39.

[40] A. Pathak, S. Kumar, V.K. Jha, Development of Building Material from Geopolymerization of Construction and Demolition Waste (CDW), Transactions of the Indian Ceramic Society, 73 **(2014)** 133-137.

[41] K. Komnitsas, D. Zaharaki, A. Vlachou, G. Bartzas, M. Galetakis, Effect of synthesis parameters on the quality of construction and demolition wastes (CDW) geopolymers, Advanced Powder Technology, 26 **(2015)** 368-376.

[42] M. Torres-Carrasco, F. Puertas, Waste glass in the geopolymer preparation. Mechanical and microstructural characterisation, Journal of Cleaner Production, 90 **(2015)** 397-408.

[43] R.A. Robayo-Salazar, J.F. Rivera, R. Mejía de Gutiérrez, Alkali-activated building materials made with recycled construction and demolition wastes, Construction and Building Materials, 149 **(2017)** 130-138.

[44] M. Vafaei, A. Allahverdi, High strength geopolymer binder based on waste-glass powder, Advanced Powder Technology, 28 **(2017)** 215-222.

[45] P. Shoaei, H.R. Musaeei, F. Mirlohi, S. Narimani zamanabadi, F. Ameri, N. Bahrami, Waste ceramic powder-based geopolymer mortars: Effect of curing temperature and alkaline solution-to-binder ratio, Construction and Building Materials, 227 **(2019)** 116686.

[46] A. De Rossi, M. Ribeiro, J. Labrincha, R. Novais, D. Hotza, R. Moreira, Effect of the particle size range of construction and demolition waste on the fresh and hardened-state properties of fly ash-based geopolymer mortars with total replacement of sand, Process Safety and Environmental Protection, 129 **(2019)** 130-137.

[47] C.-L. Hwang, M.D. Yehualaw, D.-H. Vo, T.-P. Huynh, A. Largo, Performance evaluation of alkali activated mortar containing high volume of waste brick powder blended with ground granulated blast furnace slag cured at ambient temperature, Construction and Building Materials, 223 **(2019)** 657-667.

[48] O. Mahmoodi, H. Siad, M. Lachemi, S. Dadsetan, M. Sahmaran, Optimization of brick waste-based geopolymer binders at ambient temperature and pre-targeted chemical parameters, Journal of Cleaner Production, 268 **(2020)** 122285.

[49] O. Mahmoodi, H. Siad, M. Lachemi, S. Dadsetan, M. Sahmaran, Development of normal and very high strength geopolymer binders based on concrete waste at ambient environment, Journal of Cleaner Production, 279 **(2021)** 123436.

[50] H. Ulugöl, A. Kul, G. Yıldırım, M. Şahmaran, A. Aldemir, D. Figueira, A. Ashour, Mechanical and microstructural characterization of geopolymers from assorted construction and demolition waste-based masonry and glass, Journal of Cleaner Production, 280 **(2021)** 124358.

[51] H. Ilcan, O. Sahin, A. Kul, G. Yildirim, M. Sahmaran, Rheological properties and compressive strength of construction and demolition waste-based geopolymer mortars for 3D-Printing, Construction and Building Materials, 328 **(2022)** 127114.

[52] Ş. Akduman, O. Kocaer, A. Aldemir, M. Şahmaran, G. Yıldırım, H. Almahmood, A. Ashour, Experimental investigations on the structural behaviour of reinforced geopolymer beams produced from recycled construction materials, Journal of Building Engineering, 41 **(2021)** 102776.

[53] G. Yıldırım, A. Kul, E. Özçelikci, M. Şahmaran, A. Aldemir, D. Figueira, A. Ashour, Development of alkali-activated binders from recycled mixed masonry-originated waste, Journal of Building Engineering, 33 **(2021)** 101690.

[54] T. Wohlers, T. Gornet, History of additive manufacturing, Wohlers report, 24 **(2014)** 118.

[55] M. Shellabear, O. Nyrhilä, DMLS-Development history and state of the art, Proceedings of the 4th LANE 2004, Sept. 22.-24, **(2004)**.

[56] Ö. Gökhan, Eklemeli üretim teknolojileri üzerine bir derleme, Niğde Ömer Halisdemir Üniversitesi Mühendislik Bilimleri Dergisi, 9 **(2020)** 606-621.

[57] L. Yang, K. Hsu, B. Baughman, D. Godfrey, F. Medina, M. Menon, S. Wiener, Additive manufacturing of metals: the technology, materials, design and production, Springer **2017**.

[58] M. Gouge, P. Michaleris, Thermo-mechanical modeling of additive manufacturing, Butterworth-Heinemann **2017**.

[59] ASTMF2792-12a, Standard terminology for additive manufacturing technologies, ASTM International, **(2012)**.

[60] S.C. Paul, Y.W.D. Tay, B. Panda, M.J. Tan, Fresh and hardened properties of 3D printable cementitious materials for building and construction, Archives of Civil and Mechanical Engineering, 18 **(2018)** 311-319.

[61] T. Wangler, E. Lloret, L. Reiter, N. Hack, F. Gramazio, M. Kohler, M. Bernhard, B. Dillenburger, J. Buchli, N. Roussel, Digital concrete: opportunities and challenges, RILEM Technical Letters, 1 **(2016)** 67-75.

[62] R.A. Buswell, R.C. Soar, A.G. Gibb, A. Thorpe, Freeform construction: mega-scale rapid manufacturing for construction, Automation in construction, 16 **(2007)** 224-231.

[63] B. Khoshnevis, Automated construction by contour crafting—related robotics and information technologies, Automation in construction, 13 **(2004)** 5-19.

[64] S. Lim, T. Le, J. Webster, R. Buswell, A. Austin, A. Gibb, T. Thorpe, Fabricating construction components using layered manufacturing technology, Global Innovation in Construction Conference, Loughborough University Leicestershire, UK, **2009**, pp. 512-520.

[65] N. Oxman, J. Duro-Royo, S. Keating, B. Peters, E. Tsai, Towards robotic swarm printing, Architectural Design, 84 **(2014)** 108-115.

[66] Y.W.D. Tay, B. Panda, S.C. Paul, N.A. Noor Mohamed, M.J. Tan, K.F. Leong, 3D printing trends in building and construction industry: a review, Virtual and Physical Prototyping, 12 **(2017)** 261-276.

[67] R.J. Wolfs, F.P. Bos, E.C. van Strien, T.A. Salet, A real-time height measurement and feedback system for 3D concrete printing, High Tech Concrete: Where Technology and Engineering Meet, Springer **2018**, pp. 2474-2483.

[68] R.A. Buswell, R.C. Soar, A.G. Gibb, A. Thorpe, Freeform construction application research, Advances in Engineering Structures, Mechanics & Construction, Springer **2006**, pp. 773-780.

[69] J. Beirão, N. Mateus, J.S. Alves, Modular, Flexible, Customizable Housing and 3D Printed.

[70] M. Hojati, S. Nazarian, J.P. Duarte, A. Radlinska, N. Ashrafi, F. Craveiro, S. Bilén, 3D printing of concrete: A continuous exploration of mix design and printing process, 42nd IAHS world congress the housing for the dignity of mankind, **2018**.

[71] R. Rael, V. San Fratello, Printing architecture: Innovative recipes for 3D printing, Chronicle Books **2018**.

[72] B. Panda, S. Chandra Paul, M. Jen Tan, Anisotropic mechanical performance of 3D printed fiber reinforced sustainable construction material, Materials Letters, 209 **(2017)** 146-149.

[73] B. Panda, S.C. Paul, L.J. Hui, Y.W.D. Tay, M.J. Tan, Additive manufacturing of geopolymer for sustainable built environment, Journal of Cleaner Production, 167 **(2017)** 281-288.

[74] S. Al-Qutaifi, A. Nazari, A. Bagheri, Mechanical properties of layered geopolymer structures applicable in concrete 3D-printing, Construction and Building Materials, 176 **(2018)** 690-699.

[75] B. Panda, C. Unluer, M.J. Tan, Investigation of the rheology and strength of geopolymer mixtures for extrusion-based 3D printing, Cement and Concrete Composites, 94 **(2018)** 307-314.

[76] B. Panda, M.J. Tan, Experimental study on mix proportion and fresh properties of fly ash based geopolymer for 3D concrete printing, Ceramics International, 44 **(2018)** 10258-10265.

[77] B. Nematollahi, P. Vijay, J. Sanjayan, A. Nazari, M. Xia, V.N. Nerella, V. Mechtcherine, Effect of Polypropylene Fibre Addition on Properties of Geopolymers Made by 3D Printing for Digital Construction, Materials, 11 **(2018)** 2352.

[78] B. Nematollahi, M. Xia, S.H. Bong, J. Sanjayan, Hardened properties of 3D printable 'one-part'geopolymer for construction applications, RILEM International Conference on Concrete and Digital Fabrication, Springer, **2018**, pp. 190-199.

[79] B. Nematollahi, M. Xia, J. Sanjayan, P. Vijay, Effect of type of fiber on inter-layer bond and flexural strengths of extrusion-based 3D printed geopolymer, Materials science forum, Trans Tech Publ, **2018**, pp. 155-162.

[80] A. Kashani, T. Ngo, Optimisation of mixture properties for 3D printing of geopolymer concrete, ISARC. Proceedings of the International Symposium on Automation and Robotics in Construction, IAARC Publications, **2018**, pp. 1-8.

[81] M. Chougan, S.H. Ghaffar, M. Jahanzat, A. Albar, N. Mujaddedi, R. Swash, The influence of nano-additives in strengthening mechanical performance of 3D printed

multi-binder geopolymer composites, Construction and Building Materials, 250 **(2020)** 118928.

[82] Z. Li, L. Wang, G. Ma, Mechanical improvement of continuous steel microcable reinforced geopolymer composites for 3D printing subjected to different loading conditions, Composites Part B: Engineering, 187 **(2020)** 107796.

[83] B. Panda, C. Unluer, M.J. Tan, Extrusion and rheology characterization of geopolymer nanocomposites used in 3D printing, Composites Part B: Engineering, 176 **(2019)** 107290.

[84] O. Şahin, H. İlcan, A.T. Ateşli, A. Kul, G. Yıldırım, M. Şahmaran, Construction and demolition waste-based geopolymers suited for use in 3-dimensional additive manufacturing, Cement and Concrete Composites, 121 **(2021)** 104088.

[85] B. Nematollahi, M. Xia, P. Vijay, J.G. Sanjayan, Properties of extrusion-based 3D printable geopolymers for digital construction applications, 3D Concrete Printing Technology, Elsevier**2019**, pp. 371-388.

[86] S. Muthukrishnan, S. Ramakrishnan, J. Sanjayan, Effect of alkali reactions on the rheology of one-part 3D printable geopolymer concrete, Cement and Concrete Composites, 116 **(2020)** 103899.

[87] X. Guo, J. Yang, G. Xiong, Influence of supplementary cementitious materials on rheological properties of 3D printed fly ash based geopolymer, Cement and Concrete Composites, 114 **(2020)** 103820.

[88] S.H. Bong, M. Xia, B. Nematollahi, C. Shi, Ambient temperature cured 'just-add-water' geopolymer for 3D concrete printing applications, Cement and Concrete Composites, 121 **(2021)** 104060.

[89] V. Mechtcherine, V.N. Nerella, F. Will, M. Näther, J. Otto, M. Krause, Large-scale digital concrete construction – CONPrint3D concept for on-site, monolithic 3D-printing, Automation in Construction, 107 **(2019)** 102933.

[90] G. Ma, Z. Li, L. Wang, F. Wang, J. Sanjayan, Mechanical anisotropy of aligned fiber reinforced composite for extrusion-based 3D printing, Construction and Building Materials, 202 **(2019)** 770-783.

[91] T. Ding, J. Xiao, S. Zou, X. Zhou, Anisotropic behavior in bending of 3D printed concrete reinforced with fibers, Composite Structures, 254 **(2020)** 112808.

[92] M. Xia, B. Nematollahi, J. Sanjayan, Printability, accuracy and strength of geopolymer made using powder-based 3D printing for construction applications, Automation in Construction, 101 **(2019)** 179-189.

[93] B. Panda, G.V.P.B. Singh, C. Unluer, M.J. Tan, Synthesis and characterization of one-part geopolymers for extrusion based 3D concrete printing, Journal of Cleaner Production, 220 **(2019)** 610-619.

[94] G. Ma, Z. Li, L. Wang, G. Bai, Micro-cable reinforced geopolymer composite for extrusion-based 3D printing, Materials Letters, 235 **(2019)** 144-147.

[95] B. Panda, N.A. Noor Mohamed, Y.W.D. Tay, M.J. Tan, Bond strength in 3D printed geopolymer mortar, RILEM International Conference on Concrete and Digital Fabrication, Springer, **2018**, pp. 200-206.

[96] Y.W.D. Tay, G.H.A. Ting, Y. Qian, B. Panda, L. He, M.J. Tan, Time gap effect on bond strength of 3D-printed concrete, Virtual and Physical Prototyping, 14 **(2019)** 104-113.

[97] B. Panda, G.H. Ting, A. Annapareddy, M. Li, Flow and mechanical properties of 3D printed cementitious material with recycled glass aggregates, **2018**.

[98] B. Panda, S.C. Paul, N.A.N. Mohamed, Y.W.D. Tay, M.J. Tan, Measurement of tensile bond strength of 3D printed geopolymer mortar, Measurement, 113 **(2018)** 108-116.

[99] T. Marchment, J. Sanjayan, M. Xia, Method of enhancing interlayer bond strength in construction scale 3D printing with mortar by effective bond area amplification, Materials & Design, 169 **(2019)** 107684.

[100] A. Bouaissi, L.Y. Li, L.M. Moga, I.G. Sandu, M. Abdullah, A.V. Sandu, A review on fly ash as a raw cementitious material for geopolymer concrete, Rev. Chim, 69 **(2018)** 1661-1667.

[101] Z. Zuhua, Y. Xiao, Z. Huajun, C. Yue, Role of water in the synthesis of calcined kaolin-based geopolymer, Applied Clay Science, 43 **(2009)** 218-223.

[102] W.M. Kriven, J.L. Bell, M. Gordon, Microstructure and microchemistry of fully-reacted geopolymers and geopolymer matrix composites, Ceramic Transactions, 153 **(2003)** 227-250.

[103] M. Lizcano, A. Gonzalez, S. Basu, K. Lozano, M. Radovic, Effects of water content and chemical composition on structural properties of alkaline activated metakaolin-based geopolymers, Journal of the American Ceramic Society, 95 **(2012)** 2169-2177.

[104] A. C1437', Standard Test Method for Flow of Hydraulic Cement Mortar, Annual Book of ASTM Standards, West Conshohocken, PA, USA, **(2007)**.

[105] A. Kazemian, X. Yuan, E. Cochran, B. Khoshnevis, Cementitious materials for construction-scale 3D printing: Laboratory testing of fresh printing mixture, Construction and Building Materials, 145 **(2017)** 639-647.

[106] S.C. Figueiredo, C.R. Rodríguez, Z.Y. Ahmed, D.H. Bos, Y. Xu, T.M. Salet, O. Çopuroğlu, E. Schlangen, F.P. Bos, An approach to develop printable strain hardening cementitious composites, Materials & Design, 169 **(2019)** 107651.

[107] J. Benbow, E. Oxley, J. Bridgwater, The extrusion mechanics of pastes—the influence of paste formulation on extrusion parameters, Chemical Engineering Science, 42 **(1987)** 2151-2162.

[108] R. Basterfield, C. Lawrence, M. Adams, On the interpretation of orifice extrusion data for viscoplastic materials, Chemical engineering science, 60 **(2005)** 2599-2607.

[109] J. Benbow, N. Ouchiyama, J. Bridgwater, On the prediction of extrudate pore structure from particle size, Chemical Engineering Communications, 62 **(1987)** 203-220.

[110] Y. Chen, S. Chaves Figueiredo, Ç. Yalçinkaya, O. Çopuroğlu, F. Veer, E. Schlangen, The effect of viscosity-modifying admixture on the extrudability of limestone and calcined clay-based cementitious material for extrusion-based 3D concrete printing, Materials, 12 **(2019)** 1374.

[111] X. Zhou, Z. Li, M. Fan, H. Chen, Rheology of semi-solid fresh cement pastes and mortars in orifice extrusion, Cement and Concrete Composites, 37 **(2013)** 304-311.

[112] ASTMC496/C496M-17, Standard Test Method for Splitting Tensile Strength of Cylindrical Concrete Specimens, ASTM International, West Conshohocken, **2017**.

[113] S. Timoshenko, Axisymmetric stress and deformation in a solid of revolution, Theory of elasticity, **(1970)**.

[114] J.L. Provis, J.S.J. Van Deventer, Geopolymers: structures, processing, properties and industrial applications, Elsevier**2009**.

[115] D.-W. Zhang, D.-m. Wang, Z. Liu, F.-z. Xie, Rheology, agglomerate structure, and particle shape of fresh geopolymer pastes with different NaOH activators content, Construction and Building Materials, 187 **(2018)** 674-680.

[116] K. Vance, A. Dakhane, G. Sant, N. Neithalath, Observations on the rheological response of alkali activated fly ash suspensions: the role of activator type and concentration, Rheologica Acta, 53 **(2014)** 843-855.

[117] S. Alonso, A. Palomo, Alkaline activation of metakaolin and calcium hydroxide mixtures: influence of temperature, activator concentration and solids ratio, Materials Letters, 47 **(2001)** 55-62.

[118] D. Khale, R. Chaudhary, Mechanism of geopolymerization and factors influencing its development: a review, Journal of materials science, 42 **(2007)** 729-746.

[119] O.K. Wattimena, Antoni, D. Hardjito, A review on the effect of fly ash characteristics and their variations on the synthesis of fly ash based geopolymer, AIP Conference Proceedings, AIP Publishing LLC, **2017**, pp. 020041.

[120] D. Hardjito, C.C. Cheak, C.L. Ing, Strength and setting times of low calcium fly ash-based geopolymer mortar, Modern applied science, 2 **(2008)** 3-11.

[121] J. Zhang, S. Li, Z. Li, Q. Zhang, H. Li, J. Du, Y. Qi, Properties of fresh and hardened geopolymer-based grouts, Ceramics-Silikaty, 63 **(2019)** 164-174.

[122] B. Akturk, A.B. Kizilkanat, N. Kabay, Effect of calcium hydroxide on fresh state behavior of sodium carbonate activated blast furnace slag pastes, Construction and Building Materials, 212 **(2019)** 388-399.

[123] M.L. Granizo, S. Alonso, M.T. Blanco-Varela, A. Palomo, Alkaline activation of metakaolin: effect of calcium hydroxide in the products of reaction, Journal of the American Ceramic Society, 85 **(2002)** 225-231.

[124] X. Chen, A. Sutrisno, L.J. Struble, Effects of calcium on setting mechanism of metakaolin-based geopolymer, Journal of the American Ceramic Society, 101 **(2018)** 957-968.

[125] J. Temuujin, A. van Riessen, R. Williams, Influence of calcium compounds on the mechanical properties of fly ash geopolymer pastes, Journal of Hazardous Materials, 167 **(2009)** 82-88.

[126] H. Khater, Effect of calcium on geopolymerization of aluminosilicate wastes, Journal of materials in civil engineering, 24 **(2012)** 92-101.

[127] X. Guo, H. Shi, L. Chen, W.A. Dick, Alkali-activated complex binders from class C fly ash and Ca-containing admixtures, Journal of Hazardous Materials, 173 **(2010)** 480-486.

[128] A.U. Rehman, J.-H. Kim, 3D concrete printing: A systematic review of rheology, mix designs, mechanical, microstructural, and durability characteristics, Materials, 14 **(2021)** 3800.

[129] M. Komljenović, Z. Baščarević, V. Bradić, Mechanical and microstructural properties of alkali-activated fly ash geopolymers, Journal of Hazardous Materials, 181 **(2010)** 35-42.

[130] H.Y. Leong, D.E.L. Ong, J.G. Sanjayan, A. Nazari, The effect of different Na2O and K2O ratios of alkali activator on compressive strength of fly ash based-geopolymer, Construction and Building Materials, 106 **(2016)** 500-511.

[131] U. Rattanasak, P. Chindaprasirt, Influence of NaOH solution on the synthesis of fly ash geopolymer, Minerals Engineering, 22 **(2009)** 1073-1078.

[132] R.M. Hamidi, Z. Man, K.A. Azizli, Concentration of NaOH and the effect on the properties of fly ash based geopolymer, Procedia engineering, 148 **(2016)** 189-193.

[133] A.B. Pascual, M.T. Tognonvi, A. Tagnit-Hamou, Waste glass powder-based alkali-activated mortar, Int. J. Res. Eng. Technol, 3 **(2014)** 32-36.

[134] Y. Rifaai, A. Yahia, A. Mostafa, S. Aggoun, E.-H. Kadri, Rheology of fly ash-based geopolymer: Effect of NaOH concentration, Construction and Building Materials, 223 **(2019)** 583-594.

[135] A. Palomo, M. Grutzeck, M. Blanco, Alkali-activated fly ashes: A cement for the future, Cement and concrete research, 29 **(1999)** 1323-1329.

[136] C.K. Yip, G. Lukey, J.S. Van Deventer, The coexistence of geopolymeric gel and calcium silicate hydrate at the early stage of alkaline activation, Cement and concrete research, 35 **(2005)** 1688-1697.

[137] X. Guo, H. Shi, Metakaolin-, fly ash-and calcium hydroxide-based geopolymers: effects of calcium on performance, Advances in Cement Research, 27 **(2015)** 559-566.

[138] C. Li, H. Sun, L. Li, A review: The comparison between alkali-activated slag (Si+ Ca) and metakaolin (Si+ Al) cements, Cement and concrete research, 40 **(2010)** 1341-1349.

[139] J. Gourley, Geopolymers; opportunities for environmentally friendly construction materials, Materials 2003 Conference: Adaptive Materials for a Modern Society, Sydney, Institute of Materials Engineering Australia, **2003**.

[140] S.V. Patankar, Y.M. Ghugal, S.S. Jamkar, Effect of concentration of sodium hydroxide and degree of heat curing on fly ash-based geopolymer mortar, Indian journal of materials science, 2014 **(2014)**.

[141] T.T. Le, S.A. Austin, S. Lim, R.A. Buswell, R. Law, A.G.F. Gibb, T. Thorpe, Hardened properties of high-performance printing concrete, Cement and Concrete Research, 42 **(2012)** 558-566.

[142] K. Yu, W. McGee, T.Y. Ng, H. Zhu, V.C. Li, 3D-printable engineered cementitious composites (3DP-ECC): Fresh and hardened properties, Cement and Concrete Research, 143 **(2021)** 106388.

[143] P.K.M.P.J.M. Mehta, Concrete : microstructure, properties, and materials, McGraw-Hill, New York, **2006**.

[144] M. Moini, Buildability and Mechanical Performance of Architectured Cement-Based Materials Fabricated Using a Direct-Ink-Writing Process, Purdue University Graduate School, **2020**.

[145] J.H. Lim, B. Panda, Q.-C. Pham, Improving flexural characteristics of 3D printed geopolymer composites with in-process steel cable reinforcement, Construction and Building Materials, 178 **(2018)** 32-41.

[146] J.G. Sanjayan, B. Nematollahi, M. Xia, T. Marchment, Effect of surface moisture on inter-layer strength of 3D printed concrete, Construction and building materials, 172 **(2018)** 468-475.

[147] TBEC, Turkish Seismic Earthquake Code **2018**, pp. 1-146.

[148] C. International Code, 2015 IBC : International building code, **2014**.

[149] J. Noland, G. Kingsley, U.S. Coordinated Program for Masonry Building Research: Technology Transfer, **1995**, pp. 360-371.

[150] H. Wang, H. Li, F. Yan, Synthesis and mechanical properties of metakaolinite-based geopolymer, Colloids and Surfaces A: Physicochemical and Engineering Aspects, 268 **(2005)** 1-6.

[151] T. Ding, J. Xiao, S. Zou, J. Yu, Flexural properties of 3D printed fibre-reinforced concrete with recycled sand, Construction and Building Materials, 288 **(2021)** 123077.

[152] T. Marchment, J.G. Sanjayan, B. Nematollahi, M. Xia, Interlayer strength of 3D printed concrete: influencing factors and method of enhancing, 3D concrete printing technology, Elsevier**2019**, pp. 241-264.

[153] X. Chen, S. Wu, J. Zhou, Influence of porosity on compressive and tensile strength of cement mortar, Construction and Building Materials, 40 **(2013)** 869-874.

[154] W. Lee, J. Van Deventer, The interface between natural siliceous aggregates and geopolymers, Cement and Concrete Research, 34 **(2004)** 195-206.

[155] J. Temuujin, A. van Riessen, K. MacKenzie, Preparation and characterisation of fly ash based geopolymer mortars, Construction and Building materials, 24 **(2010)** 1906-1910.